Thermal and Hydrodynamic Characteristics of Jet Impingement Quenching for High Temperature Surface

By

Aloke Kumar Mozumder

A dissertation submitted in partial fulfillment of the
requirement for the degree of

Doctor of Philosophy (Ph.D.)
in
Mechanical Engineering

Department of Energy and Materials Science
Graduate School of Science and Engineering
Saga University

September 2006

Acknowledgement

The author would like to express his appreciation to Professor Masanori Monde, Department of Mechanical Engineering, Saga University, for his advice during the author's doctoral research endeavor for the past three years. As a supervisor, he has constantly forced the author to remain focused on achieving the goal. His observations and comments helped for establishing the overall direction of the research and to move forward with investigation in depth. The author thanks Prof. Monde for providing the opportunity to work with a talented team of researchers.

The author is deeply indebted to the committee members, Prof. Masanori Monde, Department of Mechanical Engineering, Saga University, Prof. Kenji Kaneko, Department of Mechanical Engineering, Saga University, Prof. Shuichi Nagata, Institute of Ocean Energy, Saga University, and Assoc. Prof. Yuichi Mitsutake, Department of Mechanical Engineering, Saga University for the critical reading of this dissertation and for proving valuable suggestions.

The author owes a great deal to Assoc. Prof. Yuichi Mitsutake, Department of Mechanical Engineering, Saga University, for his valuable suggestions in conducting the experiment at different stages.

The author would like to thank Dr. Peter Lloyd Woodfield and Dr. Md. Ashraful Islam for their valuable help and suggestions in successful completion of this research work.

The author also would like to thank all the students who study in Prof. Monde's laboratory and to Mr. Kenichi Nakashima for his help during the manufacturing of the experimental apparatus.

Special thank is directed from the author to Dr. Jaffar Abdulla Hammad for his kind cooperation at the beginning of this research works.

Finally, the author would like to express his respect and appreciation to the Japanese Ministry of Education Culture Sports Science and Technology (Monbukagakusho) for providing scholarship during the three years of the author's study.

Contents

List of Figures and Tables

Nomenclature

a	thermal diffusivity [m^2/s]
c	specific heat [kJ/kg K]
CHF	critical heat flux
d	jet diameter [mm]
$f(\tau, \gamma, \zeta_n)$	function for depicting temperature variation on plane $\zeta = \zeta_n$ beneath the surface
$G_{j,l}^{(m,n)}$	coefficient in Eq. (A.2)
$H_{j,l}^{(m,n)}$	coefficient in Eq. (A.3)
$J_0(r), J_1(r)$	Bessel function
l_r	length in r direction of a cylindrical coordinate [mm]
l_z	length in z direction of a cylindrical coordinate [mm]
m_j	eigenvalue [root of $J_1(m_j) = 0$]
m	mass flow rate of liquid
MHF	maximum heat flux
N	order of approximating polynomial
N_j	number of eigenvalues minus one
Pa	Pascal [N/m^2]
PCZ	precursory cooling zone
$P_{j,k}^{(n)}$	coefficient derived from measured temperature variation
q_w	surface heat flux [MW/m^2]
R_{ed}	Reynolds number on the basis of jet diameter $= \dfrac{ud}{\upsilon_l}$
r	position in the radial direction of the block [mm]
r^*	radial position of wetting front during resident time [mm]
T	measured temperature [mm]
t	time (counted from the impingement of jet) [s]
t^*	resident time [s]
T^*	solid–liquid interface temperature [°C]
T_b	block initial temperature [°C]
T_c	critical temperature [°C]

T_{liq}	liquid temperature [°C]
T_{max}	limiting surface temperature that allows liquid-solid contact [°C]
T_q	quench temperature [°C]
T_{rw}	Rewet temperature [°C]
T_{sat}	saturated temperature [°C]
T_{tls}	thermodynamic limit of superheat [°C]
T_w	surface temperature [°C]
T_w^*	surface temperature at resident time (at $r = r^*$) [°C]
u	jet velocity [m/s]
W	boiling width
z	z-coordinate distance (in axial direction of the cylinder) [mm]
z_1, z_2	the distance of thermocouples location from the hot surface [mm]

Greek symbols

α	strain meter constant
ΔT	thermal potential [K]
ΔT_{sub}	liquid subcooling [$=T_{sat} - T_{liq}$]
θ_w	non-dimensional surface temperature [T/T_b]
Φ_w	non-dimensional surface heat flux
λ	thermal conductivity [kW/m K]
τ	non-dimensional time $= \frac{at}{l^2_r}$
ε	strain
ζ	non-dimensional distance in z direction (z/l_z)
γ	non-dimensional distance in r direction (r/l_r)
ρ	density [kg/m^3]
τ^*_n	non-dimensional time lag
ν	kinematic viscosity [m^2/s]

Subscripts

l	liquid
s	solid

Chapter 1

Introduction

Rapid cooling of a high temperature solid surface is described as quenching in thermal engineering. At the primary ages of material science, people did quenching by immersing solid metal pieces into a bath of water. Quenching is now widely used in many manufacturing industries for controlling high temperature and heat treatment process. In this section, various applications of quenching and its definition of different terms and the literatures of quenching will be discussed. Finally, the objectives of the present study will be included.

1.1 Application of Quenching

Quenching is used in industry for cooling and product quality control purposes. Some applications are discussed in this section.

1.1.1 In manufacturing industry

Both the physical dimensions and metallurgical and mechanical properties are important for quality products. For the precise controlling of the desired properties; the rate of cooling/quenching of the product plays a vital role. In the manufacturing world, quenching is widely used in different processes such as extrusion, casting, forging, annealing and so on.

1.1.2 Cooling of nuclear reactors

In water-cooled nuclear reactors, it is essential to control the heat removal rate from the fuel element during a loss of coolant accident (LOCA). At that time the fuel element will overheat even though the reactor is immediately shutdown. In the event of such an emergency it is necessary to provide an alternative cooling system known as emergency core cooling (ECC). For the purpose of emergency core cooling, water jets are impinged on the hot fuel element. In certain types of water cooled reactors, this emergency cooling water is sprayed into each fuel bundle from a pipe situated in the centre of the bundle. When a jet of emergency cooling water impinges on a hot fuel element, stable film boiling

occurs [1]. Convective and radiative heat transfer locally remove the stored heat and after a time (the wetting delay time or resident time) the film becomes unstable and a wet patch is initiated. This wet patch spreads and results in the formation of a stable quenching front. Understanding of the wetting delay or resident time, which occurs between jet initiation and starting of wetting front movement, is of great importance in analyzing the consequences of a loss of coolant accident. This delay time influences the total time to quench the fuel bundle and, if long can lead to excessive cladding temperatures or in the worst case a failure of the emergency cooling system. In order to investigate this wetting delay phenomena together with the other parameters, an experimental study on jet impingement quenching for a high temperature surface has been conducted. It is worth mentioning that the lack of efficient emergency cooling systems was responsible for about 55 % of the nuclear reactor accidents until 1995 [IEEE].

1.1.3 Cooling of electronic components

Electronic components produce heat during operation and the cooling process associated with this problem is called microelectronic/electronic cooling. The higher the power and speed of the electronic machinery; the higher is the heat generation rate. So, the experts in fluid and thermal science become involved with the cooling problem. Spray nozzle and impinging cooling are some of the effective cooling techniques for microelectronic circuits.

1.2 Quenching and Boiling Phenomena

Due to increasing demand for utility of quenching in industry, researchers and scientists have carried out analytical and experimental investigations for clear understanding of quenching phenomena. Most of the researchers can be divided into two groups according to the main interest, the first group includes those who are interested in the mechanical properties of metals such as hardness, toughness, strength and the second group includes those who are interested in the mechanism of heat transfer during the cooling process. In this study, a brief history for the literatures of the second group will be discussed. The quenching process is very complicated; it involves many sub-processes which are also complicated themselves. Definitions of some phenomena associated with quenching are also discussed here.

1.2.1 Definition of quenching

Quenching can be defined as a heat transfer process in which extremely rapid cooling results from bringing high temperature solid into sudden contact with lower temperature

fluid. Generally, the key feature responsible for the rapid cooling is a rewetting process which is believed to occur when the temperature of the hot surface is below a certain value referred as the rewetting, sputtering or Leidenfrost temperature. However, the Leidenfrost temperature does not appear to be a simple function of the liquid properties. Moreover, the mechanism for defining this temperature, if a single mechanism actually exits, is not well established and numerous proposals have been made [2]. According to Dua and Tien [3] surface rewetting refers to the establishing of liquid contact with a solid surface whose initial temperature is higher than the sputtering temperature, the temperature up to which a surface may wet. Due to its importance to emergency core cooling of water reactors in the event of postulated loss-of-coolant accidents, the problem of surface rewetting has gained much attention in recent years. Iloeje et al. [4] described rewetting as the onset of transition or unstable boiling in going from stable film boiling to nucleate boiling, and found that it corresponded to the minimum film boiling heat flux on the standard boiling curve.

1.2.2 Jet impingement quenching

One of the most efficient ways of cooling is jet impingement quenching. The heat transfer coefficients for this cooling system typically exceed the ones for pool boiling enormously, starting at values of about 10, 000 W/m^2K [5]. This characteristic makes this cooling system preferable for many practical applications. Figure 1.1 shows a pictorial definition of wet zone, wetting front, dry zone and wetting front velocity during quenching of a high temperature solid surface by using liquid jet impingement.

When the liquid jet is impinged on the hot solid surface, the entire hot surface does not wet immediately. The liquid splashed out from the local impinged region. The solid temperature drops to a certain value and then the liquid is allowed to move over the hot surface. After starting the wetting of the hot surface, the moving front of the wet region is

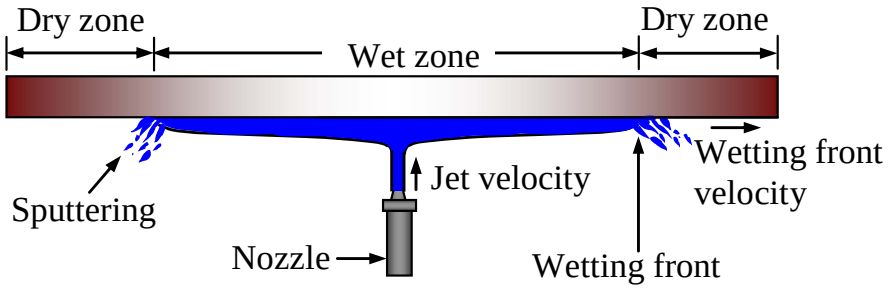

Fig. 1.1: Definition of jet impingement quenching

described as wetting front in this study. The local wall temperature at the wetting front is important for theoretical modeling of the quenching problem. There has been confusion in the specialized literatures concerning the exact definition of this parameters manifested in the variety of synonyms used to identify it, such as sputtering, quench, minimum film boiling and Leidenfrost temperature, which does not always represent the same physical phenomena [6]. After starting towards covering the entire hot surface by the impinged liquid, the wetting front moves at a certain rate over the surface which is described as wetting front velocity, u_{wf}.

1.2.3 Wetting delay / Resident time in quenching

As observed in the present study, when the liquid was first impinged on the hot surface it remained stagnant in a small impingement region for a certain period of time before covering the entire surface. This time period varied from fraction of second to a few minutes which depends on the experimental conditions. This wetting delay period is described as the resident time, t^* in the present study. The radius of the stagnation area during the resident period is described as the stagnation radius, r^*. The local wall temperature at the stagnation radius at the resident time is represented by T_w^* in this study. Figure 1.2 describes the above mentioned definition of quenching phenomena by using a cooling curve. Just after the resident time the wetting front starts moving and consequently the surface temperature drops at a faster rate. Before the resident time, the surface temperature drops slowly and almost at a constant rate though there is a sudden drop of temperature at the very beginning of the jet impingement.

1.2.4 Boiling curve

A typical pool boiling curve is shown in Fig. 1.3. Different regimes of pool boiling were first identified by Nukiyama [7]. An appreciation for the underlying physical mechanisms

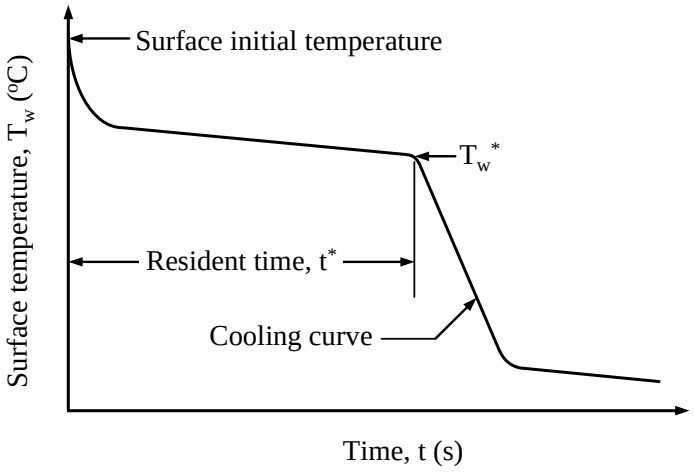

Fig. 1.2: Cooling curve during quenching

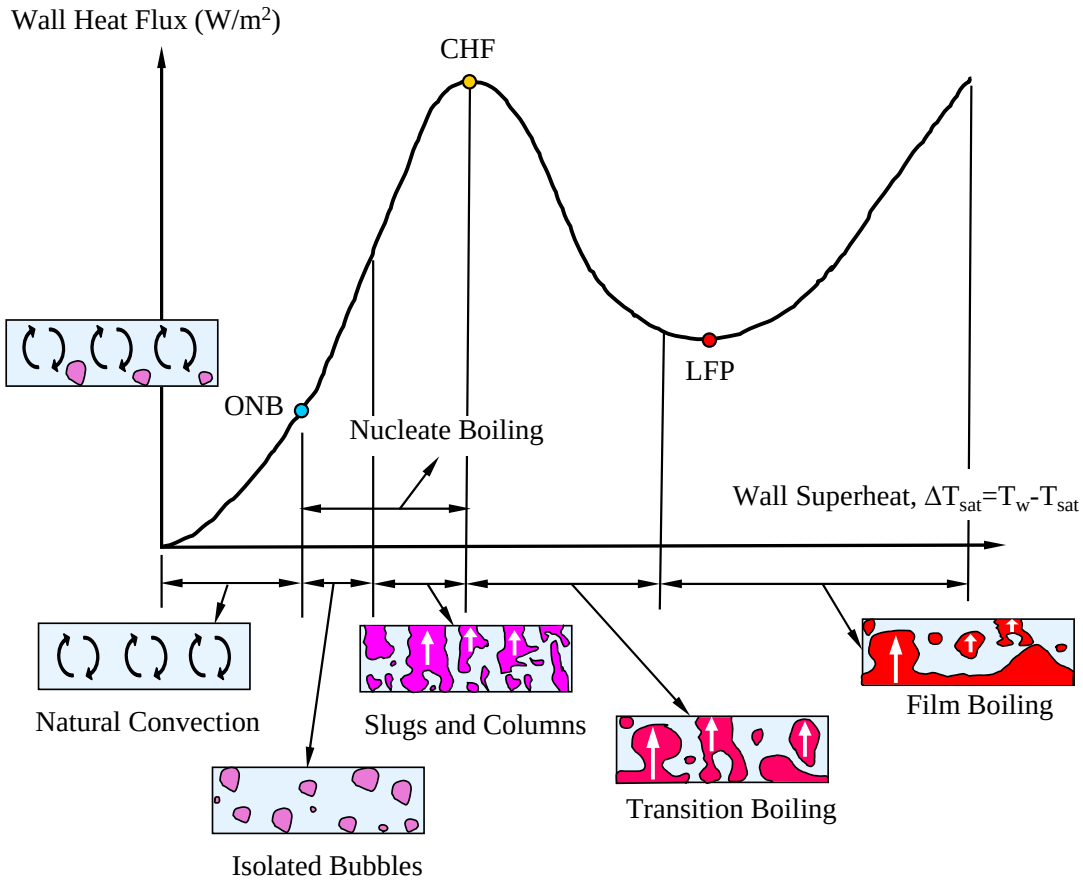

Fig. 1.3: Typical pool boiling curve for water at one atmosphere

may be obtained by examining the various modes or regimes of pool boiling as shown in Fig. 1.3. Different boiling regimes may be delineated according to the value of wall superheat, ΔT_{sat}.

Natural convection: Natural convection boiling exists when the wall superheat, $\Delta T_{sat} \leq 5$ ^{o}C. In this regime there is insufficient vapor in contact with the liquid phase to cause boiling at the saturation temperature. As the wall superheat is increased, bubble inception will eventually occur, but below the point of Onset of Nucleate Boiling, ONB, fluid motion is determined principally by natural convection effects.

Nucleate boiling: Nucleate boiling exists when the wall super heat, $\Delta T_{sat} = 5\sim30$ ^{o}C. In this range, two different flow regimes may be distinguished. Isolated bubbles form at nucleation sites and separate from the surface, as illustrated in Fig. 1.3. For the higher value of ΔT_{sat} in the nucleate boiling range, the vapor escapes as jets or columns, which subsequently merge into slugs of vapor. At the end of this regime, the heat flux reaches its maximum value which is usually termed as critical heat flux, CHF.

Transition boiling: The regime corresponding to ΔT_{sat} = 30~120 ^{o}C is termed as transition boiling, unstable film boiling, or partial film boiling. Bubble formation is now so rapid that a vapor film or blanket begins to form on the surface. At any point on the surface, conditions may oscillate between film and nucleate boiling, but the fraction of the total surface covered by the film increases with increasing ΔT_{sat}.

Film boiling: This mode of heat transfer happens when the value of ΔT_{sat} exceeds 120^{o}C and at this stage the surface is completely covered by a vapor blanket. The minimum heat flux point in the film boiling regime is sometimes described as the Leidenfrost point, LFP.

1.2.5 Maximum and critical heat flux

The upper limit of heat flux for a safe operation of heat transfer equipment is the maximum heat flux. Many analytical and experimental investigations have been conducted to clarify the basic mechanism of the maximum heat flux condition during quenching, this point is not clearly understood yet. There are two groups of researchers who studied the maximum heat flux during quenching.

Maximum heat flux: The maximum heat flux of the surface estimated from the solid side is usually described as the transient heat flux or maximum heat flux, q_{max}. The surface heat flux q_w, which cannot be measured directly, is estimated from internal energy by measured temperature inside the solid and employing certain techniques. Researchers have developed many methods to estimate the surface heat flux. Kumagai et al. [8] conducted an experimental work by cooling a hot thick metal plate by impinging a plane water jet to clarify the transition behavior of boiling heat transfer performance along the surface.

Mitsutake and Monde [9] studied experimentally the transition boiling heat transfer during cooling of a hot cylindrical block with an impinging water jet. They numerically estimated the surface heat flux by using a two-dimensional energy balance equation. They found that the maximum heat flux at a certain radial position seems to occur where nucleate boiling region occurs.

Transition boiling heat transfer by using a large pre-heated test specimen exposed to a water wall jet on its top surface was experimentally investigated by Filipovic et al. [10]. A two-dimensional transient condition was obtained numerically by using control-volume approach. They found that the reduction in the maximum heat flux with time corresponds to a decreasing slope of the longitudinal temperature distribution in the nucleate boiling regime.

Critical heat flux: One group of the researchers have studied the maximum heat flux on the surface from the liquid side which is defined as critical heat flux, CHF or steady critical heat flux. In steady state experiment, heat transfer rate is estimated from a thermal balance between the power input, usually electric, into an appropriate sample and the heat transferred to the liquid [11]. The pool boiling curve generally exhibits a maximum or critical heat flux, CHF, at the transition between nucleate and transition boiling as shown in Fig. 1.3.

Ueda et al. [12] have made a comparison between the critical heat flux and transient maximum heat flux, they found that the critical heat flux coincides with the maximum heat flux obtained by transient cooling of high thermal capacity copper test section. For cooling of a high temperature cylindrical block, Mitsutake and Monde [9] found that there is an agreement between the critical heat flux, CHF and maximum transient heat flux, q_{max} for copper block, while disagreement is noticed for brass. Ueda and Inoue [13] found that the maximum heat flux shows a somewhat higher value than the critical heat flux.

1.3 Literature Survey

Quenching and boiling are the important branches in thermal engineering. The history of boiling is more than 250 years old. A German medical doctor Johann Gottlob Leidenfrost first observed the boiling of water droplets on a red hot spoon in 1756. During this long period of time, many scientists and researchers performed a lot of investigations on quenching and boiling phenomena. Among the quenching processes, jet impingement is the most effect cooling system. In this section, a brief history of jet impingement quenching will be discussed.

1.3.1 Literature on quenching and wetting delay

Studies of jet impingement quenching for multiphase heat transfer have been performed by many researchers [14-17]. Heat flux, temperature, and the flow field by flow visualization were studied extensively in those investigations. Some studies [18-20] also performed on free surface jet impingement cooling, have given valuable background information on single phase convection heat transfer. Wetting delay is an important phenomenon in jet impingement quenching. Only a few publications however are available still now. In this dissertation, the initiative has been taken to investigate this relatively unexplored field.

Piggott et al. [21] experimentally investigated wetting delay during cooling of a hot rod using a subcooled water jet. During the quench, constant power was supplied to the rods corresponding to that initially necessary to maintain a steady temperature in air before the jet was applied. In the present study, the jet was impinged for cooling of a flat surface and no power was supplied during quenching. Owen and Pulling [1] presented a model for the transient film boiling of water jets impinging on a hot metal surface of stainless steel and nimonic alloy. In their study, wetting of the surface was assumed to occur when the temperature of the surface falls to the Leidenfrost temperature. Kumagai et al. [8] conducted an experimental investigation of cooling a hot thick copper plate by impinging a plane water jet to clarify the transient behavior of boiling heat transfer performance along the surface and the temperature profile inside the body as well as on the surface. Their experimental results indicated a time delay of approximately 100 seconds before the movement of the wetting front for a saturated jet with velocity 3.5 m/s and an initial solid temperature of 400 ^{o}C. Hammad et al. [22] reported resident times for subcooled jet impinging on block with different initial solid temperatures, 250 ^{o}C and 300 ^{o}C. While these studies have shed some qualitative light on the subject, there is an urgent need to clarify under what circumstances the wetting front will move forward and to develop practical correlations to estimate the resident time as a function of initial solid temperature, jet velocity, temperature of liquid, solid and liquid properties and solid geometry. This goal is by no means an easy task due to the complex nature of the problem.

After the jet impingement and before the wetting front movement many complicated processes and sub-processes have been observed [23, 24]. During this time, dramatic changes in the flow pattern depending on the superheat of the surface and possibly homogeneous nucleate boiling in the case of higher interface temperatures have been reported [23]. In this study, when the block temperature was higher than 300 ^{o}C, an almost explosive flow pattern was reported and a conical sheet of liquid in the case of slightly lower temperatures was observed. For the gradual cooling of a high temperature surface, both patterns were observed within the resident time, initially explosive and then the liquid sheet. In this case, the intensity level of the boiling sound was found to decrease and the rate of heat transfer increased when the flow field changed from the explosive pattern to the sheet pattern [24].

Just at the moment when the wetting front starts moving, the surface temperature and the other dominating parameters are favorable for the wetting front to move quickly

towards the circumference of the hot surface. However, exactly which parameters define a favorable wetting condition is presently uncertain. In contrast to the resident time, once the wetting front starts moving it does not take much time to completely cover the surface [16]. Hammad et al. [16] found that for any experimental condition they considered, the heat flux reaches its maximum value just after the wetting front starts moving rather than when the jet first strikes the block. Therefore in parallel with the resident time, the time required to reach the maximum heat flux condition is a strong function of the liquid subcooling and jet velocity. Thus the resident time is very important because this time also gives an indication of the time required to reach the maximum heat flux situation.

1.3.2 Literature on quenching heat flux and surface temperature

Studies of jet impingement quenching have been performed by a number of researchers [2, 14, 15, 17] who gave attention to heat flux, temperature, and the flow field by flow visualization. Some researchers [23-27] have also conducted the jet impingement quenching study together with different sub-process associated with jet impingement and they nicely reported their findings.

Knowledge of the maximum heat flux and its position is of great importance since the maximum heat flux usually corresponds to the maximum temperature gradient in the solid and therefore the largest thermal stress. In addition the maximum cooling rate is directly connected to the maximum heat flux. Thus to be able to predict and ultimately control the maximum heat flux during quenching is a key goal for boiling research.

In the present article we have decided to use the term ‘maximum heat flux’ rather than ‘critical heat flux’ (CHF) since there may be a difference between the critical heat flux appearing in steady-state experiments and the maximum heat flux arising in quench cooling experiments as discussed in the section 1.2.5. There is a wealth of literature relating to steady-state critical heat flux [5] but in contrast relatively fewer publications are available for insight into maximum heat flux during transient quenching [3, 6, 8, 10, 16, 19, 28, 29].

Barnea et al. [6] conducted experiments and performed a theoretical study of flow and heat transfer regimes during quenching of a heated vertical channel. They observed that the quench front was in the transition-boiling region, which stretched between into the dry and wet segments of the surface. Dua and Tien [3] performed an experimental study on rewetting of a copper tube by a falling film of liquid nitrogen. They observed that the maximum heat flux in rewetting occurred at the location of the wet front and its magnitude

was comparable to the average of the maximum and the minimum heat fluxes of nucleate and film pool boiling.

Filipovic et al. [10] performed transient boiling experiments using a large preheated test specimen exposed to a water wall jet on its top surface. They reported that during much of the quenching process, conditions on the test surface were characterized by propagation of a quench front in the direction of flow along the surface. Heat transfer occurred by nucleate boiling or single-phase convection upstream of the front, while film boiling existed in a precursory region downstream of the front. The front itself was at the leading edge of a transition-boiling zone, which was approximately coincident with location of maximum heat flux. They also found that the location of the maximum heat flux on the surface moved downstream with increasing time and its value decreased with time. Kumagai and Suzuki [8] also conducted a transient cooling experiment of a hot metal slab but with an impinging plane jet. They observed that local surface temperature fell rapidly when the temperature at that point reached the temperature corresponding to the high heat flux region of transition boiling.

Hall et al. [19] performed an experimental study of boiling heat transfer during quenching of a cylindrical copper disk by a subcooled, circular, free-surface water jet. Their study revealed that quenching measurements encompass three distinct boiling regimes; nucleate boiling in the impingement zone, the upper limit of nucleate boiling (maximum heat flux for the entire surface) and transition boiling which is characterized by minimum film boiling heat flux and the temperatures for the radial flow region. They correlated the radial distributions of maximum heat flux data with relations developed by others researchers from steady-state experiments for radial flow region.

Experimental measurements of the heat transfer and heat flux to a jet impinging on a heated test surface were obtained in the nucleate and film boiling regimes by Ruch and Holman [30]. Test variables were jet nozzle inside diameter, test surface orientation, and test surface temperature. A generalized correlation of the jet nucleate boiling heat flux was obtained. For Freon-113, dimensional correlations of the heat transfer and heat flux data in both nucleate and film boiling were also obtained in terms of the four test variables. Ragheb et al. [31] summarized the results of an extensive forced convection transition boiling study. Boiling curves were obtained for water at near atmospheric pressure using a high thermal inertia test section. The cooling process of a hot steel plate by a cylindrical water flow was studied experimentally and analytically by Hatta et al. [32]. Simultaneous measurements of wall temperature and vapor film thickness in an inverted annular film

boiling situation are reported by Edelman et al. [33]. The data correspond to bottom reflooding of a single tube uniformly heated with a steady electric heat source. The raw data are processed to yield the wall heat flux, heat transfer coefficient, quench front velocity, quench front temperature and void fraction, which may serve as a relatively complete comparative base for the development of theoretical models.

The characteristics of nucleate boiling with jet impingement were investigated by Ma et al. [34]. The considerations were the effects of velocity, subcooling, flow direction and surface condition on fully developed boiling and on the correspondence of the extrapolation of pool boiling with developed jet boiling. Nonn et al. [35] described an experimental study of free jet impingement cooling of simulated microelectronic heat source with dielectric liquid FC-72 (T_{sat} = 56 ^{o}C). Jet velocity was found to have the greatest influence on the thermal performance of the heat source. It can significantly increase the heat flux prior to boiling incipience as well as the magnitude of the critical heat flux (CHF). In general, the study demonstrated that the heat flux close to 10^6 W/m^2 could be dissipated at acceptable flow rates. An experimental investigation was carried out by Qiu and Liu [36] to measure the critical heat flux (CHF) of steady saturated and subcooled boiling for a round R-113 jet impingement on a flat stagnation zone.

Heat flux and surface temperature are important parameters for understanding the quenching phenomena. Some researchers [37] considered the measured temperatures close to the surface as a representative of surface temperature, while others, including the present study, used the measured temperatures and the unsteady heat conduction equation to estimate surface temperature and heat flux.

Hammad et al. [16] conducted experiments for investigating the heat transfer characteristics and wetting front during quenching of a high temperature cylindrical block by water jet at atmospheric pressure. Ochi et al. [29] also experimentally investigated transient heat transfer using circular water jet impingement. Their test piece was a flat plate. They observed that heat flux at the stagnation point (in the central region) was higher the values at further radial positions. In the stagnation region the heat flux increases with water subcooling and with jet velocity divided by the nozzle diameter. Their observation revealed that the velocity of the rewetting front increases with nozzle diameter, jet velocity and water subcooling.

In quenching experiments on large test pieces a phenomenon termed ‘wetting front’ [16], ‘quench front’ [6] or ‘wet-front’ [3] has been observed. It is a little difficult to unambiguously define what the ‘wetting front’ is. The wetting front phenomenon should

not be thought of as a single point or line but the entire transition boiling region should be understood to be a part of the wetting front. However, for convenience of discussion, in the present dissertation the wetting front is defined as follows. In all of our experiments, a black region at the outer zone of the moving liquid was observed on the basis of the video images. The wetting front is defined as the visible outer edge of this black region in the present study. Most of the time, an inner edge of this black region is also visible as shown in Fig. 4.2. A complete thermal and hydrodynamic criterion for this moving wetting front has not yet been clarified.

1.3.3 Literature on rewetting temperature and velocity

Experimental and analytical studies on rewetting/quenching phenomena in various modes have been carried out during the last four decades. From those studies, the fundamental understandings of the dominating characteristics of rewetting phenomena (rewetting temperature, rewetting velocity and maximum heat flux) are mentioned here briefly along with a historical review which can provide necessary information to have an image regarding the present status of this complicated quenching phenomena.

***Rewetting temperature*:** The temperature at the local wetting/quench front position is important for theoretical modeling of the rewetting problem. There has been confusion in the specialized literature concerning the exact definition of this parameter manifested in the variety of synonyms used to identify it, such as quench, sputtering, minimum film boiling, Leidenfrost temperature etc., which does not always represent the same physical phenomenon.

Gunnerson and Yackle [38] distinguished the quench front temperature and rewetting temperature. The quench temperature, termed here as apparent rewetting temperature, is defined as the intersection between the tangent line to the temperature-time curve (or the equivalent curve of temperature vs. axial distance) at the point where its slope is the largest, with the tangent to the curve before quenching as shown by T_q in Fig. 1.4. Apparent rewetting temperature marks the onset of a rapid surface cooling caused by an enhanced rate of heat transfer that does not necessitate liquid–solid contact. On the other hand, they defined a criterion of rewetting as direct liquid-solid contact and the establishment of a liquid-solid-vapor triple interface. Usually, the rewet temperature (Fig. 1.4) is considerably lower than the quench temperature, and, given sufficient resolution, may be detected by a slope change in the cladding temperature versus time trace under certain conditions. Such slope change, however, can likewise be caused by external

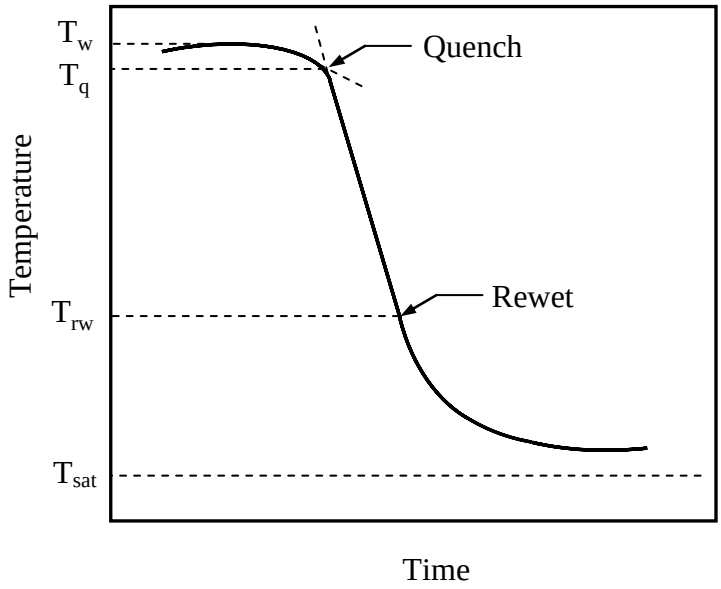

Fig. 1.4: Illustration of quench and rewet temperatures [38]

cladding thermocouple-coolant interactions. According to their investigation, rewetting required a contact angle or triple interface to be reestablished, and the liquid must recontact the solid substrate. If the liquid-solid interface temperature attained upon contact equals or exceeds a thermodynamic limiting superheat of the rewetting liquid, the liquid is repelled from the hot surface and rewetting cannot occur. Many, if not most, other studies also associate the conditions required for wetting to start or the wetting front to move with an apparent 'wetting temperature'. However the range of suggested temperatures required for wetting is vast and for water [2] ranges from solid superheats less than 100 ^{o}C to temperatures even beyond the critical temperature for the fluid. Exactly what decides this temperature or the balance point conditions for deciding the wetting front velocity is still an open question. Apparent rewetting temperature established by the intersection of tangent lines to the 'knee' of the measured temperature-time trajectories are correlated by Kim and Lee [39] as a function of the wall properties, wall initial temperature and the coolant inlet temperature and mass flux.

Chan and Banerjee [40] defined the rewetting as the re-establishment of continuous liquid contact with a hot dry surface. Carbajo [41] reported that rewetting or quenching of a hot surface occurred when the coolant re-established contact with the dry surface. Furthermore, this phenomenon took place when the temperature of the surface cooled down enough to allow a change in heat transfer region from film boiling to transition or nucleate boiling. Elias and Yadigaroglu [42] reported that the rewetting temperature or the Leidenfrost temperature is usually defined as the temperature at which a droplet eventually

wets a hot surface. Lee and Shen [43] found that the rewetting temperature seems to be independent of coolant vapor quality and coolant flow rate but affected by the initial wall temperature. Some researchers [44-46] defined the rewetting temperature as the starting of the sharp drop of the surface temperature. Lee et al. [47] described the rewetting temperature as the temperature coincides with the minimum heat flux. Elias and Yadigaroglu [48] also reviewed various published analytical and numerical rewetting models. They found that although a one-dimensional (axial) conduction model is reasonably adequate for predicting the temperature profile and the rewetting rate in saturated liquid and for low-flow-rate tests, a two-dimensional analysis is required for higher flow rates and subcooling. In practice, however, all models depend on two principal unknowns, that is, the heat transfer coefficient behind the quench front and the sputtering temperature, both of which are chosen to fit the experimental data. David et al. [49] formulated a nonisothermal microscale model of three-phase, solid-liquid-gas, contact zone in the context of rewetting phenomena. The model comprises scaled mass, momentum and energy balances, and their corresponding scaled boundary conditions. A new single-channel, transient boiling transition (BT) prediction method based on a film flow model has been developed for a core thermal-hydraulic code by Nagayoshi and Nishida [50]. This method could predict onset and location of dryout and rewetting under transient conditions mechanically based on the dry out criteria and with consideration of the spacer effect. The developed method was applied to analysis of steady-state and transient BT experiments using BWR fuel bundle mockups for verification.

***Rewetting velocity*:** Rewetting velocity is described as the rate of movement of the wetting front position over the heated surface or in short, the speed of the rewetting point. It gives an indication of how quickly the coolant contributes to effective heat removal from the hot surface. The prediction of the rewetting velocity has been the main goal of many investigators. However, there is confusion in the specialized literature about determining the location of the rewetting velocity on the heated surface. Locating the position of the wet front is very difficult either because of the very fast wet-front velocities or due to the large generation of vapor which prevents clear visibility of the wet front [3]. Dua and Tien [3] defined wetting velocity as wet-front velocity which was calculated by measuring the time taken for the wet front to pass between two marked locations on the tube surface. The time taken by the wet front to traverse this distance was measured directly by a stop watch and also by the chart recorder with the aid of an electronic marker which is pressed to

mark, on the Temperature-time plot, both of the times when the wet front passes through two specified locations on the tube.

Piggott and Duffey [51] presented the results of falling film rewetting experiments on two types of irradiated fuel pin and on a complementary range of tubes and heaters. The preliminary findings for bottom flooding were that there were smaller differences between various heaters than for falling film, and surface finish did not significantly change rewetting behavior. It was shown that subcooling local to the quench front was an important parameter in rewetting, and can be used as a basis for correlating data. Carbajo and Siegel [52] observed that the rewetting of light reactor fuel rods after a loss of coolant accident corresponds to the re-establishment of water contact with the hot surfaces. A considerable number of analytical and numerical models have been developed in order to solve the heat condition problem in the fuel pin and predict the rewetting velocity. A comparison among the existing models was performed. Oliveri et al. [53] proposed a new correlation for the prediction of the quench front velocity in the rewetting of hot dry surfaces by falling water films. This correlation is valid in the full range of the operating parameters where it proves very successful, providing a root mean square error of about 2.5 %, with respect to accurate numerical solutions of the mathematical problem involved. Peng et al. [54] clarified some of the governing phenomena and fundamental concepts involved in the wetting process, the physical models and wetting mechanisms for four different types of flow were theoretically, experimentally or qualitatively analyzed and a film flow regime map proposed. The investigation indicated that the wetting behavior and wetting mechanisms for different types of liquid flow were distinct and separate, and that the analytical treatments should be conducted individually for different circumstances. Ohtake and Koizumi [55] investigated the mechanism of vapor-film collapse by a propagative collapse for film boiling at high wall-superheat. They also reported effects of a local-cold spot on both the minimum-heat-flux temperature and the way in which the vapor film would collapse. Experimental results showed that propagation velocity of vapor-film collapse would decrease and minimum-heat-flux temperature would increase when the local-cold spot temperature was decreased. The results also showed that the minimum-heat-flux temperature increased remarkably when the local-cold spot temperature was lower than the thermodynamic limit of liquid superheat. It was proved through analytical and numerical models that local temperature at the collapse front of the vapor film, namely the local solid surface temperature at the position of liquid-solid contact, could never exceed the thermodynamic limit of superheat even if the vapor-film collapse

occurred at a high wall-superheat. Satapathy and Sahoo [56] characterized the cooling process by the formation of a wet patch on the hot surface, which has eventually been encountered by a steady moving quench front. As the quench front moves along the hot surface, two regions can be identified, a dry region ahead of the quench front and wet region behind the quench front.

The rewetting velocity was defined by Dhir et al. [57] as the quench front velocity which is obtained by taking slop of the curve representing location of quench front as a function of time. Saxena et al. [58] studied experimentally the rewetting behavior of a hot vertical annular channel with hot inner tube for bottom flooding and top flow rewetting condition. They calculated the rewetting velocity for bottom and top flooding rewetting. Peng et al. [59] investigated analytically the wetting front velocity of a thin liquid film flowing over a hot flat plate. For estimating the wetting front velocity they did not use the time counted from the beginning when the liquid first came into contact with the solid. Rather the time required for the liquid to cool the region immediately beyond the leading edge was subtracted from the actual measured time.

Sun et al. [60] observed that the rewetting velocity increased with increasing the product of the liquid subcooling and flow rate. Chen et al. [61] found that the rewetting velocity tended to decrease with increasing wall thickness. This trend was predicted on the basis of simple one-dimensional analysis.

Barnea et al. [6] conducted a theoretical and experimental analysis of quenching propagation for a heated vertical channel with subcooled water as the working fluid. They noted that as the quench front progressed along the flow channel; it removed heat from the hot surface by several heat transfer mechanisms such as axial conduction and radial convection and radiation to the coolant. They noticed two types of flow regimes downstream of the quench front. At high inlet velocities the dominant flow regime was an inverted annular flow where a liquid core flowed at the centre of the channel surrounded by a vapor annulus. At lower inlet flow rates an inverted slug flow regime typically prevailed. In both cases, the two-phase mixture downstream of the quench front acted as a precursory heat sink, which gradually decreased the surface temperature prior to quenching.

Filipovic et al [62] conducted transient boiling experiments with a preheated copper test specimen exposed to a rectangular water wall jet on its top surface. They defined quench front velocity as the velocity at which the front sweeps along the hot surface. Their investigation revealed that increased subcooling and flow velocity accelerated propagation

of the quench front. They attributed this to intensifying the rate of energy removal in the wet portion of the test specimen. They also found that larger initial test specimen temperatures resulted in smaller wetting front velocities. This can be understood in that increasing the amount of energy stored in the specimen increases the time needed to extract energy and, thus reduces the quench front velocity. Another important phenomenon disclosed from their investigation was that the quench front velocity increased as the front propagated along the test specimen. They explained this observation by noting that the specimen temperature in the precursory cooling zone ahead of the wetting region decreases with time resulting in an increased velocity of the front as it propagates along the surface.

Hammad [63] conducted experiments with the same experimental setup of the present study. The experiment was performed for the blocks with initial temperature from 250 to 300 ^{o}C and the average wetting front velocity was estimated on the basis of video images. The wetting front velocity for a particular experimental condition (radial position averaged) for short resident time was presented. Hammad [63] showed that the average wetting front velocity increased with jet subcooling and jet velocity and decreased with increase of block initial temperature. It was also apparent that for short resident time conditions, the wetting front velocity was the maximum for steel among three materials (copper, brass, steel) for the same experimental conditions.

With the movement of the wetting front, the position of maximum heat flux (MHF) also moves. Experimental studies on the movement of the MHF position are important for a clear understanding of quenching since the highest heat transfer rate and maximum temperature gradients occur in this region. For developing a theoretical model of jet quenching, the MHF point and wetting front propagation are prerequisites.

1.4 Difficulties of This Study

Due to the increasing demand for use of jet impingement quenching in practical applications, scientists and researchers have conducted a lot of experimental and analytical investigations on quenching. A clear understanding of this complicated phenomena has not yet been done. The following difficulties have been usually encountered during the study of quenching:

1. No complete analytical solution/model of quenching phenomena has been accomplished yet by any scientists or researchers.

2. Physical understandings of this complicated quenching phenomena has not yet cleared.

3. The quenching process involves many sub-processes which themselves are complicated. Therefore, understandings of those sub-processes are also necessary for complete understanding of the quenching process.

4. For complete modeling of quenching, the thermal and hydrodynamic states of the impinged liquid in the vicinity of the heated surface are essential. Still now no clear idea for measurement or estimation of the liquid state at the surface vicinity has been obtained.

5. Key features associated with quenching are indispensable to explain this complicated phenomena physically. At the moment, it is also a difficult job to identify the distinguishable characteristics in quenching. There may be some unfamiliar dominating characteristics; insufficient knowledge of which makes the image of quenching unclear until now.

1.5 Objectives

This is an experimental work; the primary aim of this study is to obtain a large range of data for making relations among the physical parameters of the experiment. A high speed video camera is used to analyze the hydrodynamic phenomena during quenching. A two-dimensional inverse solution technique for heat conduction is employed to obtain the surface thermal parameters from the temperature data measured beneath the surface. Sound intensity during quenching is also recorded. Together with all the above mentioned means, the following objectives are stated for the present work:

1. Estimation of the surface temperature and surface heat flux with the aid of the inverse solution and to compare the results for different experimental conditions.

2. Measurement/estimation of the resident time for each of the experimental conditions and to compare the results.

3. Developing correlations among the parameters associated with the resident time and temperature. In particular, different solid materials, different jet velocities, sub-coolings and initial solid temperatures have been included.

4. The position and magnitude of maximum heat flux are among the important criteria for understanding the quenching phenomena. One of the important aims of the present study is to investigate the parameters that control the position of maximum heat flux and to predict its magnitude as a function of experimental parameters. The parameters like initial block temperature, jet velocity, liquid subcooling and block material properties are considered predominantly in this study. Correlations for maximum heat flux are also proposed in this study.

5. One important objective of the present study is to investigate the rate of movement of maximum heat flux, MHF point in the radial direction and to search for the parameters that dominate this propagation velocity. The surface thermal and hydrodynamic parameters together with the block inside temperature distribution and its effect on the MHF propagation velocity are also analyzed in this study.

6. The boiling width and its dominating parameters in jet impingement quenching are investigated in the dissertation.

7. The quenching phenomena that happened just after the commencement of jet impingement is considered for clarifying the heat transfer mechanism.

1.6 Scope of This Dissertation

An experimental investigation for water jet impingement quenching of a high temperature solid surface has been covered within this dissertation. It includes seven chapters as follows:

Chapter one: It contains an introduction of jet impingement quenching which consists of application of jet impingement quenching, fundamental definition of different terms in quenching, history of quenching and the objectives of this study.

Chapter two: It deals with the experimental set-up and procedure. It also includes experimental ranges and uncertainty analysis.

Chapter three: This chapter consists of the results and discussions regarding the wetting delay phenomena. It represents the thermal, visual and audible data and their analysis.

Chapter four: Maximum heat flux characteristics together with its correlation are proposed in this chapter.

Chapter five: Wetting front propagation and the MHF propagation velocity are investigated in this chapter.

Chapter six: One possible effect of boiling width for estimating the heat flux and its influence on other parameters in quenching phenomena are deliberated in this chapter.

Chapter seven: In this final chapter the concluding remarks are delineated.

From Chapter three to six, the results and discussions of the present experimental investigation are described. A conceptual interpretation regarding the phenomena those happened immediately after the impingement of liquid jet on the hot solid surface is highlighted in Appendix A.

Chapter 2

Experiment

Various components of the experimental setup and test procedure for collecting the thermal, audible and visible data during quenching of the hot cylindrical blocks are discussed in this chapter. Detailed description of the major components of the experimental apparatus, experimental ranges and estimation uncertainty are also delineated in this chapter.

2.1 Experimental Procedure

The experimental set-up shown in Fig. 2.1 contains five major components, a heated block, a fluid flow system, a data acquisition system, a high-speed video camera and a sound measuring unit. At the beginning of the experiment, the water container (11) is filled with distilled water up to a certain level which can be seen through the level gauge (10). The pump (7) produces a water jet through the nozzle (12) of diameter 2 mm, which is located centrally 44 mm from the test surface (1). A shutter (13) is mounted in front of the nozzle to prevent water from striking the block (1) prematurely and to maintain a constant water temperature by forcing it to run within a closed loop system. The desired temperature of the water is obtained by controlling the main heater (9), auxiliary heater (6) or by adding cooling water to the cooler (8). The desired initial temperature of the block (1) is achieved by heating it with an electrical heater mounted around the block. A dynamic strain meter (16) is attached at two points of the flow line before the nozzle for measuring differential pressure from which jet velocity is calculated and this velocity is adjusted by a regulating valve. Nitrogen gas is fed around the heated surface by opening the cylinder valve (15) to create an inert atmosphere and consequently, prevent oxidization of the test surface. The whole experiment is conducted at one atmospheric pressure. When all the desired experimental conditions are fulfilled, then the shutter (12) is opened for the water jet to strike the center of the flat surface of the heated block. The high speed video camera (3) starts simultaneously at the signal of the shutter opening to record the flow pattern over the heated block surface and at the same time, the sixteen thermocouples measure the

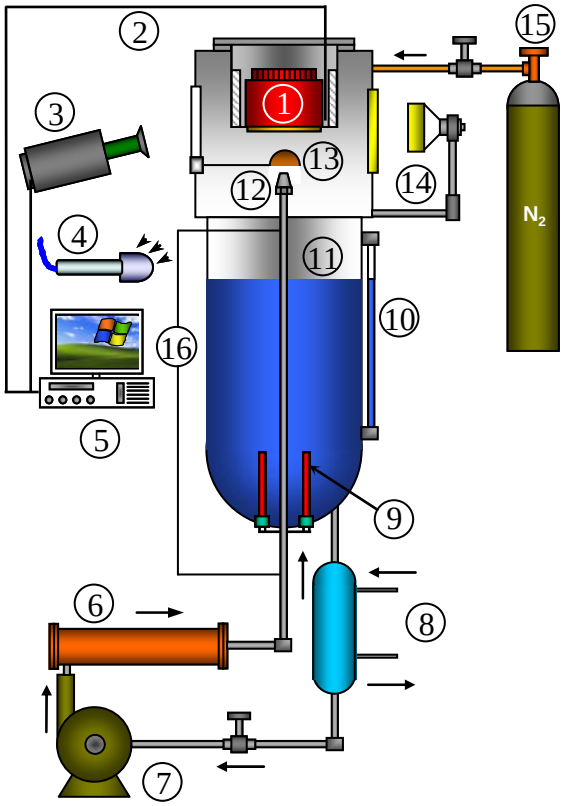

1. Tested block, 2.Thermocouple wire, 3. High-speed video camera, 4. Microphone, 5.Data acquisition system, 6. Auxiliary heater, 7 Pump, 8.Cooler, 9.Main heater, 10. Level gauge, 11.Liquid tank, 12.Nozzle, 13. Rotary shutter, 14. Spot light, 15. Nitrogen cylinder 16. dynamic strain meter (for measuring jet velocity)

Fig. 2.1: Schematic diagram of the experimental set-up

temperatures inside the heated block. Sound has been also recorded simultaneously with the microphone (4) for some conditions.

2.2 Heated Block

The heated block is of cylindrical shape with 94 mm diameter and 59 mm height as shown in Fig. 2.2. In order to make it easy to fix the thermocouples inside the heated block, a small section of the block was made removable but no cuts were made through the test surface itself. The effect of this removable section is limited to one corner of the block in an area more than r = 30 mm, where it is found from video observation that there is a departure from symmetry in the expanding of the wetting front. Sixteen thermocouples (CA-type, 1 mm sheath diameter and 0.1 mm wire diameter) are located at two different depths, 2.1 mm and 5 mm from the surface as described elsewhere [64]. At each depth,

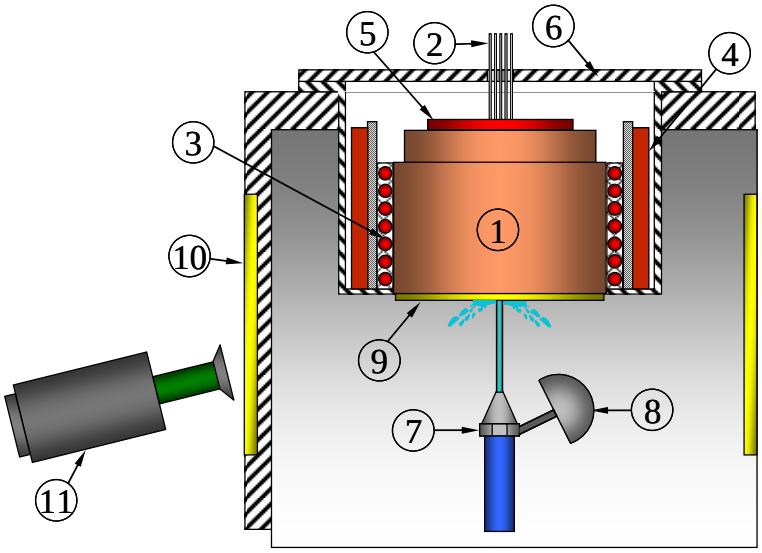

1. Tested block, 2.Thermocouple wires, 3. Sheath heater, 4. Band type heater, 5. Plate heater, 6. Block holder, 7 Nozzle, 8. Rotary shutter, 9.Test surface, 10. Glass window, 11. High speed video camera

Fig. 2.2: Schematic diagram of the test section and heating element

eight thermocouples are inserted along the r-axis. To protect the heated test surface from oxidation, it was plated with a thin layer of gold, 16 μm, which has an excellent oxidation resistance and also a good thermal conductivity; $\lambda \approx 317$ W/mK. The surface roughness is 0.2~ 0.4 μm. Figure 2.2 shows the assembly of the block, where it is mounted in a block holder and is heated by an electrical sheath heater with 0.94 kW capacity, that is coiled around the block circumference. To thermally insulate the block and to keep a uniform heat flux at the surfaces, two auxiliary heaters are used; one of them is of band type, 0.65 kW, and is placed around the block circumference, while the second is of plate type, 0.5 kW, and is placed on the upper part of the block as illustrated in Fig. 2.2.

With the continuation of the same experimental work, a portion of the experiment was conducted with new blocks (Fig. 2.3) having same dimensions as of the old blocks and the main change is that there is no cut for inserting the thermocouples. The thermocouple locations were rearranged a bit. The thermocouple spacing was about 5 mm for the old blocks and was 6 mm for the new blocks. With the new blocks the data seems reasonably accurate up to the radial position 40 mm. Almost no significant difference of the observed phenomena was noticed with the new blocks. The conducted experimental range for the initial block temperature T_b was 250-400 ^oC for the old block.

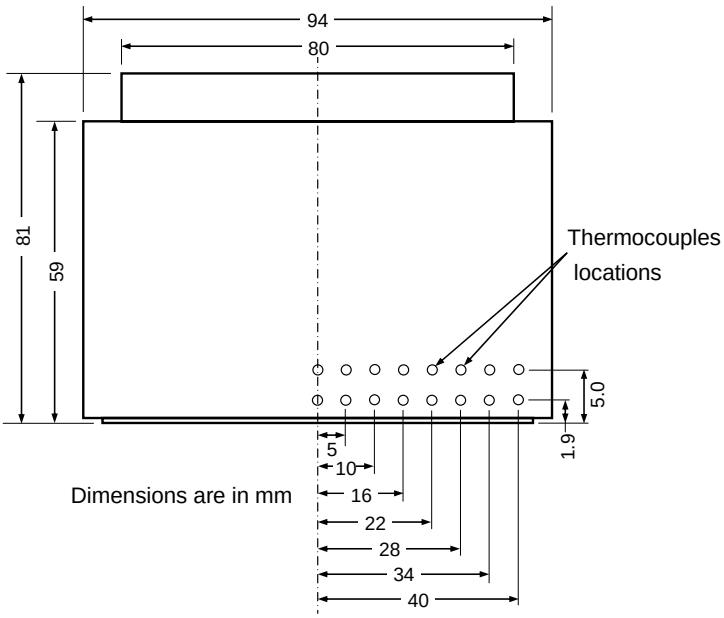

Brass and Steel

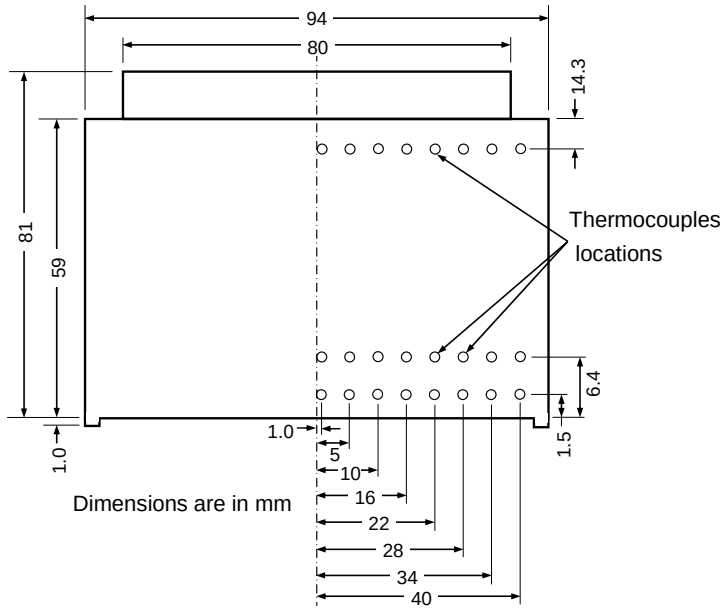

Copper

Fig. 2.3: Dimensions of the cylindrical blocks with thermocouple locations

2.3 Data Acquisition System

The thermocouples are scanned sequentially at 0.05 second intervals, with 8.0 ms needed to read all of the thermocouples using 16-bit resolution with an analog-digital converter. The duration of the total data acquisition period was adjusted to suit the experimental conditions so that in all cases the experiment continued until the quench was

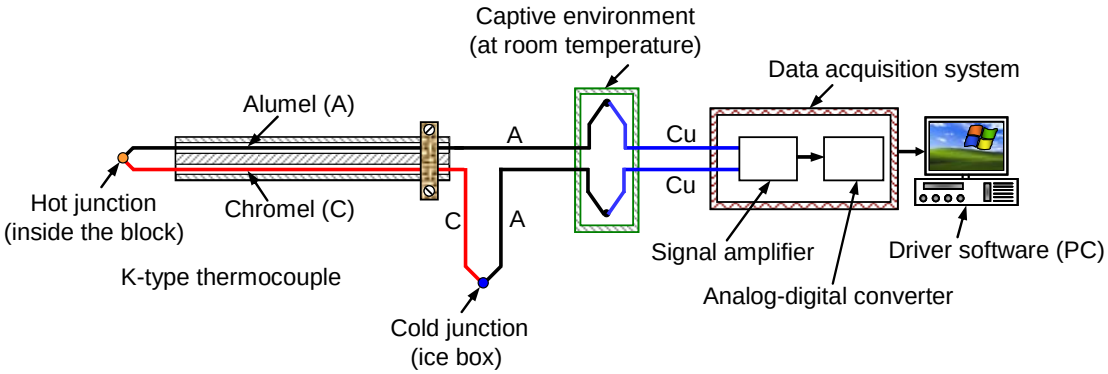

Circuit diagram for thermocouple connection

Photograph of data acquisition system

Fig. 2.4: Schematic view of temperature measuring system

Fig. 2.5: Photograph of high speed video camera

completed. The uncertainty in the temperature measurements is ±0.46 °C, while the uncertainty in the placement of the thermocouples is estimated to be ±0.1 mm. The time lag for the response of the thermocouples is estimated to be less than 0.1 sec.

2.4 Visual Observation

Fluid movement over the heated surface during the quenching was captured by a high-speed video camera. The captured picture was with a maximum resolution of 1,280×1,024

pixels and a maximum rate of 10,000 frame/s. From individual frames of the video images, the wetting front movement and the splattering of liquid droplets were analyzed.

2.5 Audible Observation

For some cases, a microphone was simultaneously employed during quenching to record the sound. The recorded sound signal (electrical voltage) was then normalized against the peak voltage during the recording giving a representation of noise level before and after the wetting front propagation.

2.6 Experimental Ranges

The experiment has been conducted for eight initial block temperatures, four jet subcoolings, four jet velocities and three different block materials as shown in the Table 2.1. The jet diameter was 2 and 3 mm. The analysis with the 3 mm jet has not been covered within this dissertation. Unless otherwise stated, the jet diameter is to be considered as 2 mm in the present study.

2.7 Uncertainty of Measurement

The uncertainty values for different primary/measured quantities are shown in Table 2.2. The estimation procedure for uncertainty associated with the present experimental work has been discussed in Appendix C.

Table 2.1 Experimental ranges for parameters

Block Material	Steel [St] (0.45% Carbon), Brass [Br] (70% Cu, 30% Zn), Copper [Cu] (commercially pure)
Initial temperature, T_b [^oC]	250, 300, 350, 400, 450, 500, 550, 600
Jet velocity, u [m/s]	15, 10, 5, 3
Jet subcooling, ΔT_{sub} [K]	80, 50, 20, 5
Pressure	1 atmosphere
Coolant	Distilled water
Nozzle diameter, d (mm)	2

Appendix C can be referred for the thermo-physical properties of the test section materials.

Table 2.2 Uncertainty of the primary measured quantities

Variables	Uncertainty
Block initial temperature, T_b[^oC]	± 0.46 ^oC at T_b = 250 ^oC
Jet velocity, u [m/s]	± 5.22 % at T_{liq} = 20 ^oC
Jet sub-cooling, ΔT_{sub} [K]	± 0.2 ^oC at T_{liq} = 50 ^oC
Thermocouple position [mm]	± 0.1 mm

2.8 Analysis of Experimental Data

The thermocouples' reading was obtained beneath the test surface. This was done because it is impossible to get the thermal history directly just from the surface at which the jet is impinged without greatly disturbing the flow and boiling phenomena. The thermal history beneath the test surface was used for estimating the surface history by using a two-dimensional inverse solution for unsteady heat conduction. The procedures for obtaining this thermal history at the surface along with the audible and visual data are discussed in this section.

2.8.1 Temperature data

Temperatures were measured beneath the hot surface inside the block on which the jet was impinged. These temperatures were then used to estimate the surface temperature and surface heat flux because it was impossible to measure the surface temperature directly during quenching with the present apparatus. A two-dimensional inverse solution for heat conduction adopted from Monde et al. [65] and Hammad et al. [66] was applied for estimating the surface parameters based on the measured temperature. Temperature was measured at eight different locations for each particular depth inside block. To improve the space resolution of the calculation procedure [67] additional points were interpolated between the measured points taking into account time and space trends in the data, so that the number of reference points was increased from 8 to 29. Some improvements to implementation of the inverse calculation procedure suggested by Woodfield et al. [67] were incorporated also. The procedure for estimation of surface temperature and surface heat flux from inverse solution has been described in Appendix A. It is worth mentioning here that the values of material thermal properties such as density, specific heat and conductivity used in the inverse solution have been taken at 250 ^oC. The experimental

range for initial block temperature used in the present study is 250-600 ^{o}C as given in Table 2.1. No significant changes due to material properties are expected within this temperature range.

In the present work the closest thermocouple to the centerline of the test piece was at a radial position of 4 mm (for the old blocks). Thus only results for a radial position greater than about 5 mm are reported in most of the analysis of the present study.

Temperature distributions within the whole solid for axial positions greater than 2 mm from the surface given in chapters 5 and 6 were calculated using the thermocouple readings from the 2 mm depth and an analytical solution to the direct heat conduction problem derived using the techniques in Carslaw [68]. The assumption was made that heat loss through the side and top of the test piece could be ignored in comparison to the large heat flux due to the impinging jet when calculating the temperature distribution within the solid. For positions closer than 2 mm from the surface the inverse problem was solved in a manner similar to Appendix B. The inverse solution for the surface temperature distribution was based on two depths of thermocouples and therefore did not require any assumptions about the boundary condition at the top of the test piece.

2.8.2 Visual observation data

During the quenching process, the thermal and hydrodynamic phenomena changed with a fraction of a second and it was very difficult to capture for a particular moment. A high-speed video camera was used to capture the video image for certain duration of time. The recorded video images were then played frame by frame so that a change within 0.0001s (as the speed is 10,000 frame/s) could be obtained. Some video images obtained in this way together the other simultaneous phenomena are discussed in this study.

2.8.3 Acoustic data

A change of sound intensity, when the hot surface started cooling down at a very faster rate was notified. To ascertain a relation among the thermal, hydrodynamic and this acoustic phenomenon, the noise level was measured by using a micro phone simultaneously with thermocouple readings and high-speed video camera. The noise intensity was then plotted against time to have an image of its decaying or increasing trend with time. The change of sound intensity level together with the other dominating phenomena is highlighted in this dissertation.

2.9 Particulars of Equipments

The specifications of the equipments used during the experiment are listed in Table 2.3.

Table 2.3 Particulars of the equipments used

Equipments	Specification	Manufacturer
High Speed Video-Camera	Type: V-153 Maximum resolution: 1,280x1,024 pixels Maximum speed: 10,000 frame/s	NAC, Japan
Dynamic Strain Meter	Model: YA-503A	KYOWA Electronic Instrument Ltd., Japan
Differential Pressure Gauge	Model: PDU-2KA Capacity: 2 kg_f / cm^2 Liner pressure: 300 kg_f /cm^2	KYOWA Electronic Instruments Co. Ltd., Japan
AD converter	Model: AD12-16TA (98)H	Contec, Japan
Digital Multi-meter	Model: TR6855	TAKEDA RIKEN, Japan
D. C. Amplifier	Model: AH 1108	NEC Remote control AMP Japan
Digital multi-thermometer	Model: TR2114H/TR21143	Advantest Corporation, Japan
Personal Computer	Optiplex G120	Dell
Chromel-Alumel (CA-type) sheathed thermocouple	Sheath diameter: 1.0 mm Wire diameter: 0.1 mm	Sukekawa Electronic Inc., Japan
Pump	Model: H106-JSBCO-2P Total head: 40m Capacity: 5 *l*/min	Nikuni Machinery Industrial corporation Limited, Japan
Micrometer	No. 51082	PIKA SEIKO LTD., Japan
Microphone	Model: MLI FD-01 Directivity: Omni-direction Frequency range:50Hz~13kHz Max. input sound pressure: 120 dB	MIDI Land, Inc.

Chapter 3

Wetting Delay and Jet Quenching

Jet impingement Quenching is one of the most effective cooling systems. The objective of this quenching is to get a faster cooling effect from a high temperature solid surface. From the present experimental study, it was not always possible to get a drastic cooling effect immediately after the commencement of the jet on the heated surface. A varying delay period is observed during quenching. In this chapter, the observed phenomena regarding the wetting delay period during the quenching of the present experiment are discussed.

3.1 Wetting Delay Period

It is important to clarify the meaning of the key parameters for the present investigation before discussing the phenomena in detail. The wetting delay period in the present study is defined as the time from when the jet first strikes the hot surface until the wetting front starts moving as also described in the section 1.2.3. It can be thought of as the time during which the wetting front or region of interaction between the jet and hot solid is residing at or near the center. For this reason, the wetting delay period is expressed by the term 'resident time' in the present study. The expression 'resident time' in connection with jet quenching first appeared in the work of Hammad [22] and is synonymous to 'wetting delay time' used by Piggott et al. [21]. The resident time should not be thought of as purely a film boiling time since the present observation clearly indicates that surface wetting in the central region can occur a considerable time before movement of the wetting front.

3.2 Visual and Audible Observations during Quenching

For conditions where the material was copper or brass, the initial temperature was high, the jet velocity was low and the subcooling was low, when the jet first struck the center of the hot surface, liquid did not cover the entire heated area immediately. Rather as is shown in Fig. 3.1(a) the liquid quickly spreads over a small central region about two to four times the jet diameter and then was splashed out or deflected away from the surface. The size of this region of liquid/solid interaction remained relatively fixed for a considerable period of

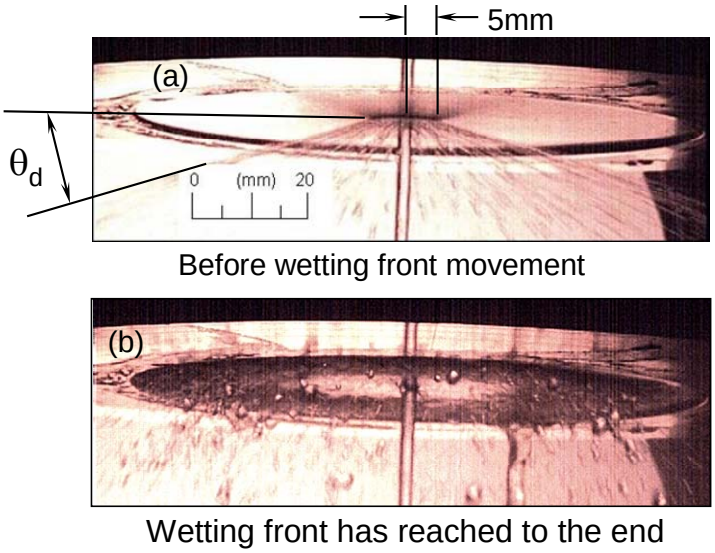

Fig. 3.1: Video images during quenching [Cu, T_b = 400 ^oC, ΔT_{sub} = 20 K, u = 3 m/s] (a) t (= 554 sec) < t* (= 555 sec), (b) t (= 576 sec) > t* (= 555 sec)

time. Finally the wetting front began to move across the surface and the departing angle, θ_d increased with radial position.

Figure 3.1(a) shows just one of the flow patterns observed before movement of the wetting front. As has been reported elsewhere [24], depending on the conditions, the observed flow pattern can pass through a sequence of stages. If the initial temperature was higher than about 300 °C for a copper block, when the jet first struck the surface an explosive flow pattern where the jet broke into thousands of tiny droplets was observed. As the solid cooled, the flow field became less chaotic and in some cases, liquid droplets could be seen departing in rings from the surface with a frequency of approximately 1000 rings per second. Following this, the angle between the departing droplets and the surface increased and a small conical sheet of liquid appeared. For some conditions, the sheet was clearly visible, but in other cases such as is shown in Fig. 3.1(a), the sheet broke into droplets very close to the surface.

Accompanying the changes in flow pattern, there were a number of changes in the boiling sound before and after the wetting front movement. Figure 3.2 illustrates the recorded sound for a set of conditions where the changes in phenomena were particularly clear. The resident time in this case was about 200 s. During the first 120 s, the explosive flow pattern mentioned above could be observed and the boiling sound was quite loud. Following this, the sharp splattering sound died down and the experiment became very quiet as the flow pattern changed to the conical liquid sheet. The sheet then disappeared

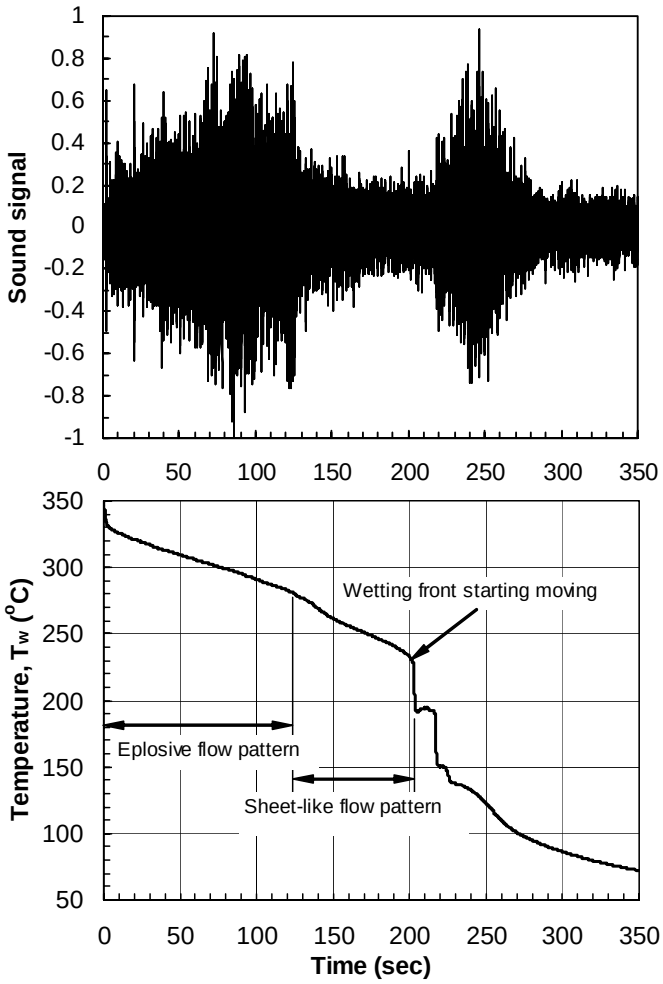

Fig. 3.2: Sound intensity at 30 cm from the test surface during wetting front propagation [T_w at r = 5 mm, Cu, T_b = 350 ^oC, ΔT_{sub} = 50 K, u = 3 m/s]

and the wetting front started to move forward. A short time after movement commenced the sound level increased and the sharp boiling sound could be heard again. The loudest sound approximately corresponded to the time of the maximum heat flux for the experiment. Finally the sound diminished as boiling ceased and the mode of heat transfer changed to single-phase convection.

The history of the boiling sound shown in Fig. 3.2 and the video images have some important implications for the nature of the phase change phenomena before and after the resident time. The sharp splattering sound is most likely the result of some form of nucleate boiling. Now to obtain the liquid superheat and nucleation sites required for nucleate boiling liquid/solid contact is necessary. Thus Fig. 3.2 indicates that liquid/solid contact occurs long before the movement of the wetting front in what may be described as a kind of transition boiling phenomena [24]. During the first 120 seconds in Fig. 3.2, cycles of brief liquid/solid contact followed by separation probably occur at a very high frequency. During the next 80 seconds, the surface temperature is lower, the phase-change

is less explosive and solid/liquid contact continues. Visual observations suggested that surface wetting might have been almost continuous in the central region during this time from about 120 seconds to 200 seconds but for some reason the wetting front did not move forward.

Towards establishing criteria for defining the time when the wetting front moves forward, in relation to the above observations we can conclude that the resident time does not correspond to the time when the liquid first directly contacts the solid. Nor does it appear to correspond to the time when continuous wetting is first established beneath the jet. Rather the completion of the resident time, t*, ultimately must relate to overcoming a thermal, hydrodynamic, heat flux or some other balance at the wetting front itself.

Another interesting observation is that in spite of the different flow phenomena during the resident time, the size of the region of interaction between the liquid jet and solid was noted to remain relatively fixed before movement of the wetting front. For the copper block, the radius of this region, r*, was found to be 5±1 mm for a range of conditions and for brass, r* = 8±3 mm. For example, in the case shown in Fig. 3.1, from the time just after the jet struck the surface until one second before the wetting front moved as shown in Fig. 3.1(a), the apparent wetting front remained at a constant radial position (r* = 5 mm).

Finally, the video images show that the resident time can be much larger than the time for the wetting front to move across the surface. For the case in Fig. 3.1 the resident time was 555 seconds in contrast to the 22 seconds required for the wetting front to reach the circumference of the cylinder. A similar trend has been observed for all experimental conditions with a moderately higher value for the resident time and for those cases the resident time was higher than the propagation period by a few times to 100 times.

3.3 Surface Temperature and Heat Flux Distribution

Typical surface temperature and heat flux distributions with position and time (estimated from Monde et al. [65] and Hammad et al. [66]) are shown in Fig. 3.3. It is clear from Fig. 3.3 that the cooling curve can be roughly divided into four regions. These are an initial transient (0 to 5 s), steady cooling (5 to 86 s), wetting front movement across the surface (86 to 106 s) and finally, single-phase convection. During the first few seconds of the case in Fig. 3.3 the temperature near the center quickly fell by about 40 °C. This is most likely a transient effect due to the step change in heat flux that occurs when the jet first strikes the center of the test surface. From 5 s up to the estimated resident time (86 s) the surface

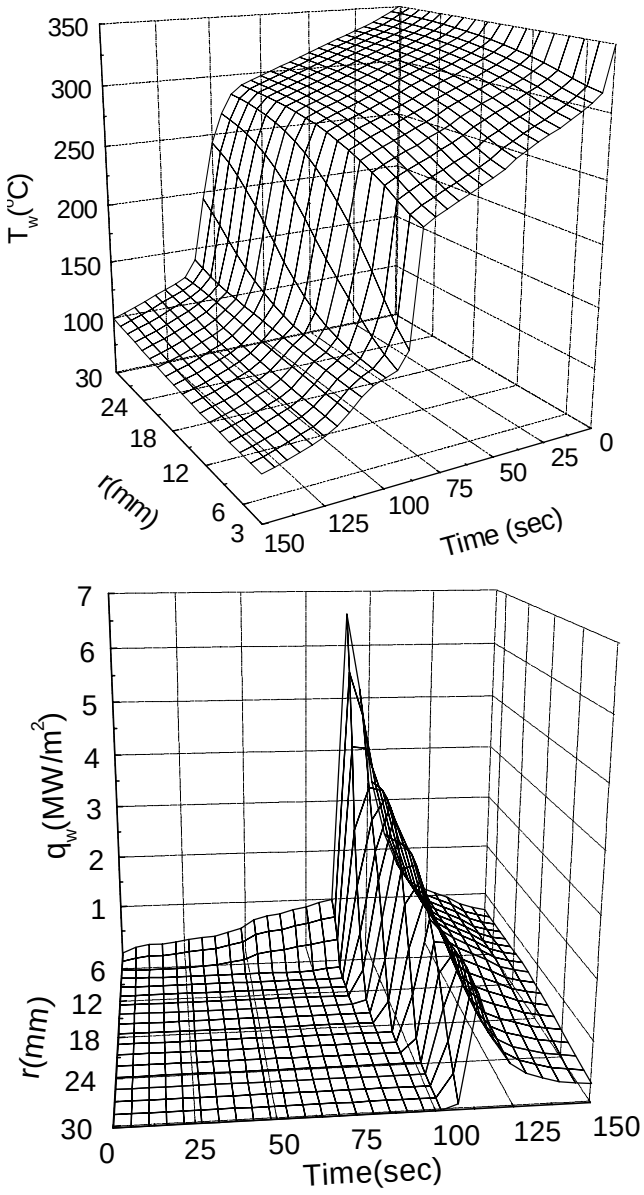

Fig. 3.3: Estimated surface temperature and heat flux from measured temperatures

temperature dropped at a slow and almost uniform rate with time. Then as the wetting front started moving several major changes took place. The heat flux suddenly increased, the surface temperatures began to fall rapidly and radial temperature gradient became much steeper. During the 20 seconds that it took for the wetting front to reach the circumference, the entire surface temperature distribution dropped by around 100 °C. Finally both the heat flux and cooling rate diminished as single-phase convection became dominant.

In examining the cooling curves and heat flux distributions there are two key points that are expected to elucidate. The first is what conditions are established at the instant the wetting front starts movement. The second is what factors may influence how long it takes

for these conditions to be established. If these two issues can be resolved, much progress can be made towards developing a theoretical model for predicting the resident time.

For the case shown in Fig. 3.3 it is clear that before movement of the wetting front the temperature near the center is steadily decreasing and the heat flux is steadily increasing. At the instant when the wetting front started moving forward the temperature at the edge of the wetted region (r = 5 mm) was 242 °C and the heat flux at this position was about 1 MW/m^2. Rather than constants for every experiment, both of these values are found to be strong functions of the experimental conditions as will be discussed in section 3.6.

A further interesting result that has emerged from consideration of the cooling curves is that the maximum heat flux point always occurred just after movement of the wetting front. In Fig. 3.3, within two or three seconds from when the wetting front started moving, the heat flux increased by a factor of about seven to reach its peak value and the temperature just upstream of the wetting front fell to about 140 °C. For all the experimental conditions, the heat flux increased by a factor in the range from 5 to 60. The temperature at the maximum heat flux point was found to always lie in the range from about 120 °C to 220 °C for all the combinations of conditions given in Table 2.1. However, since the maximum heat flux always occurred after wetting front movement, it may be considered an effect of wetting rather than the direct cause of wetting front movement.

While it appears that a simple set of criteria for wetting front movement is not immediately obvious from the results of different experimental conditions it is worth noting that higher initial solid temperatures usually resulted in longer resident times. This is strong evidence that factors affecting the overall rate of cooling of the solid at higher temperatures have an important influence on the resident time. During the first 86 s in Fig. 3.3 the almost steady cooling rate observed will be a function of heat flux to the jet in the central region, the size of the wetted region and losses to the environment surrounding the dry region by single phase convection and radiation. We may expect that the total heat capacity of the block also will be important since for a given total heat flux, the bulk temperature of a larger block will drop more slowly.

3.4 Regimes for Wetting Delay

An examination of the cooling curves for all of the data indicated that each set of conditions in Table 2.1 could be classified into one of three regimes for the resident time. It has been elected to describe the categories as (a) quick cooling, (b) moderate cooling and

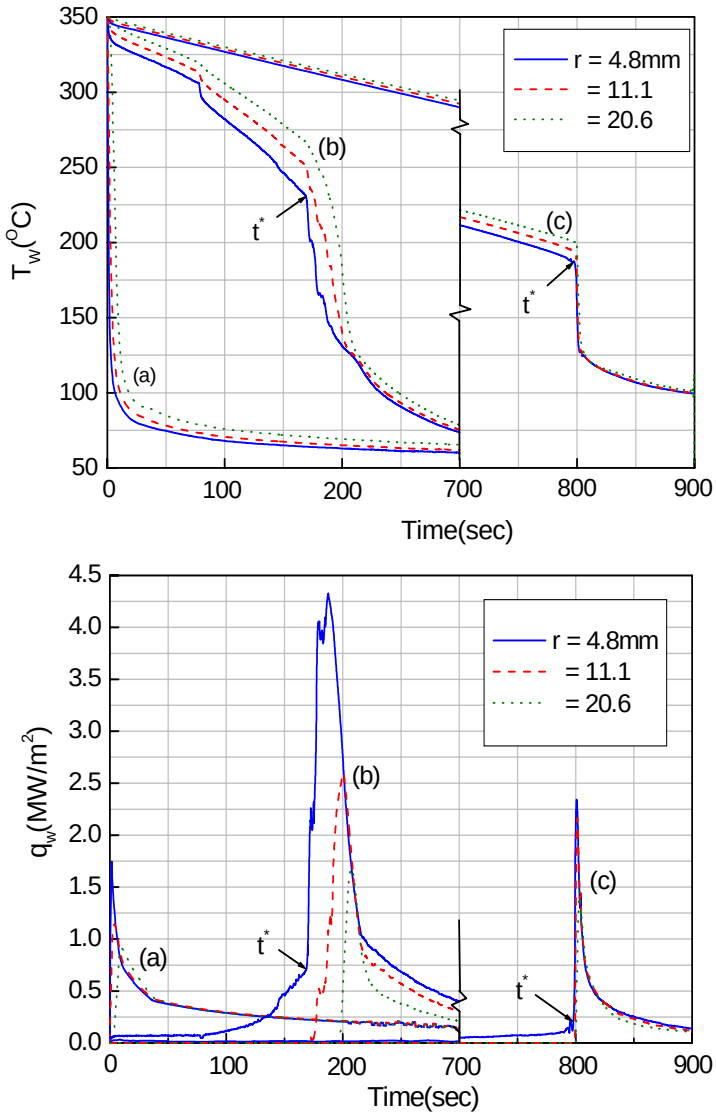

Fig. 3.4: Regimes of resident time [cooling curve and heat flux during quenching]

(a) St, T_b = 350 °C, ΔT_{sub} = 50 K, u = 3 m/s

(b) Cu, T_b = 350 °C, ΔT_{sub} = 50 K, u = 3 m/s

(c) Cu, T_b = 350 °C, ΔT_{sub} = 5 K, u = 3 m/s

(c) slow cooling. Figure 3.4 gives typical examples of the three categories. The case (a) in Fig. 3.4 shows a cooling curve for carbon steel. In this case it took only a fraction of a second for the wetting front to start movement and the surface temperature cooled very rapidly immediately after the jet struck the surface. The case (b) in Fig. 3.4 shows a moderate cooling case that occurred for a copper block with a jet subcooling of 50 K. In this case the resident time is 170 s and the curves have a slight irregularity at around 80 s, which corresponds to a change in sound and flow pattern described in section 3.2 (cf. Fig. 3.2). A slow cooling case (c) is also shown in Fig. 3.2 where the material is copper and the

jet subcooling is 5 K. Here the resident time is 800 s and the cooling rate is almost constant during this time.

In this study, all the measured resident times for steel were a fraction of a second while a large proportion of the results for copper could be classified as either moderate or slow cooling. For the quick cooling situation, the surface temperature drops from its initial temperature to close to the corresponding liquid temperature very soon after the jet impingement. During this time, the wetting front begins to move slowly across the surface and the heat flux reaches its maximum value. The different behavior among the three materials is most likely the result of the ability of the material to supply heat to the region of the surface where the liquid contacts the surface. For copper the thermal conductivity is high so that heat can be supplied easily to balance the heat flux demanded by the jet and maintain a high surface temperature. In contrast, the heat conductivity of carbon steel is about one tenth that of copper so the surface cools quickly if the heat flux is high.

Another important feature that is different among the three regimes is the spatial temperature gradient at the resident time and during propagation of the wetting front. For shorter resident time regime (a), the radial temperature gradient is quite large at and after the resident time. In contrast, for regime (c) the solid surface temperature is much more uniform. A comparison of the cooling curves at t* for different radial positions in Fig. 3.4 shows this. In the case (c) at t* the difference in temperature between the radial position r = 4.8 mm and r = 20.6 mm is only about 20 °C. For the case (a) the temperature difference between these two points during movement of the wetting front, for example at about 10 seconds, is over 100 °C. Therefore, for larger resident times, the temperature gradient in the radial direction is small and the radial propagation of the wetting front (wetting front velocity) is faster. Inversely, it is observed that a higher temperature gradient in the radial direction corresponds to slower wetting front velocity for quick cooling conditions.

Finally it is worth mentioning that the period of time between when the wetting front starts moving until the maximum heat flux condition is generally greater in the moderate cooling regime (b) than the slow cooling regimes. The curve for the heat flux in the case (b) shows that the heat flux peak occurs 18 s after the wetting front starts moving where for case (c) this delay is about 5 seconds.

3.5 Effect of $u\Delta T_{sub}$

A further distinction between the fast and slower cooling regimes and some interesting trends for the resident time becomes clear if this time is plotted against the parameter,

$u\Delta T_{sub}$. Figure 3.5 shows three different trends that consistently appear for each of the four initial temperatures considered for a copper block. In the case of longer resident times, the resident time, t* is a strong function of $u\Delta T_{sub}$ as shown by the solid lines in Fig. 3.5. For a resident time between 1 and 30 seconds (tentatively defined) the trend becomes almost vertical as shown by the dashed lines. This indicates an abrupt change in the resident time within the vicinity of some critical value of $u\Delta T_{sub}$. For very small resident times less than one second the trend changes again as is shown by the dotted lines.

For the different initial temperatures shown in Fig. 3.5, the general trend is that for higher initial temperatures the curve shifts to the right. Also all curves show a decrease in t* with an increase in the velocity-subcooling factor. This shows that the resident time increases with an increase in initial temperature. A possible explanation for these features is as follows. Note that both u and ΔT_{sub} are parameters from the liquid side only and that for a given geometry and material, the initial temperature of the solid is an indicator of the quantity of heat initially stored in the solid. Also it is generally found in jet boiling experiments that increasing the jet velocity or increasing the subcooling both lead to higher

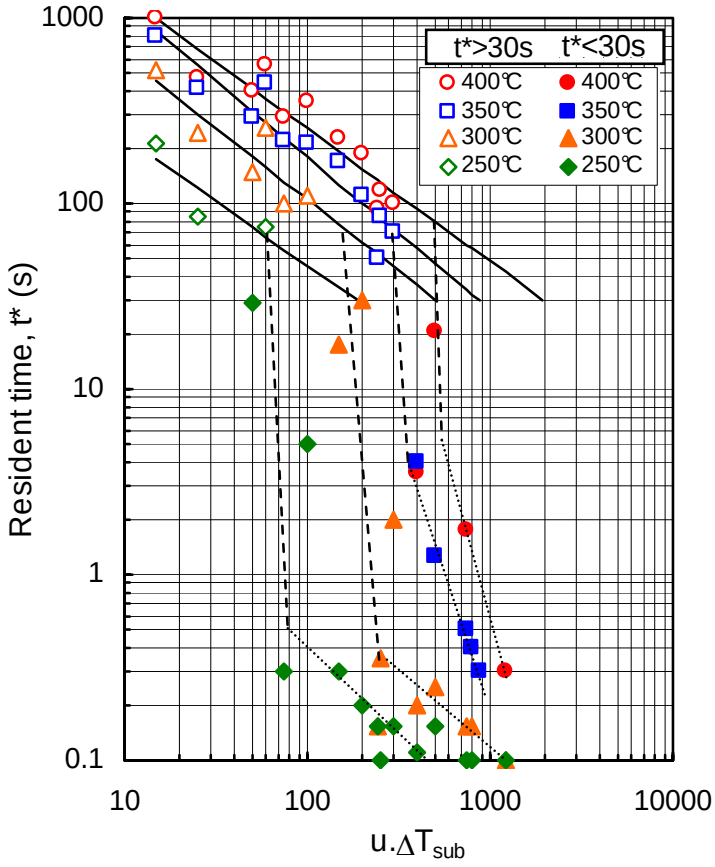

Fig. 3.5: Variation of resident time for copper with different initial temperature as a function $u\Delta T_{sub}$

heat fluxes. Thus the parameter, $u\Delta T_{sub}$, is perhaps one indicator of the ability of the liquid side to extract heat. In other words, a higher value of $u\Delta T_{sub}$ implies a higher heat flux, which makes the solid cool faster leading to shorter resident times. A higher initial temperature roughly means that more heat must be removed before the conditions where the wetting front moves forward are reached. It should be noted however, that this hypothesis does not account for the effect of $u\Delta T_{sub}$ on the temperature at which the wetting front moves forward. This will be discussed in section 3.6.

Another interesting feature in Fig.3.5 is that the critical value of $u\Delta T_{sub}$ also increases with an increase in initial temperature. This critical value forms the boundary between the moderate and fast cooling regimes described in section 3.4. The reason for the sudden change between the regimes is presently unclear. However, it may be that the fast cooling regime is the result of quickly reaching the conditions for wetting front movement during the initial localized transient cooling just after the jet contacts with the surface. This initial transient cooling can be seen in Fig. 3.3 during the first 5 s near the center of the surface. If, as in Fig. 5, the conditions favorable for wetting front propagation are not reached during this initial period of rapid cooling then the whole solid must cool down before wetting front movement. This results in a much longer resident time.

The result shown in Fig. 3.5 is for copper only. Similar trends were observed for brass also except that curves were generally to the left of those for copper. For steel, the resident time was less than one second for T_b = 250-400 ^oC. For T_b = 450-600 ^oC, steel shows a similar trend of copper as shown in Fig. 3.5.

3.6 Correlation for Surface Temperature at Resident Time

Of great importance to the present study are the precise conditions that occur when the wetting front begins to move. From an understanding of the classical boiling curve one would suspect that among all the conditions, the surface superheat at the wetting front is likely to be a key factor. Figure 3.6 shows the surface temperature at the resident time at the wetting front (r = 5 mm) for a certain range of experimental conditions for copper. Far from being a single constant value however, the temperature, T_w*, ranges from 170 °C to 385 °C. There is a clear trend in relation to the parameter $u\Delta T_{sub}$ and to the initial temperature of the solid.

In Fig. 3.6, solid symbols are used for data with t*< 30 s. For these shorter resident times the temperature of the wetting front at t* is almost independent of $u\Delta T_{sub}$ and is a

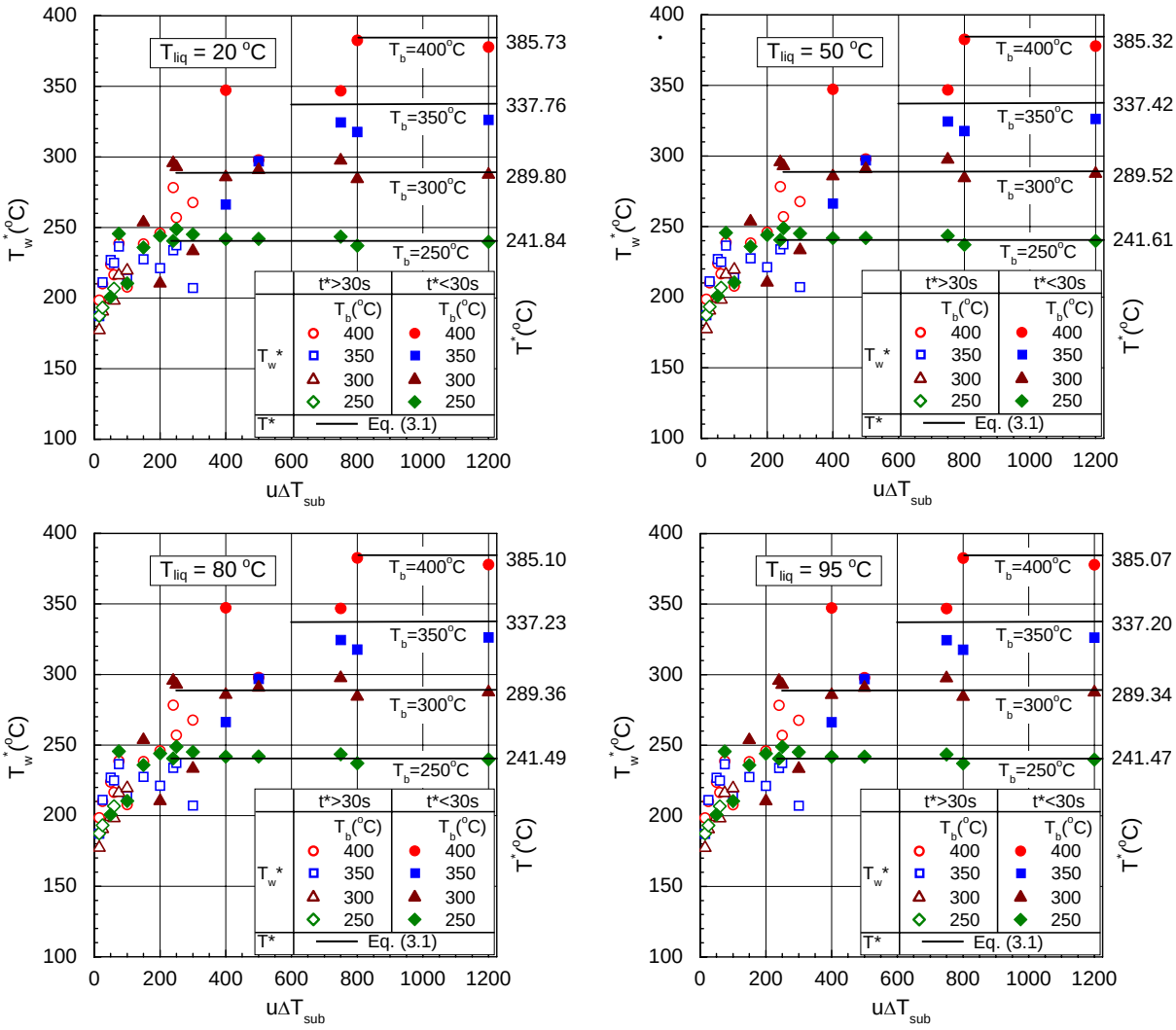

Fig. 3.6: Variation of surface temperature (at resident time at wetting front) and interface temperature for copper with different initial temperatures

strong function of the initial temperature of the solid. In fact for large values of $u\Delta T_{sub}$ all curves appear to asymptote to values of T_w^* a little below the initial temperature. It is interesting to compare these data with the interface temperature, T*, estimated from the sudden contact to two semi-infinite bodies. Equation (3.1) gives the analytical solution for T* [68]. Making use of Eq. (3.1), the solid lines are drawn in Fig. 3.6 for the interface

$$T^* = \frac{T_b - T_{liq}}{1 + \sqrt{(\rho c \lambda)_l / (\rho c \lambda)_s}} + T_{liq} \qquad (3.1)$$

temperature based on the four different initial temperatures. The measured temperatures for large values of $u\Delta T_{sub}$ agree quite well with T*. Thus Eq. (3.1) may be appropriate for estimating the wetting front temperature at the resident time in the cases where the resident time is very short.

The hollow symbols in Fig. 3.6 represent experimental data for t*>30 s. These data are classified as from the moderate or slow cooling regimes in section 3.4. In the case shown for copper here, this set of data appears to be a strong function of $u\Delta T_{sub}$ but only a weak function of the initial solid temperature. Thus we can observe from Fig. 3.6 that the surface temperature at which the wetting front can move forward becomes higher as $u\Delta T_{sub}$ becomes larger until the temperature is close to the interface temperature for the liquid and the solid. At this point the wetting front can move forward almost immediately and the resident time becomes very short. Therefore the parameter, $u\Delta T_{sub}$ can be considered to contribute in two ways to shortening the resident time. First, as mentioned in section 3.5, by increasing the cooling rate of the solid and secondly, by increasing the temperature at which the wetting front can move forward.

The data for copper with t*>30 s shown in Fig. 3.6 could perhaps be approximated as a linear function of $u\Delta T_{sub}$. However, a much better correlation which is also applicable for brass with t*> 30 s can be achieved by making T_w* a function of the initial temperature of the solid, $u\Delta T_{sub}$, and properties of the liquid and solid material. Since from Eq. (3.1) we suspect the interface temperature may play an important role we have included the dimensionless ratio of $\rho c\lambda$ for liquid and solid. Using the method of least mean squares to determine the constant and the exponents, Eq. (3.2) gives an empirical correlation for T_w*.

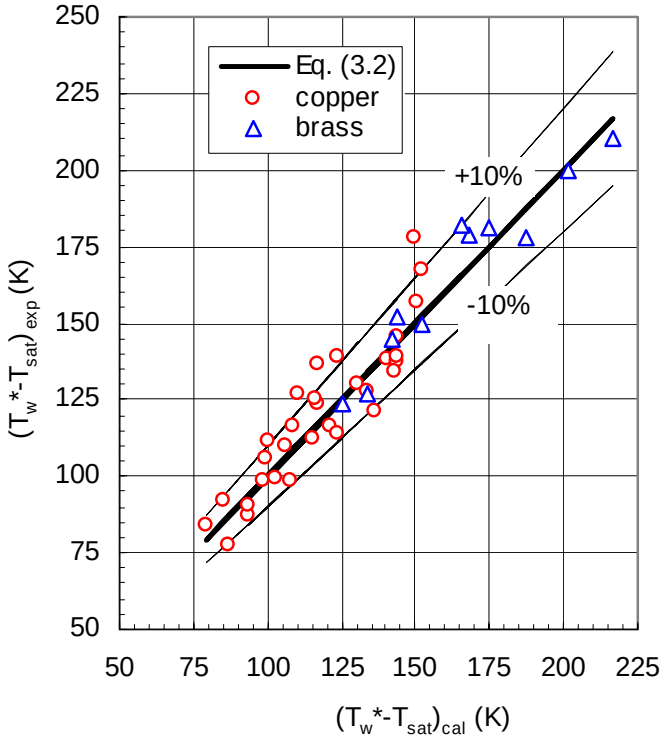

Fig. 3.7: Experimental data and proposed correlation (for t*>30 s) of surface temperature, T_w* at resident time at wetting front

$$\frac{T_w{}^* - T_{sat}}{T_b - T_{liq}} = 157\left\{\frac{(\rho c\lambda)_l}{(\rho c\lambda)_s}\right\}^{0.49}\left(\frac{2r^*}{d}\right)^{-0.49}\left(\rho cu\Delta T_{sub}\right)_l^{0.14}(T_b - T_{liq})^{-0.68} \qquad (3.2)$$

Figure 3.7 illustrates how well Eq. (3.2) represents the experimental data for both copper and brass with resident times greater than 30 seconds. Most of the data is within ±10% of the proposed relation. Equation (3.2) is not non-dimensional because the role of the parameters related to temperature differences is left unclear yet. The meanings of these parameters should be clarified in future studies.

3.7 Correlation for Resident Time

From the preceding sections, the parameters related to the resident time seem to be $\rho cu\Delta T_{sub}$, $(T_w{}^*-T_{sat})$, (T_b-T_{liq}) and r*/d. It may be worth mentioning that the heat flux transferred through heat conduction from the solid to liquid is generally proportional to $\sqrt{(\rho c\lambda)_s/t}$ with units [W/m^{2}K]. Finally the aim is to predict the resident time, t*, when the wetting front starts moving. Therefore, it is tentatively deriven a correlation predicting the resident time based on the above parameters. The temperature (T_w*) at the wetting front at t* is obtained from Eq. (3.2) and then using this temperature the resident time can

$$\frac{\sqrt{(\rho c\lambda)_s/t^*}(T_w^* - T_{sat})}{(\rho cu)_l(T_{sat} - T_{liq})} = 14\left(\frac{2r^*}{d}\right)^{0.72}\left(\rho cu\Delta T_{sub}\right)_l^{-0.41}(T_b - T_{liq})^{-0.99} \qquad (3.3)$$

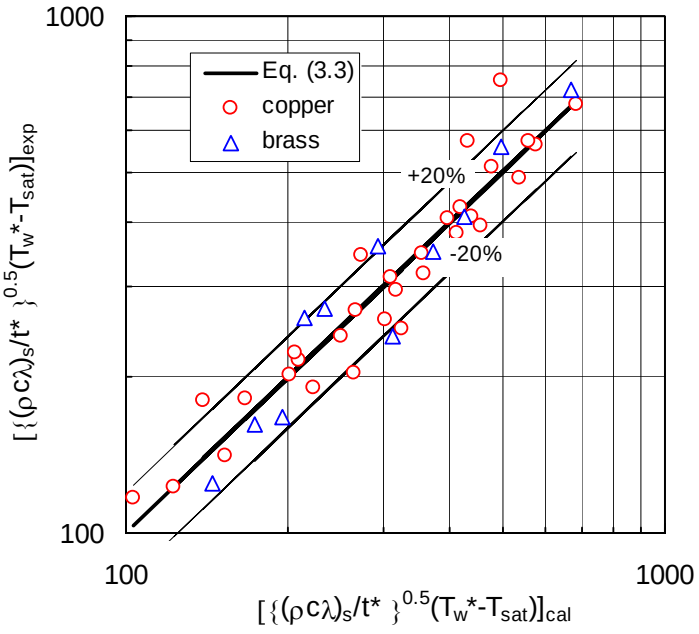

Fig. 3.8 : Experimental data and proposed correlation (for t*>30 s) of resident time

be predicted with fairly good agreement by Eq. (3.3) as is shown in Fig. 3.8. Again the constant and exponents in Eq. (3.3) were determined by the least mean squares method. Equation 3.3 is applicable to all data for copper and brass considered in this study that resulted in resident times greater than 30 seconds. Equation (3.3) is also dimensional, which should be improved by taking into account parameters related to the temperature differences.

3.8 Summary and Comments

Comments and conclusions of the present chapter are stated in this section. Emphasis has been given here to find out the parameters that govern the resident time during quenching. With the combination of key parameters a correlation for resident time and the surface temperature at resident at wetting front have been proposed.

For moderate/slower cooling condition, the surface temperature drops 100-150 ^{o}C within 10-40 s just after the wetting front start moving and then the heat flux increases dramatically. The value of maximum heat flux is (5-60) times higher than the heat transfer value just before the wetting front movement. For moderate/higher resident times, the duration of wetting propagation (the time between when the wetting front starts moving and when it reaches to the end) does not change so much (10-40 s) relative to the resident time for different experimental conditions. The resident time is much larger than the propagation period (it varies from few times to 100 times). The wetting front starts moving when the surface temperature (T_w^*) drops to the corresponding solid-liquid interface temperature (T*) for very short resident times. Resident time is a strong function of the solid material thermal properties and jet subcooling. Jet velocity and block initial temperature also effect the resident time. This time can be well categorized on the basis of the factor $u\Delta T_{sub}$. The proposed correlation for resident agrees within ± 20 % of the experimental values and this agreement is ± 10 % for the surface temperature correlation.

The proposed correlation is at the tentative stage at the moment. It has not yet been non-dimentionalized. If the effect of the parameters that are used as a group becomes clearer, the correlation will be more significant. Future investigation is indispensable for this complicated phenomenon.

Chapter 4

Maximum Heat Flux

Maximum heat flux distribution is among the important criteria for understanding the quenching phenomena. The maximum cooling effect is obtained from the position where the heat flux reaches its maximum value. The orientations of maximum heat flux during quenching over the heated surface are discussed in this chapter. The dominating parameters for the maximum heat flux and their correlations are also delineated.

4.1 Heat Flux, Temperature and Boiling Curve

The cooling curve and surface heat flux distribution for a moderate resident time condition have been included in Fig. 3.3. To explain the distribution of maximum heat flux for a short resident time condition, one further example of the surface temperature and heat flux orientation is presented in Fig. 4.1. As described in the Chapter 3, for many conditions, after the jet first struck the hot surface, the wetting region stayed for a while in a small region near the center before wetting the entire surface. This wetting delay characteristic is also described by Mozumder et al. [69] where cooling curves have been categorized in three types; long resident time, moderate resident time and short resident time. Figure 4.1 is a representative plot of short resident time conditions where the wetting front starts moving almost immediately after the first striking of the jet.

The cooling curve in Fig. 4.1 shows that the temperature close to the center of the test piece drops from 400 to 100 ^{o}C within 2 s after the jet first strikes. During this time, the heat flux increases drastically and reaches its maximum value. It takes about 10 s for the outer radial positions to come to the temperature 100 ^{o}C. The peak in the heat flux curve moves outwards in the radial direction as the liquid wets the surface. After 10 s, there is almost no variation of radial temperature distribution and the overall surface temperature of the block comes to around 80 ^{o}C. Finally the surface temperature drops gradually and slowly.

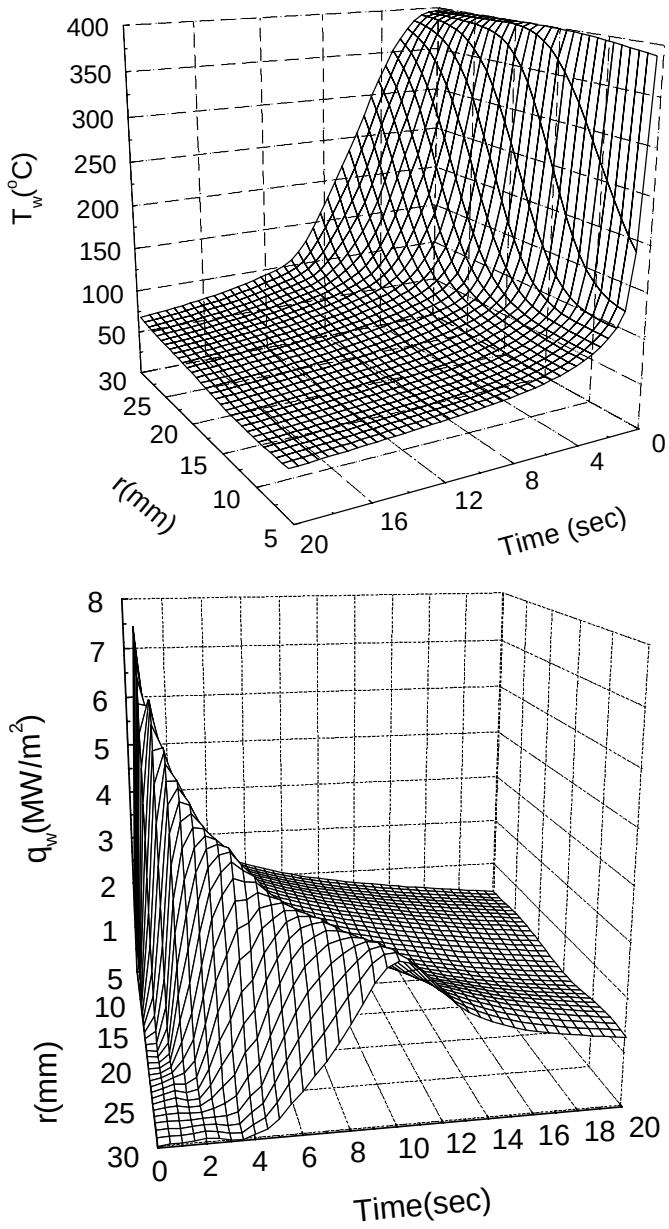

Fig. 4.1: Cooling curve and heat flux distribution during quenching for brass (T_b = 400 °C, ΔT_{sub} = 80 K, u = 15 m/s)

The key feature of the heat flux distribution in Fig. 4.1 is the moving of the maximum heat flux point. The rapid drop in temperature evident in the cooling curves is a direct result of the movement of the maximum heat flux point. For the experimental condition shown in Fig. 4.1, the heat flux is much less than 1 MW/m^2 before the movement of the wetting front. When the wetting front starts moving, the heat flux 5 mm from the center reaches about 7.5 MW/m^2. This kind of trend was observed for many of the experiment conditions for this study. Generally the heat flux after the wetting front begins moving was found to be in the range of 5-60 times higher than before movement especially for slow cooling conditions (low sub-cooling and smaller jet velocity conditions). It should be

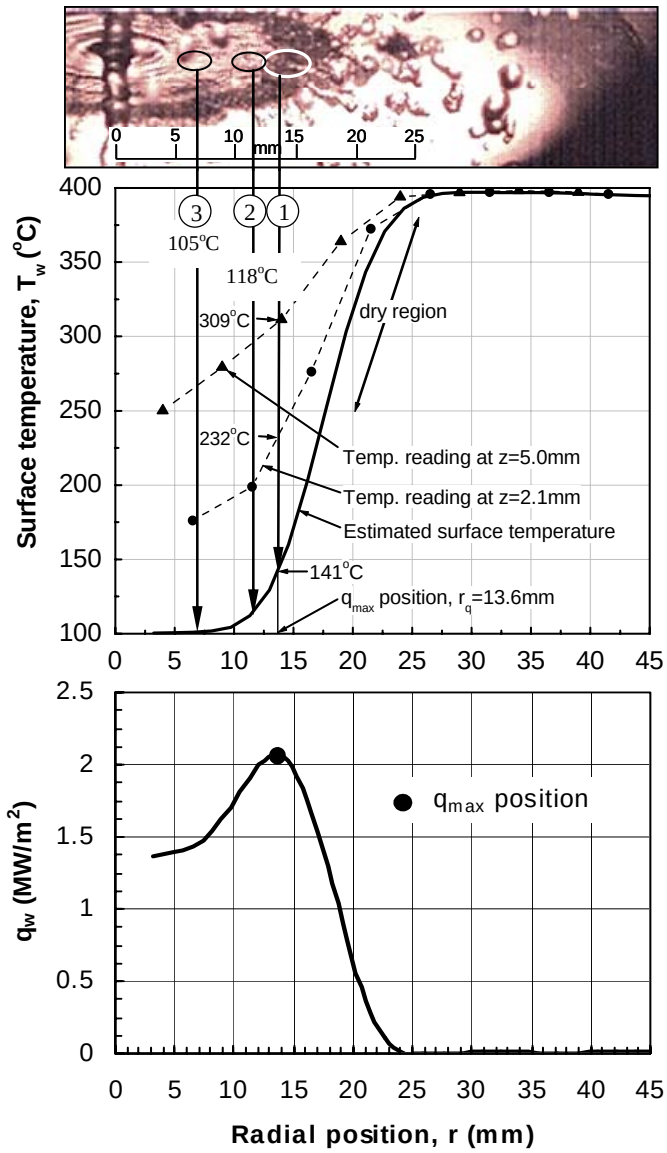

Fig. 4.2: Regimes of boiling and maximum heat flux during wetting front propagation (St, T_b = 400 ^oC, ΔT_{sub} = 50 K, u = 3 m/s, t = 4.3 s)

mentioned here that the heat flux before the movement of the wetting front is much smaller than that after the movement may be due to repetition of wet and dry on the hot surface before the wetting front movement. The heat flux during the wetting time would be equal to that when the wetting front just moves. It is interesting that the magnitude of the maximum heat flux decreases with increasing radial position.

Quench cooling is a particularly a complex phenomenon because different boiling modes occur simultaneously at different spatial positions relative to the wetting front. For this reason, it is useful to discuss the heat flux distribution with reference to corresponding boiling curves.

Figure 4.2 represents the surface temperature and heat flux distribution in the radial direction along with a video image captured during the wetting front movement. The surface temperature, heat flux and the wetting front position are for 4.3 s after the first impingement of the jet. The picture can be divided into three regions: (a) no visible boiling (r = 0-12 mm) (b) vigorous boiling heat transfer (r = 12-18 mm) and (c) dry region (r = 18-45 mm). The region with no visible boiling activity is most likely single phase convection near the center with the onset to nucleation boiling beginning a little upstream of the vigorous boiling region in the zone marked (2).

The maximum heat flux point in the boiling curve traditionally represents the boundary between nucleation boiling and transition boiling. In Fig. 4.2 the maximum heat flux point appears at a radial position of 13.6 mm (≈14 mm), which is just inside the vigorous boiling region. As mentioned above, the region with r = 10 to 12 mm belongs to no visible boiling region but since the surface temperature is very high it is expected that nucleate boiling occurs but bubbles collapse quickly due to the high sub-cooling and consequently no vigorous boiling is observed. Thus in terms of the different modes of heat transfer the image in Fig. 4.2 may be interpreted as (i) single phase convection (0-10 mm) (ii) nucleation boiling (10-14 mm), (iii) transition boiling (14-18 mm) and (iv) single phase convection to vapor phase plus radiation (18-47 mm).

The surface temperatures and heat fluxes determined from the inverse solution are consistent with this interpretation. In the single phase convection region the surface temperature is close to the saturation point. For example at the position marked ③ in Fig. 4.2 the superheat is about 5 K, which is reasonable for single phase forced convection heat transfer. At the point ② the surface superheat has increased to 18 K and heat flux increases monotonically with radial position towards the maximum, which is consistent with nucleation boiling in subcooled forced convection. At the maximum heat flux point, the surface superheat is 41 K. This again is higher than typical values for saturated nucleate pool boiling but reasonable for jet impingement with a subcooled liquid. In the dry region the surface temperature climbs rapidly from about 250 °C to the block initial temperature of 400 °C and the heat flux becomes very small.

Since the wetting front moves outwards in the radial direction each point on the surface will experience different boiling modes at different times depending on its position relative to the wetting front. This is apparent in Fig. 4.3 where cooling curves for individual points

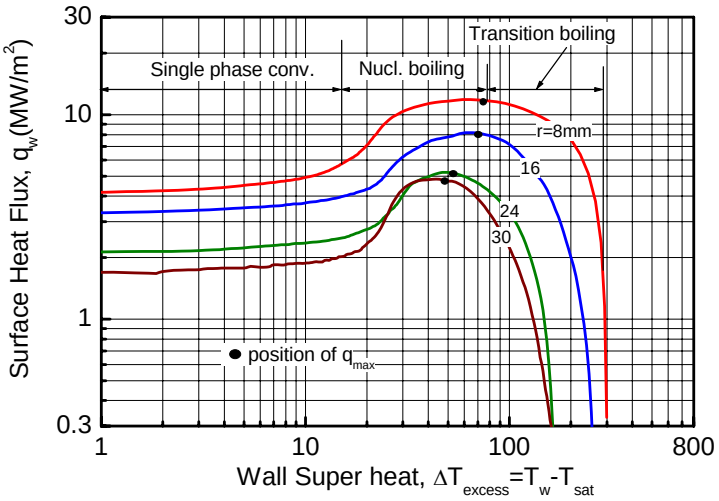

Fig. 4.3: Position of maximum heat flux in the regimes of boiling curve (Cu, T_b = 400 ^oC, ΔT_{sub} = 80 K, u = 15 m/s)

on the surface are plotted as boiling curves. The curves can be divided into four regions: single-phase convection, nucleation boiling, transition boiling and film boiling. The maximum heat flux serves as the boundary between nucleate boiling and transition boiling. It may be observed from Fig. 4.3 that for each boiling mode, the heat flux is generally greater for smaller radial positions. This may be due to a greater heat transfer enhancement from forced convection closer to the impingement zone and a tendency for the coolant temperature to rise with increasing radial position.

The most important finding from Fig. 4.3 is the surface temperature when the maximum heat flux occurs (i.e. T_w at q_{max}). When the maximum heat flux happens the surface temperature is 150-180 ^oC (for r = 8-30 mm according to this figure where T_b = 400 ^oC, ΔT_{sub} = 80 K, u = 15 m/s). This temperature is always within a certain range for any radial position and any experimental condition. It is found that for the most of the conditions (shown in Table 2.1); the range of the surface temperature when the maximum heat flux occurs is 120-200 ^oC. It is also found from the present study that the T_w at q_{max} increases with the increase of liquid sub-cooling which is a general trend of boiling but still this change of T_w always falls within the range of 120-200 ^oC. Temperatures within this range are higher than the surface temperature required for saturated nucleate boiling in pool boiling.

4.2 Movement of Maximum Heat Flux Point

The mechanism for triggering the movement of the wetting front has still not been clarified. Nevertheless, in general it is found that the commencement of the movement of

the wetting front corresponds approximately to the appearance of the moving peak in the heat flux curve. For some conditions the maximum heat flux seems to appear slightly after the first visible observation of wetting front movement, but for the case in Fig. 4.1 these events are almost simultaneous.

The commencement of movement of the wetting front is also accompanied by visible and audible changes in the flow phenomena. Generally the boiling sound becomes loudest as the wetting front begins moving and liquid droplets are splashed away from the surface at a steep angle. Much vapor is generated due to rapid phase change associated with the maximum heat flux condition and the sound results from nucleate and transition boiling. These phenomena continue as the maximum heat flux point moves across the surface.

The mechanism that determines the speed of the wetting front also has not been clarified yet but it is likely that both heat flux and surface temperature play direct or indirect roles. To draw an analogy from steady state CHF experiments, CHF has been considered a boiling crisis where the 'dry out' point begins to occur at the outer edge of the heater [5]. In the present experiment we have a situation that appears similar where the boiling reaches a crisis point (maximum heat flux) just upstream of the wetting front. Beyond the wetting front the heater surface seems to be dry. Thus we may expect that in quenching experiments, rapid generation of vapor associated with the maximum heat flux will play an important role in the hydrodynamics to determine the movement or the position of the wetting front.

From the thermal perspective, the maximum heat flux also makes a direct contribution to the thermal conditions of the surface ahead of the wetting front. Heat is transferred in the negative radial direction through the solid to the high heat flux zone. Thus the rate at which the solid surface is cooled in front of the wetting zone is a function of the solid thermal properties and the heat flux distribution within the wetted region. This is an important consideration since Fig. 4.3 indicates that the changes in boiling modes are connected to similar surface superheats for different radial positions.

Whatever the precise mechanism, it is likely that the wetting front shifts its position to keep a balance between the rate at which the solid side supplies heat and some hydrodynamic limitations of the liquid side to extract heat. The balance point itself may be due to a combination of hydrodynamic and thermal effects.

4.3 Effect of Radial Position on Maximum Heat Flux

Figure 4.4(a) compares a well-known relation for critical heat flux (CHF), q_c developed by Monde et al. [70] with present results for the maximum heat flux, q_{max} as a function of radial position. In this figure the heavy solid line (q_c) should be compared with the data having the symbols of circles (both solid and hollow). Two different characteristics as shown in Fig. 4.4(a) is presented by region: I (r_q = 5-11 mm) with hollow symbols and region: II (r_q = 11-25 mm) with solid symbols. For a radial position less than about 11 mm (denoted as region I), the maximum heat flux decreases gradually with increasing r_q. In the region II, q_{max} also decreases more rapidly and the slope of this curve on the log-log plot is similar to that of the Monde prediction [70]. Solid symbols indicate Region II where the trend is similar to the CHF equation result, q_c. This suggests that there may be a connection between the mechanism for deciding the maximum heat flux in the present experiments and the CHF for steady-state experiments.

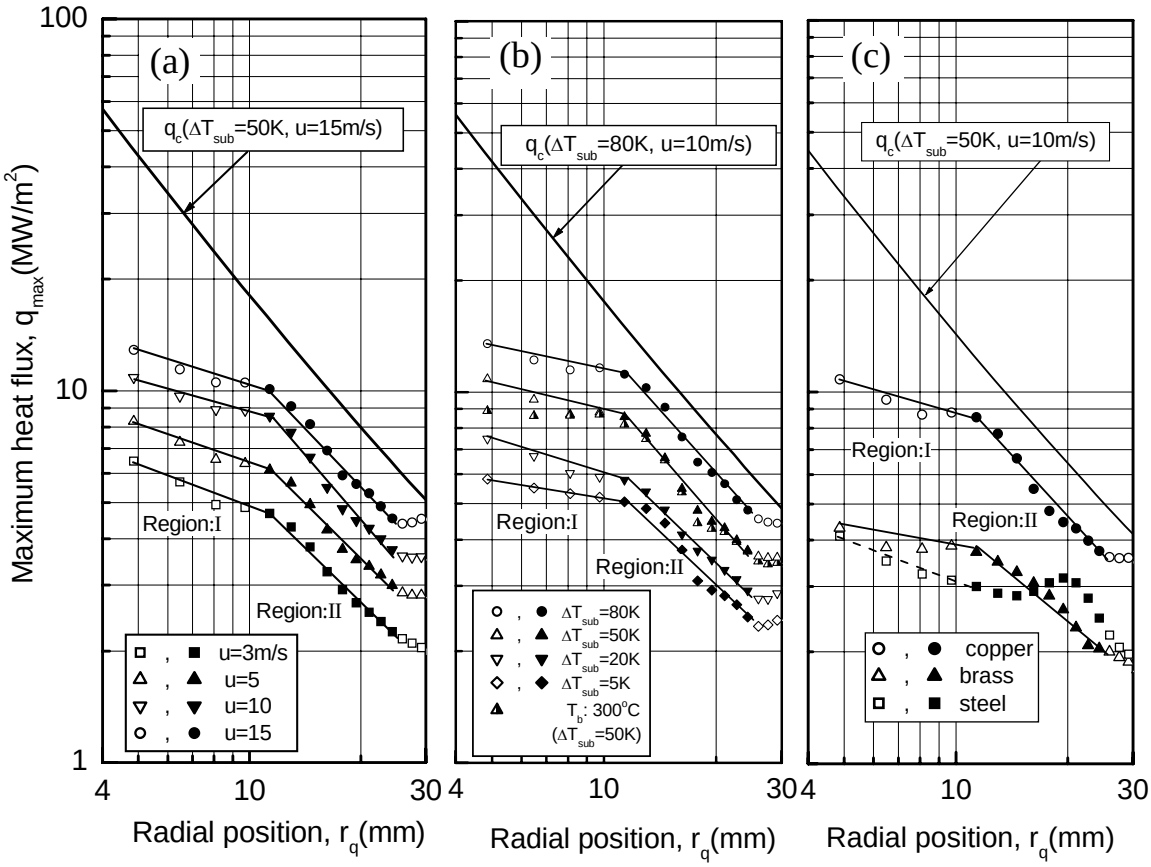

Fig. 4.4: Variation of critical and maximum heat flux with radial position for different
(a) jet velocities (Cu, T_b = 400 °C, ΔT_{sub} = 50 K)
(b) subcoolings (Cu, T_b = 400 °C, u = 10 m/s)
(c) materials (T_b = 400 °C, ΔT_{sub} = 50 K, u = 10 m/s)

Wolf et. al [5] suggested that the decrease in CHF with increasing heater size is the result of poorer convection heat transfer further from the impingement region of the jet. However, from a different angle, Monde [71] was able to explain the decrease in CHF with heater diameter in terms of an overall heat balance and a hydrodynamic stability model by Haramura and Katto [72]. If the diameter (D) of the heater is large in comparison to the diameter of the jet, the relation derived by Monde [71] suggests the critical heat flux will be approximately proportional to $D^{-2/3}$ for saturated condition. This is in accord with much experimental data for saturated impinging jet CHF. Monde [70] extended the flow model to account for jet subcooling showing that the subcooled CHF is an even stronger function of the heater diameter since the liquid becomes heated towards the saturation point as it flows in the radial direction. As shown in Fig. 4.4(a) the maximum heat flux in the present study is approximately proportional to $(r_q)^{-1}$ in the region II.

A general observation for the present quenching experiment is that the vigorous boiling region increases in area as the wetting front moves outward in the radial direction. This is the result of the greater circumference and also an increasing width of the boiling region. The effect is evident in Fig. 4.1 where the heat flux distribution near the peak becomes broader and flatter as the peak moves outward in the radial direction. Thus a balance between supply of coolant and increasing available surface area is certainly a possible explanation for the decrease in maximum heat flux with increasing radial position shown in Figs. 4.4(a-c).

It is a little difficult to explain the change in character of the curves at around r_q = 11 mm (the border of regions I and II) in Fig. 4.4(a). All data in the figure are from the parallel flow region of the jet since this region starts around 2 jet diameters downstream of the stagnation point [5]. However, it is worth noting that this changing point in Figs. 4.4 (a-c) corresponds approximately to the point where the developing boundary layer will reach the free surface if the flow is assumed laminar [73].

4.4 Effect of Initial Block Temperature on Maximum Heat Flux

Generally it is found that the effect of the initial block temperature on maximum heat flux is small. A comparison of the right half solid upward triangles (◭) with the hollow (△) and full solid (▲) upward triangles in Fig. 4.4(b) is a typical example of the effect. The half solid triangles are for an initial temperature of 300 °C while the hollow and full solid triangles are for an initial temperature of 400 °C. For both cases, the subcooling and velocity are 50K and 10 m/s respectively. In this particular case the largest differences

appear at the smaller radial position where the heat flux is slightly higher for the higher initial temperature.

The main effect of the initial block temperature is on the time it takes to reach the maximum heat flux. This is consistent with the observation that the maximum heat flux usually occurs when the surface temperature is in the range 120-200 ^{o}C. A higher initial temperature means it takes longer time for the block to cool down to bring the surface temperature within this range.

While there may be a weak correlation between the initial temperature and maximum heat flux, in the correlation proposed in the present study we have assumed that q_{max} is independent of T_b.

4.5 Effect of Block Material on Maximum Heat Flux

One of the most surprising findings in the present study is the effect of the solid material on the maximum heat flux. This is in contrast to critical heat flux for steady experiment, which has been found to be independent of the heater material. Figure 4.4(c) gives a typical example of the effect of block material on the maximum heat flux. The data are for an initial temperature of 400 °C, a subcooling of 50 K and a jet velocity of 10 m/s. All three materials were given the same surface treatment and were plated with gold. It should be noted, however, that in spite of precautions, some oxidation and surface aging could be observed on each of the surfaces after many experiments. Nonetheless it is expected that the effects shown reflect the influence of the thermal properties of the bulk material rather than the surface condition or properties of oxidation.

Among three materials, copper shows the highest value of maximum heat flux, which is more than two times that of steel whose value is the minimum. Copper, brass and steel show a similar trend up to the radial position r = 15 mm. In the region r = 15-25 mm the trend of maximum heat flux with radial position is similar for copper and brass. However, for steel the maximum heat flux rises to reach a local peak at r_q = 20 mm and then falls again. This peculiarity for steel was observed for all experimental conditions.

Differences in thermal conductivity of the block material may be the key factor responsible for the higher maximum heat flux for copper than steel or brass. According to Table C.2 at 250 ^{o}C, copper has a thermal conductivity, λ of about 372 W/mK, which is over 2.5 times that of brass (λ = 146 W/mK) and eight times that of steel (λ = 47 W/mK). The basic trend is that the maximum heat flux increases with increasing thermal

conductivity (or diffusivity) but not in direct proportion as may be deduced from Fig. 4.4(c).

In terms of the temperature distribution within the solid, quenching results in localized cooling near the surface for steel in contrast to copper/brass where the entire heated test piece quickly feels the effect of the maximum heat flux on the surface. It may be that this difference is partly responsible for the peculiar effect of radial position on q_{max} for steel. From video images it could be observed that after the wetting front starts moving in the radial direction it proceeds to the circumference without any further delay at any position for copper and brass. In the case of steel, however, at around the radial position 15-20 mm, the wetting front movement appears to suddenly become slower and then after almost stopping, the wetting velocity gradually increases and the front reaches to the end of the test piece. This behavior seems to suggest a hydrodynamic effect that perhaps was not obvious in the cases of copper and brass due to the strong influence of vigorous boiling on the flow behavior both upstream and downstream of the maximum heat flux point.

From Fig. 4.4(c) it is clear that brass and steel have closely comparable magnitudes of maximum heat flux value but the nature of the change in maximum heat flux with radial position is most similar between copper and brass. For this reason we have not included the data for steel in the present proposed correlation for q_{max} together with copper and brass.

4.6 Effect of Jet Velocity on Maximum Heat Flux

The variation of q_{max} with jet velocity has been presented in Fig. 4.5 for three different radial positions. Effect of velocity on q_{max} has been also shown in Fig. 4.4(a). Maximum heat flux increases gradually with increasing jet velocity. The jet velocity directly affects the flow rate of coolant to the test surface and has a strong bearing on convection heat transfer and the fluid hydrodynamics. If the flow model proposed by Monde [70] is applicable in the vicinity of the maximum heat flux point then the velocity directly affects the flow rate of coolant to the film of liquid on the surface. For V-regime (the regime where jet velocity is very important for critical heat flux) steady-state CHF, Monde [71] found that the critical heat flux is proportional to $u^{1/3}$ for saturated jets and the correlation proposed by Monde [70] suggests that the exponent should increase with greater subcooling. In Fig. 4.5, a comparison also has been made between maximum heat flux and critical heat flux with the variation of jet velocity. The symbol of solid upper triangle is for q_c at radial position of 17.8 mm and the hollow triangle is for q_{max} at the same radial

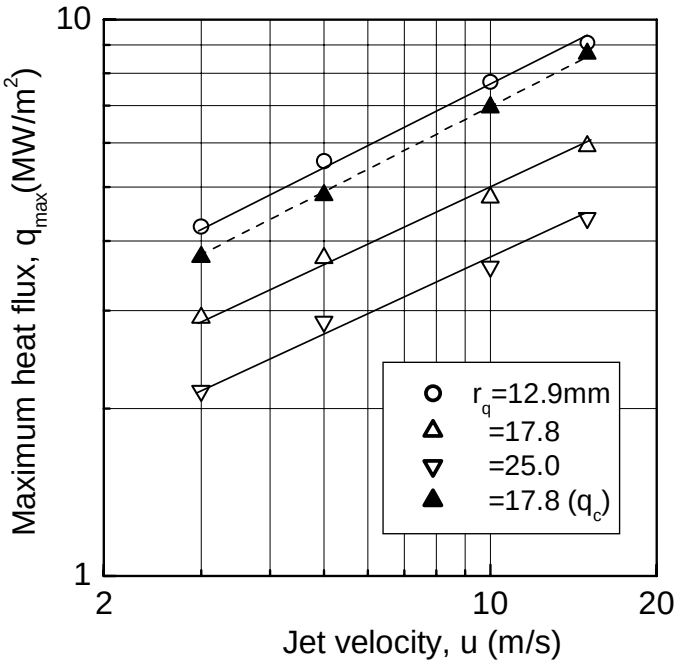

Fig. 4.5: Variation of maximum heat flux with jet velocity for different radial positions (T_b = 400 ^oC, ΔT_{sub} = 50 K)

position. A similar trend of q_c and q_{max} with the variation of jet velocity has been observed from this figure.

4.7 Effect of Subcooling on Maximum Heat Flux

Figure 4.4(b) also represents the variation of maximum heat flux with radial position for different subcoolings. With the increase of subcooling the maximum heat flux increases significantly. For reference, the estimated critical heat flux, q_c (for ΔT_{sub} =80K, u=10m/s) is also included in Fig. 4.4(b).

Figure 4.6 represents the variation of q_{max} with ΔT_{sub} for three different radial positions which are within the region II. Here q_{max} increases with subcooling. Higher subcooling increases the thermal potential between the solid and the impinged liquid which results in higher q_{max}. A similar trend has been observed for all experimental conditions. Comparison of q_{max} (hollow upward triangle) and q_c (solid upward triangle) with the variation of subcoolings for a particular radial position (r=17.8mm) has been also shown in Fig. 4.6. One important finding from this figure is that the maximum heat flux has a similar trend to critical heat flux with respect to the effect of liquid subcooling.

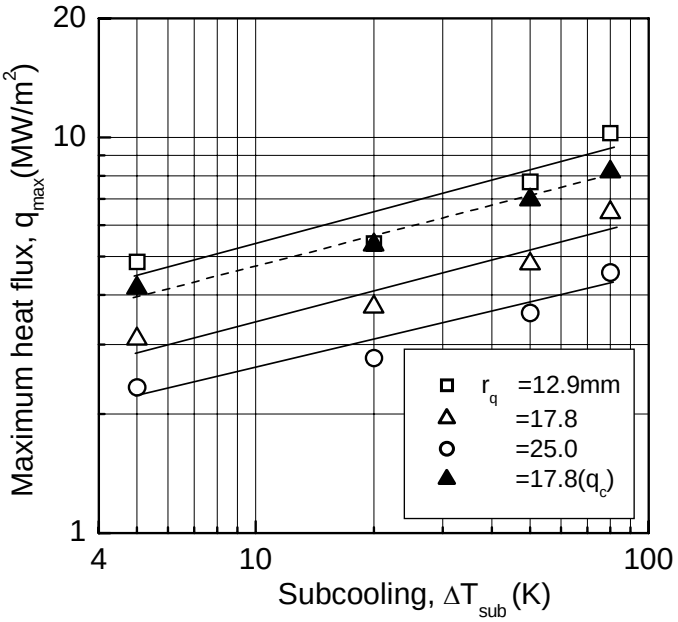

Fig. 4.6: Variation of maximum heat flux with subcooling for different radial positions (T_b = 400 ^{o}C, u = 10 m/s)

4.8 Causes for Difference between Critical and Maximum Heat Flux

As shown in Figs. 4.4(a-c) the value of maximum heat flux, q_{max} is always smaller than the critical heat flux, q_c for any radial position. The rate of decrease of q_{max} with radial position is similar with that of q_c in the region r_q=11-25mm. In this region the difference between q_c and q_{max} is smaller than the region with smaller radial position. Many factors may be responsible for making this difference.

However, an important clue can be found in Fig. 4.4(c). In this figure, for the same jet velocity and subcooling the maximum heat flux is quite different depending on the solid material. This demonstrates that in contrast to critical heat flux, the thermal properties of solid material have a significant effect on the maximum heat flux during quenching. In particular the material with lower thermal conductivity has a lower maximum heat flux and the results for copper are closest to q_c. This is a strong evidence that the thermal properties of the material place a limit on the maximum attainable heat flux during quenching. In other words there is a limit to the maximum rate at which the solid side can supply its stored heat to the surface. This limit is not present for steady-state CHF experiments where in contrast an external source or direct heating provides a constant supply of heat to the heater surface.

4.9 Influence of Limitations of the Inverse Solution Procedure

It should be mentioned that it is a little difficult to alternatively explain the large difference between the result for copper and steel in Fig. 4.4(c) by a diminishing accuracy for the inverse solution comparing copper and steel. Figure 4.2 includes the actual measured temperature at a depth of 2.1mm. From this figure it can be seen that the sensors detected about 65% of the change from initial temperature at the surface. For copper under similar conditions the sensors at the first depth detected over 80% of the change in surface temperature. This change is much larger than the noise in the thermocouple reading, which was estimated to be less than 0.1K. For the cases in Fig. 4.2 and Fig. 4.4(c) the velocity of the q_{max} point in the region II was about 2 to 4 mm/s for all materials. It is considered that this is slow enough so that the thermocouple response time is not a significant problem in this region. Also the penetration depth of the thermal wave is great enough to be detected easily by the sensors for all materials. Under similar conditions, numerical simulations [67] suggest the inverse solution should be quite accurate for all these materials.

The inverse solution result itself should be interpreted as an average over time and space. The time resolution cannot be greater than the response time of the sensors (about 0.1 s) or the time required for a thermal wave to penetrate to a depth of 5.0 mm (0.2 s for steel and 0.02 s for copper). The space resolution for the inverse solution is also limited to about 5.0 mm. Therefore the results for maximum heat flux are best understood as an average in space over about 5.0 mm.

According to Woodfield et al. [67] when the width of the high heat flux region is smaller than the pitch between the positions of two consecutive thermocouples, the inverse solution under-predicts the q_{max} value. This may help to explain why in the central region, less than about r_q = 11 mm, q_{max} was determined to even further from q_c. Near the central area the boiling region is narrow and as the wetting front moves outwards it becomes wider [16]. The boiling region in the central area (r = 10 mm) is about 2 mm wide and this value at r = 25 mm is about 5.5 mm (Brass, T_b = 300 ^oC, ΔT_{sub} =50 K, u = 5 m/s). The distance between two thermocouples beneath the test surface of the present study is approximately 5 mm. Therefore, near the center, as the width of the maximum heat flux region is smaller than pitch between consecutive thermocouples, the maximum heat flux in the central region is estimated to be lower than the actual value. This increases the difference between q_{max} and q_c. On the other hand, further from the centre, the boiling region (the region of maximum heat flux) is wider than that of thermocouples gap which prevents the under

prediction of q_{max} from the inverse solution. For this reason, q_{max} is more accurate for greater radial positions.

Furthermore, the response of thermocouples might play a role for under predicting the value of q_{max} in the region I. The drop of temperatures with time is higher in smaller radial position than that of larger radial position. The thermocouples might not cope with this faster drop of temperature which results in decrease of accuracy of maximum heat flux estimation in smaller radial position. The wetting front velocity in the region I is much higher than that of the region II. This higher velocity might be responsible for under predicting the q_{max} value. But due to slow wetting front velocity this has not happened in the region II. The developed correlation and the focus of study in the present investigation belong to the region II and the estimation accuracy of the parameters in this region is high from all points of view.

4.10 Correlation for Maximum Heat Flux

As discussed earlier, during quenching the solid material cannot supply enough heat to the liquid which has the consequence that q_{max} is always smaller than q_c. q_{max} in the present study is the maximum heat flux from transient experiments and q_c is the critical heat flux from steady state experiments conducted by Monde et al. [70]. In well designed steady state experiments due to the external power source the solid material can supply heat to the surface as if the solid conductivity is infinite. Therefore, it may be assumed that if it would possible to conduct transient experiments with material having infinite conductivity, then the q_{max} and q_c values should be close together. On the basis of this interpretation, a correlation of q_{max} is proposed in this study starting from the following critical heat flux correlation developed by Monde et al. [70] for subcooled impinging jets at steady state conditions:

$$\frac{q_c}{q_{co}} = \frac{1+\sqrt{1+4CJa}}{2} \tag{4.1}$$

$$\frac{q_{co}}{\rho_g h_{fg} u} = 0.221(\rho_l / \rho_g)^{0.645}\left[\frac{2\sigma}{\rho_l u^2 (D-d)}\right]^{0.343}(1+D/d)^{-0.364} \tag{4.2}$$

$$C = \frac{0.95(d/D)^2(1+D/d)^{0.364}}{(\rho_l/\rho_g)^{0.43}\left[2\sigma/\rho_l u^2(D-d)\right]^{0.343}} \tag{4.3}$$

where, $D = 2r_q$ for the present study.

In the present investigation, experimentation has been conducted for three material copper, brass and steel. Due to different characteristics of steel as discussed in the section 4.5, it is not included together with copper and brass in the proposed correlation. Furthermore, Figs. 4.4(a-c) reveal that q_{max} data can be categorized into two regions, region I (r_q = 5-11 mm) and region II (r_q = 11-25 mm). The trend of region II is similar with that of q_c.

Figs. 4.4(a-c) highlight the similarity between q_c and q_{max} as a function of r_q. It is also found that q_{max} shows the same trend as q_c expressed by Eqs. (4.1-4.3) when plotted as a function of jet velocity, u, and jet subcooling, ΔT_{sub}. In all cases q_{max} is smaller than q_c by a factor which differs depending on the solid material properties. Therefore, it is considered that the key difference between q_{max} in transient experiments and q_c in steady state experiments can be accounted for by a correction involving thermal properties of material. Here, the steady state condition is replaced by a combination of material thermal properties $\sqrt{\rho c \lambda}$ which plays an important role in transient heat transfer when two semi infinite bodies suddenly comes into contact. In addition, from the previous discussion it is desirable that q_{max} approaches q_c as the thermal conductivity of the solid approaches infinity. On the basis of this interpretation a relation between q_{max} and q_c is proposed by Eq. (4.4).

$$\frac{q_{\max}}{q_c} = 1 - 5.5\sqrt{\frac{(\rho c \lambda)_l}{(\rho c \lambda)_s}} \tag{4.4}$$

The coefficient 5.5 in Eq. (4.4) has been estimated using least mean squares method from the data of q_{max} of the present experiment (for T_b = 250-400 ^oC). Equation 4.4 is valid in the region II. Figure 4.7 represents the agreement between the data for q_{max} of copper and brass and the correlation. Most of the data is within ± 30 % of the proposed correlation. The few data points that fall outside of this range (inside the dotted area) mostly correspond to conditions where the wetting front starts moving almost immediately after the jet first strikes the surface. In general, when the jet velocity and jet subcooling are high the data tends to be more scattered, but even in such cases most of the data is within the ± 30 % range. The scatter in Fig. 4.7 may be due partly to the time response of the thermocouples during very rapid cooling.

The block initial temperature, T_b in some cases was found to have a weak influence on q_{max} which was not included in the proposed correlation. Therefore, T_b may contribute to the scattering of data. Also, the proposed correlation in the present study has been initiated from the correlation of q_c of Monde et al. [70] which itself has ± 20 % scattering [74].

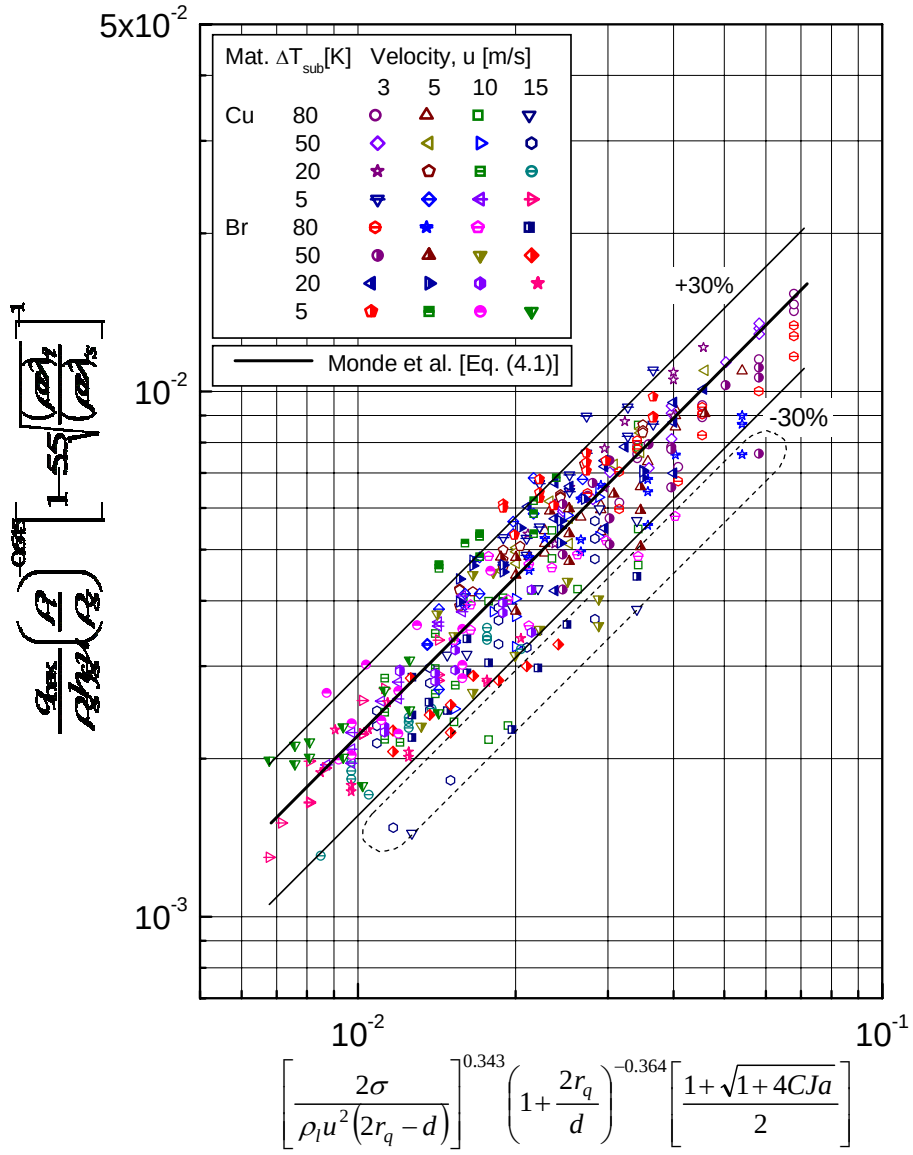

Fig. 4.7: Comparison of q_{max} data for copper and brass with the proposed correlation (for the region II)

In Fig. 4.8, the proposed correlation is compared with data for steel. The scattering is very high which might be due to the different characteristics of steel relative to copper and brass as described in the section 4.5. Future study should clarify the behavior of q_{max} for steel and the q_{max} in region I for copper and brass.

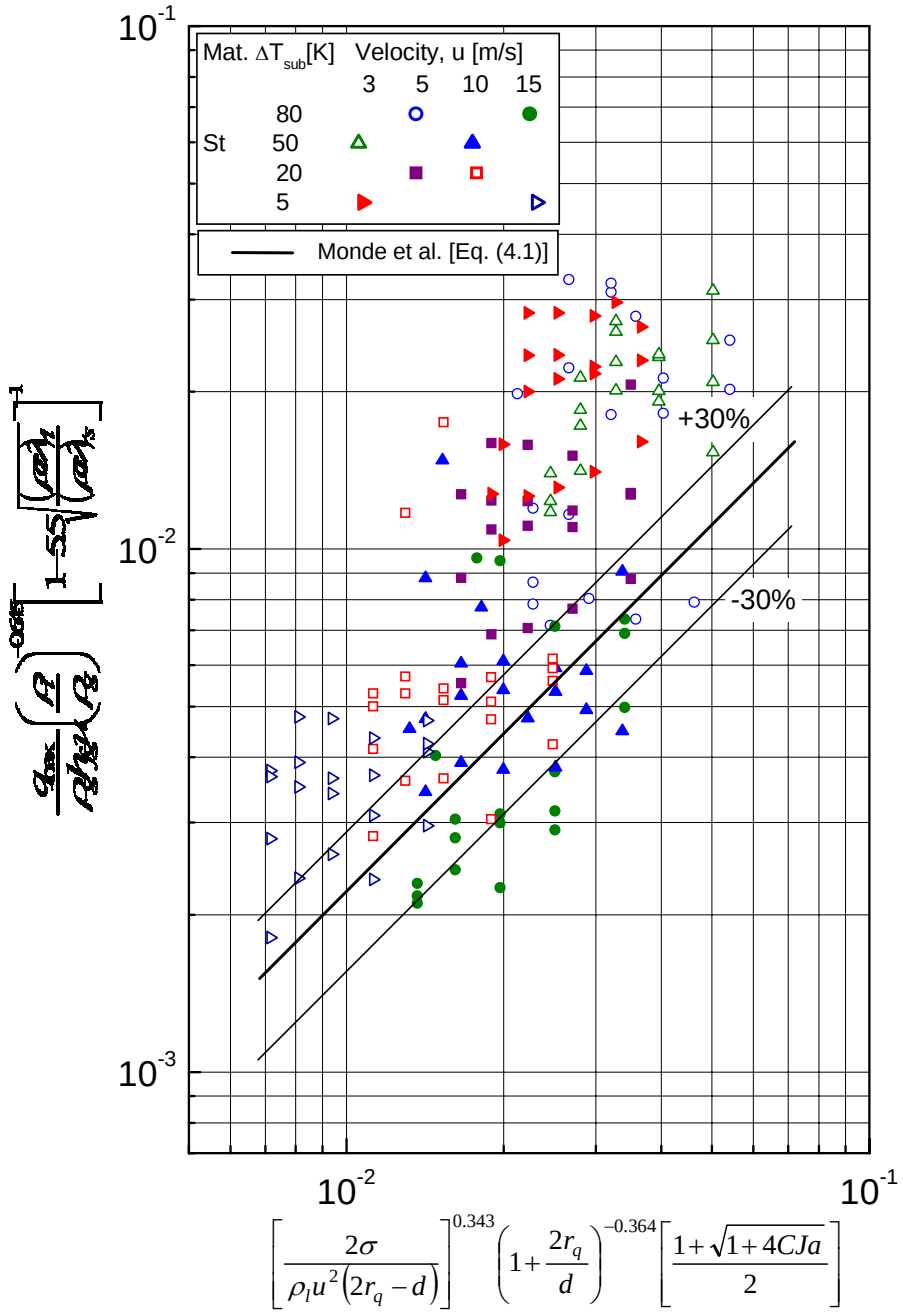

Fig. 4.8: Comparison of q_{max} data for steel with the proposed correlation (for region II)

4.11 Summary and Comments

The parameters that influenced the characteristics of maximum heat flux and interrelations among them have been highlighted in this chapter. The values of the q_{max} and T_w originated from the inverse solution should be best understood as an average over time and space. To increase the accuracy of the estimated values from this transient experiment, closer thermocouple spacing and faster response thermocouples are essential. But to decrease the thermocouple spacing, more holes inside the block is necessary for inserting

those thermocouples which will change the physical geometry of the block. Therefore, an optimum thermocouple spacing could be estimated in future studies.

The maximum heat flux position always resides within the visible boiling region where the mode of heat flux is predominantly nucleate boiling. The value and distribution of the maximum heat flux are influenced by jet velocity, thermal properties of solid material and jet subcooling. The initial value of the solid temperature seems to be less influential for maximum heat flux value. As the maximum heat flux always appears within a certain temperature range (120-200 ^{o}C) the block initial temperature should be a less influential parameter for q_{max} values. For any experimental condition the value of maximum heat flux decreases with increasing the radial position though the rate of decreasing of heat flux is different at different radial positions. There is some exception for steel also. At smaller radial position, subcooling has big influence on maximum heat flux but at higher radial position this influence becomes weaker. A reasonable agreement for the proposed correlation of maximum heat flux has been also demonstrated in this chapter.

Chapter 5

MHF Propagation Velocity

When the wetting front moves from the center towards the circumferential region, the position of maximum heat flux, MHF point also moves with the wetting front but with a certain time and position lags. The movement of the position of MHF is one of the important criteria for a clear understanding of the quench phenomena. This is because the point that gets the maximum cooling effect moves with MHF position. In this Chapter the propagation rate of the MHF point and its dominating parameters will be highlighted.

5.1 Thermal and Hydrodynamic Phenomena on the Surface

It is important to clarify some further terms for discussing the present quenching phenomena. Figure 5.1 exhibits a video clip, surface temperature and heat flux distribution during quenching of 400 ^{o}C steel block by 50 K subcooled liquid with 3 m/s jet. From Fig. 5.1 it is clear on the basis of visual observation that the liquid covers up to r =18 mm in 4.8 s from the first impingement. This area of radius 18 mm is described as ‘wet zone’. The outer dark area inside the wet zone is designated as ‘boiling zone’ which is about 4 mm (r = 14~18 mm) after 4.8 s for this particular experimental condition. The visible leading edge of this dark area is termed as the wetting front. This dark region is the most effective cooling zone. Due to nucleate boiling and formation of many bubbles, the video clip becomes darker in the boiling zone than in the other remaining part of the wet zone. The temperature gradient is very high in this region and the MHF position also belongs to this zone (at r = 15 mm) as shown in Fig. 5.1. The temperature at the central wet region (r = 0~14 mm) is less than 125 ^{o}C which indicates that the possible dominating mode of heat transfer in this region is single phase forced convection.

In Fig. 5.1, the region (r = 18~24 mm) immediate beyond the wetting front appears dry but the temperature gradient and the rate of heat transfer seem very high. The surprisingly high heat flux in this region partly may be due to the limitations of the measuring technique. Due to inverse solution settings, the heat flux in Fig. 5.1 should be interpreted

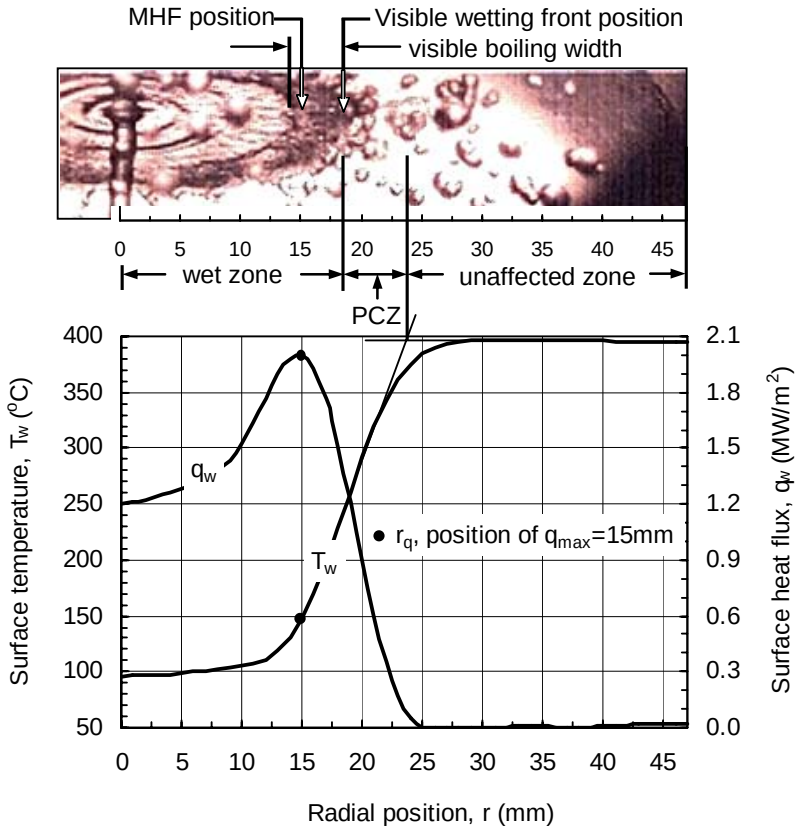

Fig. 5.1: Hydrodynamic phenomena on the surface together with the cooling curve and surface heat flux at t = 4.8 s (St, T_b = 400 °C, ΔT_{sub} = 50 K, u = 3 m/s)

as an average over a distance of about 5 mm. This region has been marked as 'precursory cooling zone' (PCZ) as shown in Fig. 5.1. The term 'precursory cooling zone' is also used by Filipovic et al. [62]. Notice that in much of this region the surface temperature gradient is almost constant and in pretty well corresponds to the maximum radial temperature gradient. In the present study the leading boundary of the PCZ is defined as the intersection point between a tangential line starting at the maximum radial temperature gradient position and another tangent at the position of the minimum positive radial temperature gradient ahead of the front at any instant in time (as shown in Fig. 5.1). In Fig. 5.1 this boundary occurs at about r = 24 mm. The definition has a convenient correspondence to the apparent 'elbow' in the radial temperature profile. It can be understood that the liquid has not yet covered this region and heat is conducted through the solid from this precursory cooling zone (PCZ) towards the inner high heat transfer boiling zone.

The most outer region (r = 24~47 mm) is designated as the 'unaffected zone', where the surface temperature has almost the initial value corresponding to when the wetting front started moving. The heat transfer from this region is by convection to the gas phase, by radiation (which is almost negligible) and to a small extent by conduction to the supporting

experimental apparatus. Most of the surface belongs to this category before the wetting front movement. It should be noted here that the example shown in Fig. 5.1 is for a short resident time condition. In the case of a long resident time, the surface temperature of the 'unaffected zone' actually drops down from its initial value before the wetting front movement. This temperature drop is due largely to conduction of heat towards the central region where the jet is impinging during the resident time. The boiling mode in the central region is film or transition boiling. In this sense the whole solid is actually affected by the quench phenomena but not by the high heat flux associated with wetting. Therefore the 'unaffected zone' is taken to mean the region unaffected by wetting occurring after the resident time and is understood to exist for any resident time during the wetting front movement.

5.2 Maximum Heat Flux Point Propagation

When the wetting front starts moving, the surface temperature drops sharply, a consequence of which the surface heat flux increases dramatically and heat flux reaches its maximum value. The wetting front moves from the central region towards the circumferential region and its position leads the position of MHF point by a certain radial position gap as shown in Fig. 5.1. In Fig. 5.2(a), both the position of the wetting front (from the video image) and the MHF position as a function of time are shown. Due to the limitation of the thermocouple positioning and spacing it is difficult to resolve the maximum heat flux position and hence velocity correctly for $r < 5$ mm. Therefore the results presented in Figs. 5.2(a) and (b) and throughout this article are for radial positions greater than 5 mm where the results are most accurate.

Figure 5.2(a) demonstrates that the position of MHF always lags the wetting front by a certain radial distance, which is kept almost same during the quench. It should be noted here that the wetting front propagation and the MHF point propagation are different phenomena but they are related and their velocity and trend in position are very close. For all cases in the present study where comparison was done with video images we have found that the wetting front movement precedes the movement of maximum heat flux position. The wetting front position has been measured from the video images and the MHF position has been estimated on the basis of the inverse solution. The estimation of MHF position is easier and it is possibly more important than the wetting front position in terms of thermal stress and rapid cooling for practical applications. This is because the drastic surface temperature drop and steep thermal gradients are closely followed by

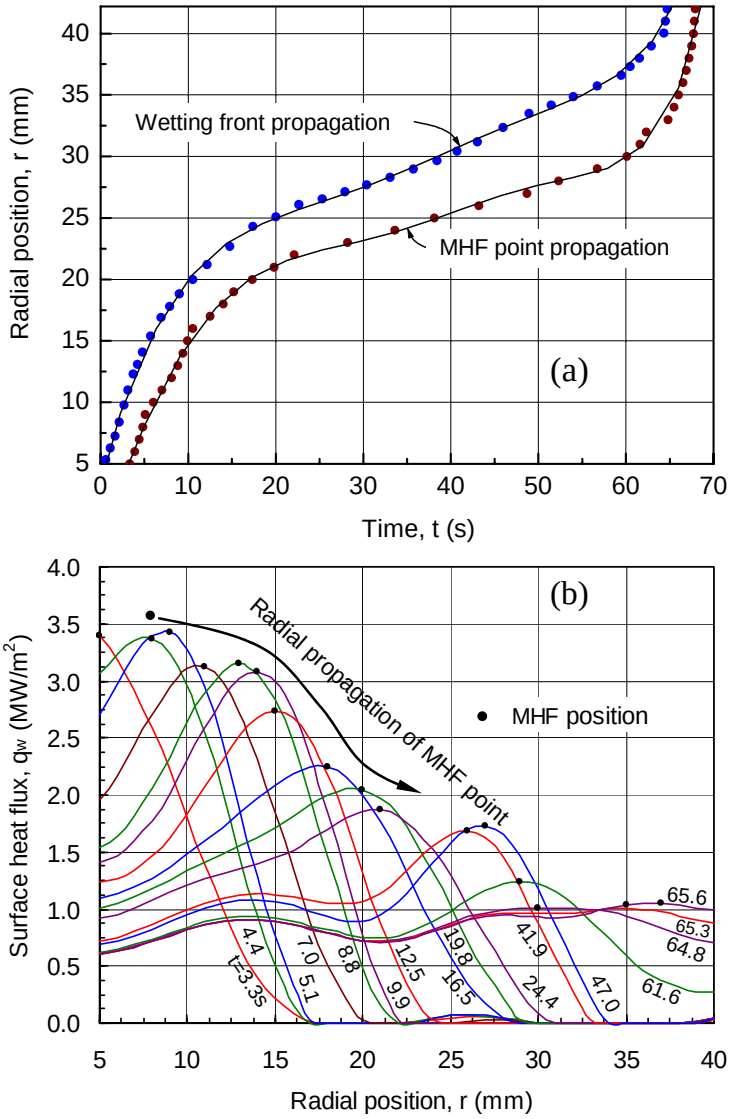

Fig. 5.2: Propagation of maximum heat flux (MHF) and wetting front position (St, T_b = 600 ^oC, ΔT_{sub} = 50 K, u = 5m/s)

and associated with the MHF point. For these reasons, in the present study, more emphasis will be given on the MHF velocity than the wetting front velocity. Just at the position of the visible edge of the wetting front the probable mode of heat transfer is transition boiling while at the position of maximum heat flux the mode is nucleate boiling as discussed in the Chapter 4 and also reported by Mozumder et al. [75].

Figure 5.2(b) also shows a typical heat flux distribution with radial position for different times. The circle symbols indicate the MHF position. For the purpose of analysis of the MHF point propagation, all the data of MHF positions were taken from a similar plotting. Fig. 5.2(b) reveals that the MHF value decreases significantly with increasing radial position and time. This has been found true for a wide range of conditions [75].

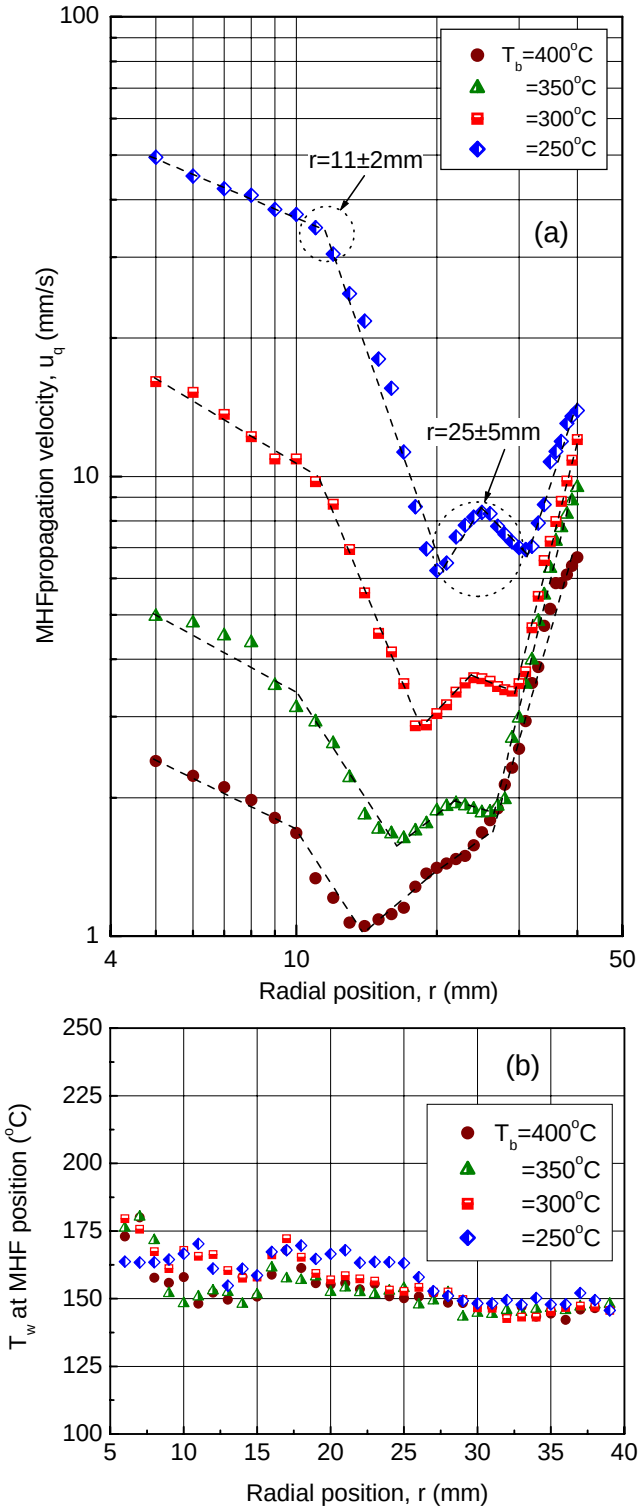

Fig. 5.3: Effect of block initial temperature on MHF propagation velocity (Cu, ΔT_{sub} = 50 K, u = 15m/s, t* < 1 s for all the above conditions)

To determine the MHF velocity, the MHF position data are fitted by the least-squares method to a suitable polynomial as a function of time and then the polynomial equation is differentiated. Figure 5.3(a) for example, also shows the MHF propagation velocity as a

function of radial position. The MHF propagation velocity for most of the cases in this study begins at a high value near the center, which decreases slowly and then more rapidly at a radial position of r = 11 ± 2 mm. The MHF velocity drops to an almost constant value around the position r = 25 ± 5 mm and finally the MHF velocity again increases sharply. The dotted circles in Fig. 5.3(a) indicate these changing trends. The pattern is typical (for most of the experimental conditions shown in Table 2.1) and also can be observed in Fig. 5.2(a) for both the visually observed wetting front and MHF point. A possible mechanism for this behavior of the MHF velocity will be discussed below. Note here that the attained minimum MHF velocity is often an order of magnitude smaller than that obtained MHF velocity near the center of the test piece.

5.3 Block Initial Temperature and MHF Propagation Velocity

Figure 5.3(a) represents the variation of MHF propagation velocity, u_q with radial position for different block initial temperatures. The effect is dramatic. With the increase of block initial temperature MHF velocity decreases for a particular radial position. Note that for all cases in Fig. 5.3, the jet velocity and subcooling were the same. This result is in contrast to maximum heat flux, which is not so sensitive to the initial solid temperature for any given radial position [75]. Also the surface temperature at the maximum heat flux point for different radial positions is shown in Fig. 5.3(b). As can be seen, the surface temperature at the MHF point is almost independent of the block initial temperature. With this in mind Fig. 5.3 leads to the almost inescapable conclusion that solid temperature is important in the mechanism for wetting front propagation. It is difficult to imagine any reason for the decrease in MHF velocity with higher initial temperatures other than the fact that the solid surface must cool for the maximum heat flux point to propagate. The MHF point moves slower if the initial solid temperature is higher simply because for a similar surface heat flux it must take longer to cool the surface ahead of the front. Nonetheless, it is still unclear as to what criteria or mechanism determines the temperature to which the surface must cool.

There is another very important factor for consideration, which is related to the initial block temperature. This is the resident time. Note that in Fig. 5.3(a) for all cases wetting started almost immediately after the jet impinged on the surface. For all the experimental conditions, the surface temperature when the wetting front starts moving is not necessarily the same as the initial solid temperature when the jet first impinged on the surface. It entirely depends on the wetting delay period (or resident time). If the resident time is long,

the surface temperature drops down during the resident period and consequently the wetting front encounters a lower solid temperature when it starts moving. In contrast to short resident times, it is observed that for long resident times the bulk temperature of the solid when the wetting front moves is far below the block initial temperature. Therefore, it is essential to note that the solid temperature distribution when propagation of the MHF point commences is more important than the actual initial temperature when the jet first impinged on the surface. Thus as will be shown below, we found that by categorizing the data on the basis of resident time, many puzzling trends in MHF propagation velocity could be explained well.

The wetting delay period or resident time has been categorized in three groups; short resident time (less than 1 s), moderate resident time (1-200 s) and long resident time (higher than 200 s) in Chapter 3. In Fig. 5.4, three different regimes of resident time have been presented to have an image for the surface temperature (at r = 5 mm) with time. For different resident times the temperature distribution on the surface just at the time when the wetting front started moving is different. For example, the temperature at t* = 987 s for the long resident time curve (a) in Fig. 5.4 is about 190 °C. This is over 200 ^{o}C lower than the initial temperature of 400 °C. At this time the bulk temperature for the solid is also much lower than the initial temperature. In contrast, for case (c) the wetting front starts moving in less than one second and the bulk temperature for the solid and hence most of the surface is still close to the initial temperature of 250 °C. Note that for case (c) the subcooling is greater than for case (a) and the initial temperature is lower. Therefore without considering the resident time, we should expect that the propagation velocity would be faster for case (c) than for (a). However, Fig. 5.4 shows the MHF velocity is actually faster for case (a). The reason is simply that the bulk temperature of the solid is lower than 250 °C when the MHF point started moving in case (a) in spite of the initial temperature of 400 °C when the jet first struck the surface.

A similar story appears comparing cases (a) and (b) in Fig. 5.4. Both the subcooling and the velocity are higher for case (b) than for case (a). Therefore we should expect that case (b) could extract heat faster and hence have a faster propagation velocity for the MHF point. However, Fig. 5.4 reveals that for radial positions less than 30 mm, the moderate resident time case (b) has a much slower MHF velocity than case (a). This time it is because the solid temperature is much higher for case (b) when the MHF point started moving than for case (a).The total time for the quench is of course much longer for case (a)

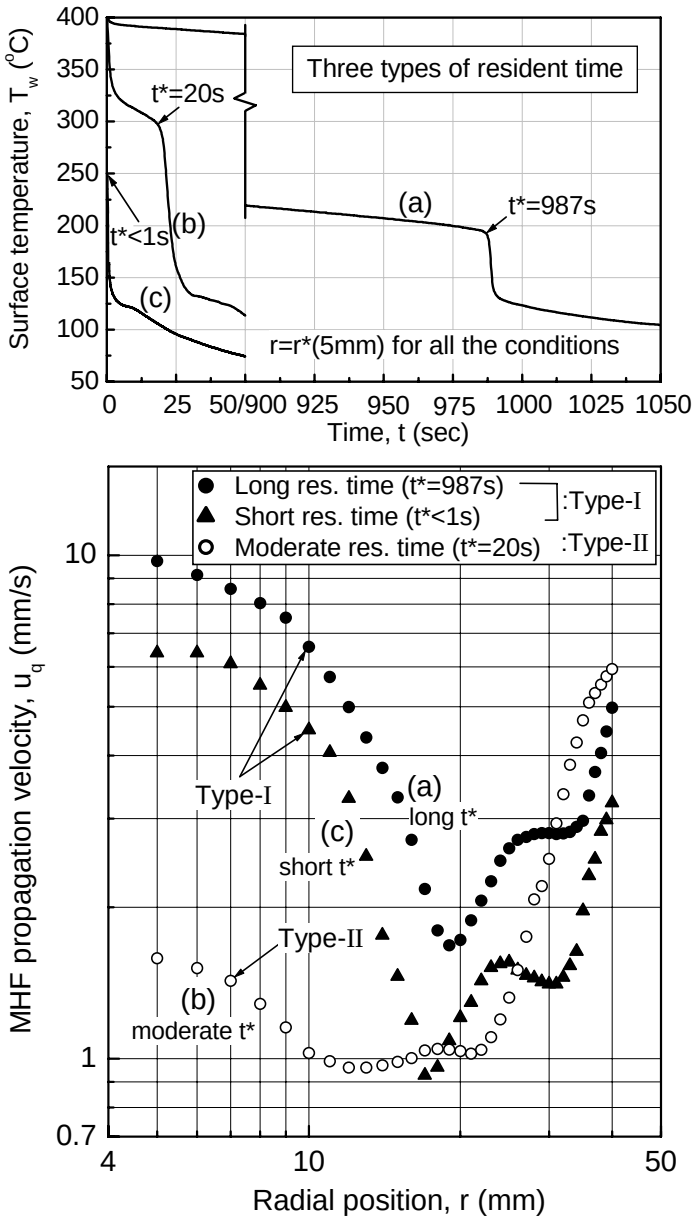

Fig. 5.4: Categorization of MHF propagation velocity on the basis of resident time
(a) Long resident time: copper, T_b = 400 ^oC, ΔT_{sub} = 5 K, u = 3 m/s
(b) Moderate resident time: copper, T_b = 400 ^oC, ΔT_{sub} = 50 K, u = 10m/s
(c) Short resident time: copper, T_b = 250 ^oC, ΔT_{sub} = 80 K, u = 3m/s

than for (b) as should be expected since the velocity and subcooling are higher in case (b). Note that the shape of the MHF propagation velocity curve for case (b) is somewhat different to cases (a) and (c) in Fig. 5.4. We have labeled curves with this character as type-II while curves with the character of (a) and (c) as type-I. Generally, type-II trends in the propagation velocity occurred for moderate resident times while either short or long resident times corresponded to type-I.

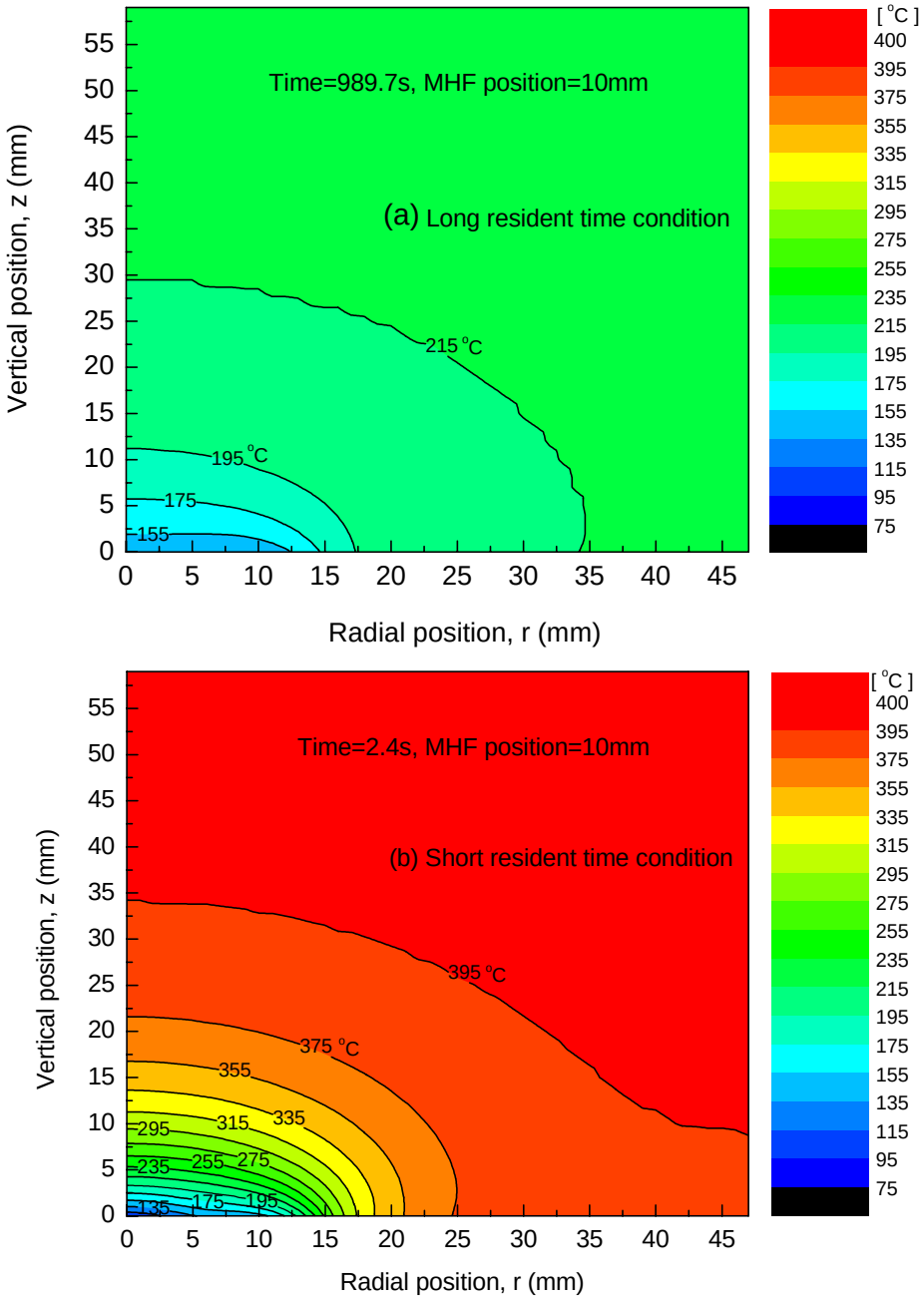

Fig. 5.5: Block inside temperature distribution for short and long resident time
(a) Cu, T_b = 400 °C, ΔT_{sub} = 5 K, u = 3 m/s, t* = 987 s (long)
(b) Cu, T_b = 400 °C, ΔT_{sub} = 80 K, u = 15 m/s, t* < 1 s (short)

It should be mentioned that it is an over simplification to talk about the solid cooling to a 'temperature' during the resident time since the temperature distribution is two-dimensional. However, it is certain that for long resident times the whole test piece does cool before propagation of the MHF point. Figure 5.5(a) shows the temperature distribution in the solid about 3 seconds after resident time for case (a) in Fig. 5.4 calculated using the thermocouple measurements assuming the top and left boundaries are well insulated. Even though the initial temperature was 400 °C, quite clearly the whole test

piece has cooled to below 250 °C. The maximum heat flux position is at r = 10 mm. From this point to the center, the surface temperatures are less than 155 °C. For comparison, a short resident time condition is given in Fig. 5.5(b). Again the maximum heat flux position is at 10 mm. Clearly in Fig. 5.5(b) the bulk of the solid is still close to the initial temperature of 400 °C.

5.4 Effect of Jet Velocity on MHF Propagation Velocity

The result in Fig. 5.3 suggests strongly that heat transfer is a dominating mechanism for determining the propagation rate of the MHF point. We should expect that any circumstances that result in faster surface cooling will also lead to a higher MHF propagation velocity. However, as shown in Fig. 5.4, we must keep in mind that increasing the velocity or liquid subcooling invariably leads to shorter resident times and hence a higher solid temperature when the front starts moving. The effect of the higher solid temperature may be greater than that due to increasing the heat flux so that the surprising effect occurs where for example increasing the jet velocity can reduce the MHF propagation velocity if the resident time is long.

In Figs. 5.6(a) and (b), the variation of MHF propagation velocity with radial position for different values of jet velocity has been shown. Figure 5.6(a) reveals that MHF propagation velocity increases with jet velocity for the short resident time conditions. For short resident time conditions (higher jet velocity and higher subcooling conditions), the wetting front starts moving immediately though at that time most of the surface temperature is high. If the jet velocity is high, the rate of heat extraction from the surface is high which results in an increase of MHF propagation velocity. This trend also continues up to the moderate resident time regime. On the other hand, when the resident time is long (smaller jet velocity and smaller subcooling conditions), MHF propagation velocity decreases with the increase of jet velocity (Fig. 5.6(b)). Within the long resident time regime, increasing the jet velocity decreases the resident time and hence the solid temperature is higher when movement of the MHF point commences. Therefore the MHF propagation velocity usually becomes slower when the jet velocity is increased in the long resident time regime.

In Fig. 5.6(b) the data for u = 15 m/s shows an exception to the above trend. Again this can be explained in terms of heat transfer. While the higher jet velocity resulted in a higher solid temperature in the unaffected zone when the MHF point started movement, the

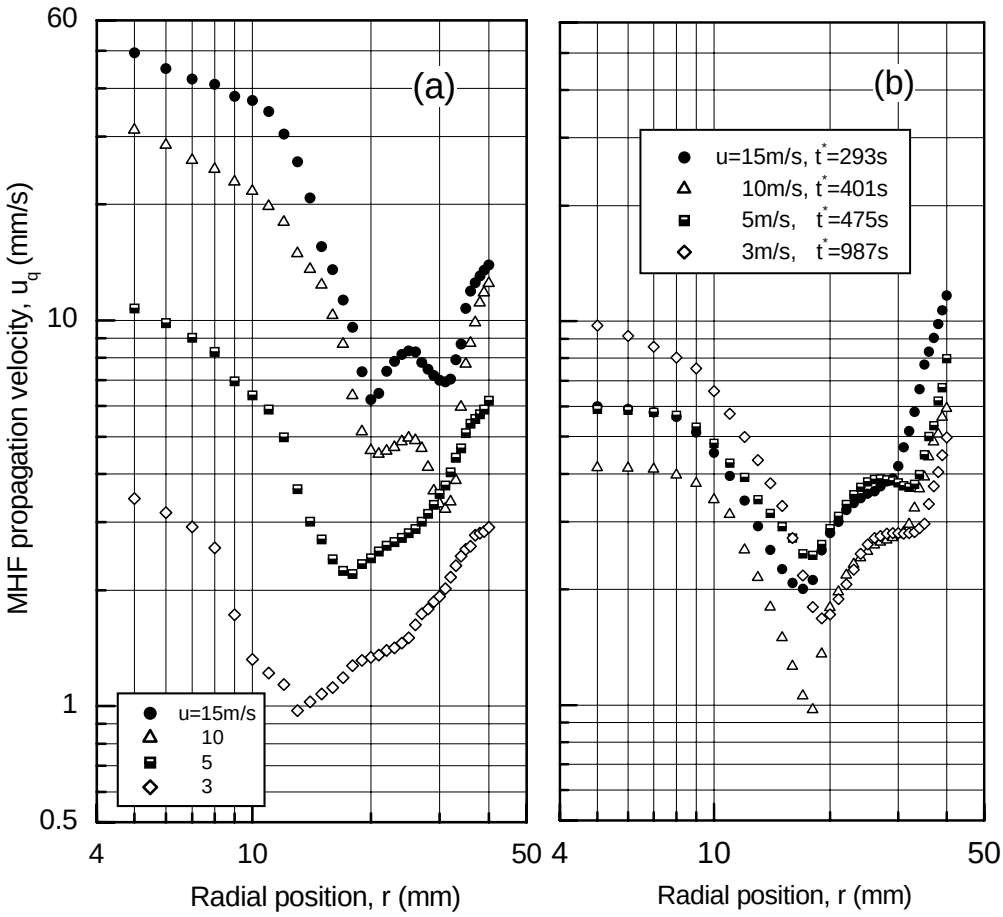

Fig. 5.6: Effect of jet velocity on MHF propagation velocity
(a) Cu, T_b = 250 ^oC, ΔT_{sub} = 50 K (short resident time conditions)
(b) Cu, T_b = 400 ^oC, ΔT_{sub} = 5 K (long resident time conditions)

effect of the higher cooling ability of the 15 m/s jet was greater than the slowing effect of the higher solid temperature. Thus the MHF point moved faster for the case of u = 15 m/s than for u = 10 m/s in Fig. 5.6(b). Exceptions such as this exist for long resident time data particularly when the resident time is reduced to close to the moderate resident time regime.

5.5 Effect of Subcooling on MHF Propagation Velocity

Among various parameters, subcooling is the most dominating for the resident time as discussed in Chapter 3 and also represented by Mozumder et al. [69]. The surface temperature, T_w with time for different subcoolings has been shown in Fig. 5.7, which also clearly represents the trend of cooling curves for different resident times. The smallest subcooling takes the longest resident time (t* = 987 s) and the surface temperature at resident time is the lowest among all the conditions presented in Fig. 5.7. The variation of MHF velocity with radial position for different subcoolings has been also represented in

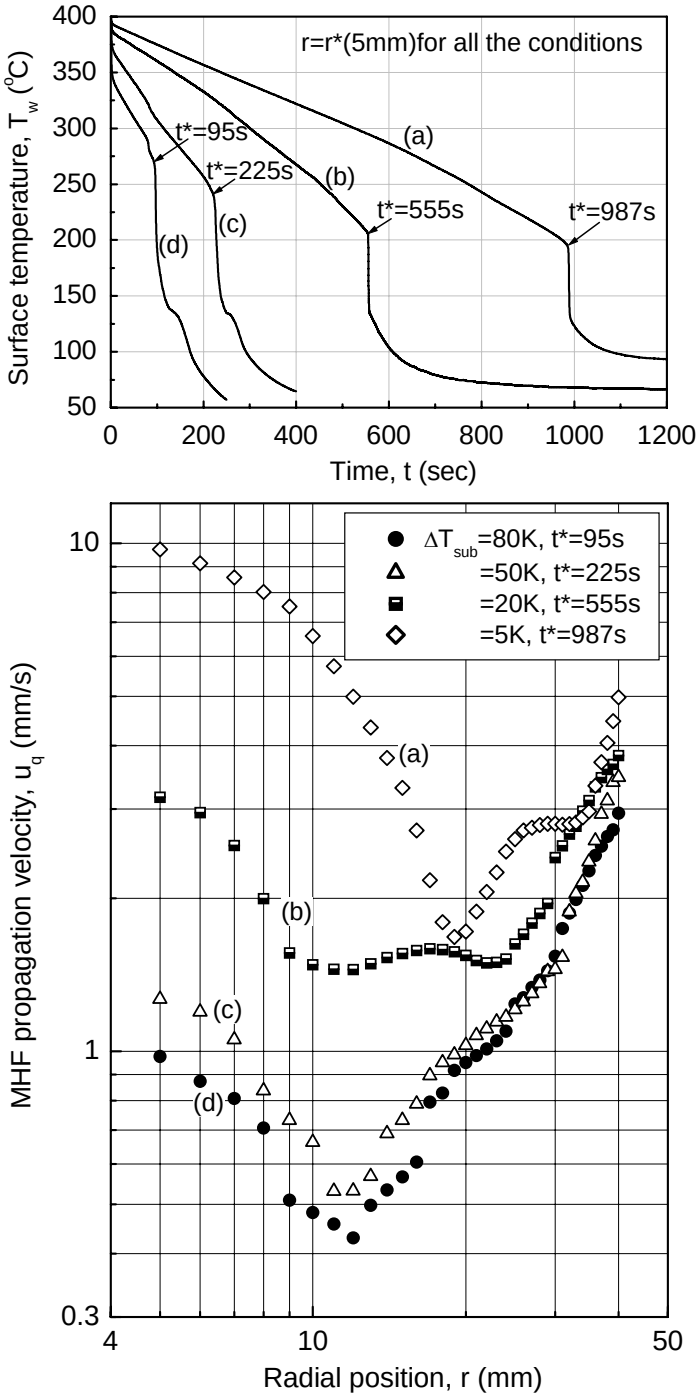

Fig. 5.7: Effect of subcooling on MHF propagation velocity (Cu, T_b = 400 °C, u = 3 m/s) (a) ΔT_{sub} = 5K, (b) ΔT_{sub} = 20 K, (c) ΔT_{sub} = 50 K, (d) ΔT_{sub} = 80 K

Fig. 5.7. According to Fig. 5.7, with the increase of jet subcooling the MHF velocity decreases for a particular radial position. Except for (d), all the conditions in Fig. 5.7 belong to the long resident time regime. Smaller subcooling takes a long time for the wetting front to start movement and consequently the overall surface cooling takes place during this time, which resulted in faster propagation of MHF position. For this reason,

higher MHF velocity is obtained if the subcooling is lower for the long resident time regime. For the short and moderate resident time regimes, the trend is the opposite because the surface temperature in the unaffected zone when the wetting front starts moving is close to the initial temperature of the block.

5.6 Radial Temperature Gradient and MHF Propagation velocity

As mentioned earlier, the surface temperature is the most decisive factor for the velocity of q_{max}. The wetting front or the position of q_{max} moves in the radial direction from the center towards the circumferential region. Therefore, to move in the radial direction for the wetting front, temperature at different radial positions i. e. radial temperature gradient should be an influential factor. Figure 5.8 represents the variation of radial temperature gradient, dT_w/dr with radial position and the corresponding q_{max} velocity for long and short resident time conditions. The radial temperature gradient just at the forward position of the wetting front is a dominating parameter for the q_{max} propagation rate which is also mentioned in the section 5.1. So the value of dT_w/dr has been taken form its forward position and then plotted it with the same position of q_{max}. From Fig. 5.1 it will be clearer. In this figure the q_{max} position is 15 mm (small solid circle) and the value of dT_w/dr is estimated just from a bit higher radial position. Because heat is conducted at a higher rate from this forward region and the value of dT_w/dr is very high at this region which should be responsible for the propagation rate of q_{max}. Then when dT_w/dr is plotted in Fig. 5.8, the corresponding radial position is 15 mm (not higher that 15 mm). Initially both the radial temperature gradient and q_{max} velocity is high and it is true for all the resident time regimes. In Fig. 5.8, only short and long resident time conditions have been shown. The impinged liquid carries higher thermal and hydraulic potential up to a certain radial position from its initial movement and this potential makes the wetting front capable to overcome a higher radial temperature gradient. For this reason, initially the q_{max} velocity is high though the radial temperature gradient is high. After that both the dT_w/dr and q_{max} velocity decrease with radial position. This is true that with decrease of dT_w/dr, q_{max} velocity should increase but in this case solid thermal potential decreases and same time both the thermal and hydraulic potential of the liquid also decreases as it crosses gradually to a greater radial distance. The net balancing results in decrease of q_{max} velocity. The decreasing trend of dT_w/dr continues up to the circumferential region as shown in Fig. 5.8. In this region the radial temperature gradient is so small that the balancing shifts to further

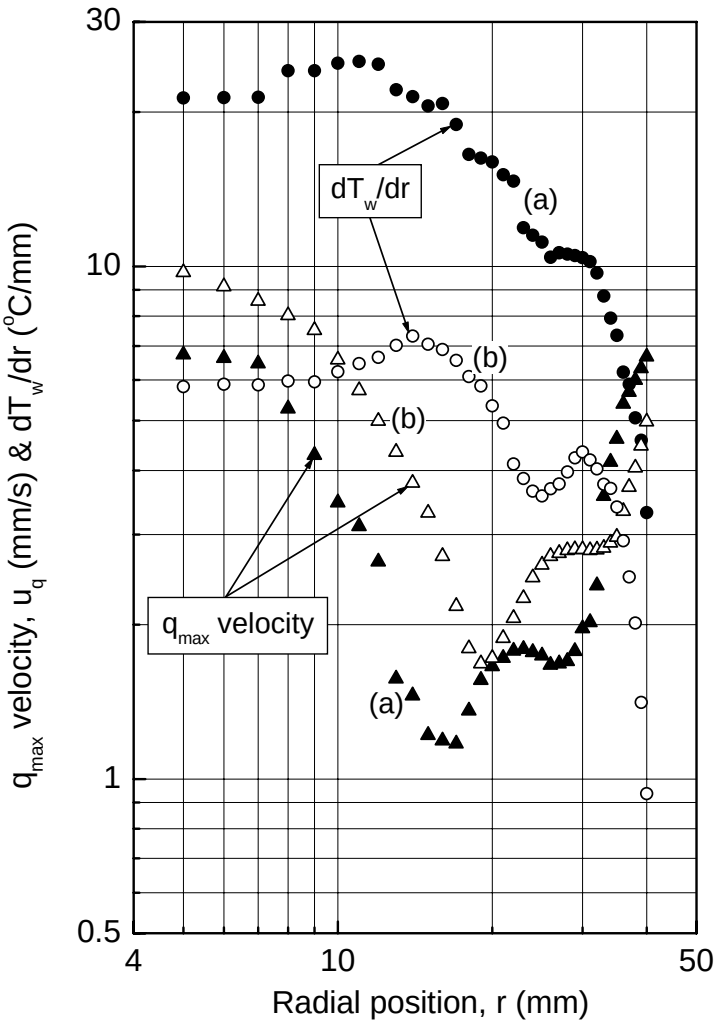

Fig. 5.8: Effect of radial temperature gradient (dT_w/dr) on q_{max} velocity
(a) Cu, T_b = 400 °C, ΔT_{sub} = 80 K, u = 15 m/s (t*<1 s)
(b) Cu, T_b = 400 °C, ΔT_{sub} = 95 K, u = 3 m/s (t*=987 s)

increase of q_{max} velocity though the deterioration of liquid thermal and hydraulic potential continues (as the liquid moves to a greater radial distance).

The trend of q_{max} velocity with radial position is similar for both short and long resident time conditions as shown in Fig. 5.8 but their value for a particular radial position is not the same. For long resident times, the value of dT_w/dr is smaller and the corresponding q_{max} velocity is higher which is expected according to the earlier discussion. In case of short resident times, dT_w/dr is higher and the corresponding value of q_{max} velocity is smaller for a particular radial position which also follows the previous explanation.

Block inside temperature distribution for a particular time and the flow situation on the surface at that time have been presented in Fig. 5.9. The figure also shows the position of maximum heat flux, r_q. Three different regions, 'Wet zone', 'Precursory Cooling Zone, PCZ' and 'Unaffected Zone' as discussed in the section 5.1 also represented in this figure.

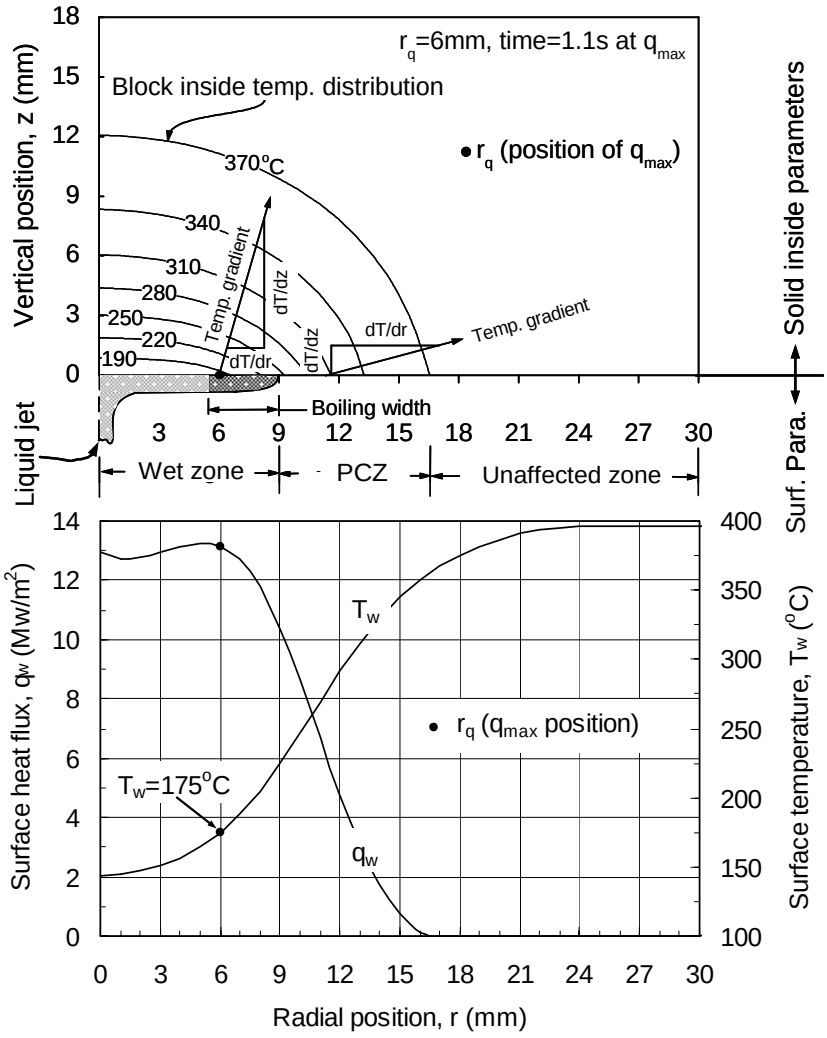

Fig. 5.9: Block inside temperature distribution together with surface temperature and heat flux (Cu, T_b = 400 ^oC, ΔT_{sub} = 80 K, u = 15 m/s)

The constant temperature lines (isotherms) inside the test block have been shown here. The significance of plotting the isotherms inside the block is that the isotherms/constant temperature lines can easily indicate the direction of heat flow inside the solid. Heat flow is always in the perpendicular direction of isotherms. The isotherms shown in this figure are more or less horizontal near the 'Wet zone' and they are close to vertical in the zone 'PCZ'. Therefore, the direction of heat flow on the surface and inside the solid just at the upper portion of the wet zone is almost downward vertical which is nearly horizontal towards the centre at the surface in the PCZ as also shown by the two arrow heads (heat transfer is in the opposite direction of the temperature gradient) in Fig. 5.9. The surface temperature and heat flux distribution has also shown in this figure. By comparing both the surface and the block inside parameters, it can be revealed from the figure that in front of

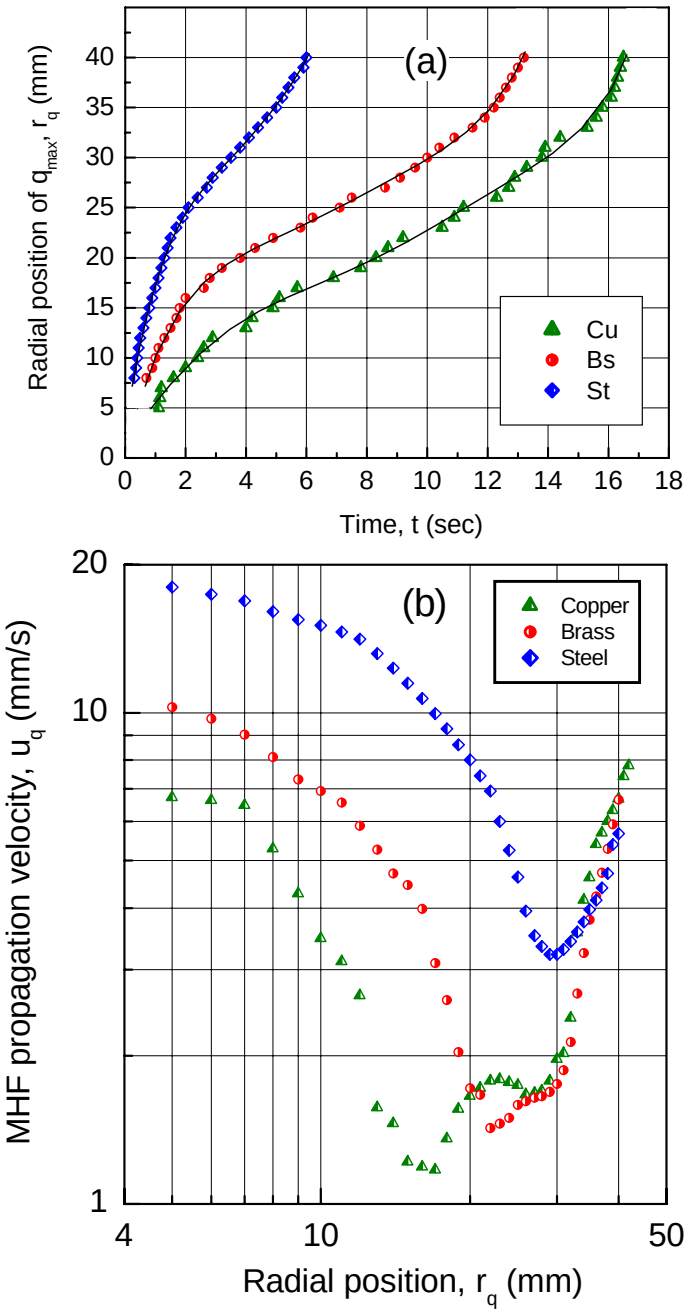

Fig. 5.10: Comparison of q_{max} velocity for three different materials (T_b = 400 ^oC, ΔT_{sub} = 80 K, u = 15 m/s)

the wetting front position, the heat transfer direction is almost in the opposite direction of wetting front propagation. The wetting front has to cool this higher temperature and then it is allowed to move. Therefore, a higher value of dT_w/dr is responsible for a lower q_{max} velocity.

5.7 Material Effect on MHF Propagation Velocity

A comparison for the propagation of maximum heat flux point with time for three different materials copper, brass and steel are represented in Fig. 5.10(a). The corresponding MHF

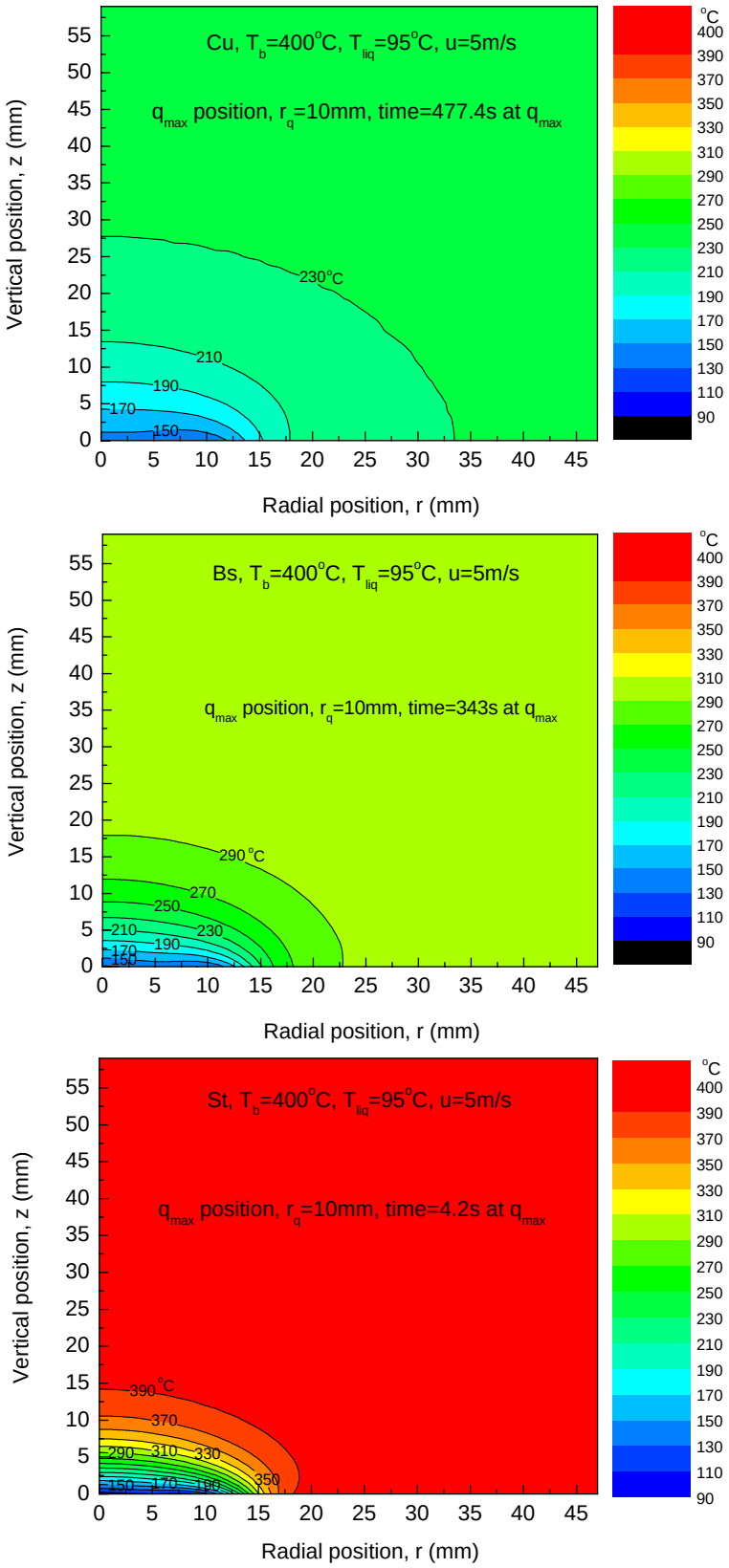

Fig. 5.11: Block inside temperature distribution for a particular position of q_{max} for three different materials (T_b = 400 °C, ΔT_{sub} = 5 K, u = 5 m/s)

point velocities are shown in Fig. 5.10(b). The data in Fig. 5.10 are from the same experimental conditions (T_b = 400 ^oC, ΔT_{sub} = 80 K, u = 15 m/s) with three different materials and belong to the short resident time regime. The MHF propagation velocity for steel is the highest and copper has the lowest value. Due to higher conductivity of copper (λ = 372 W/mK), it can transfer heat with a higher rate but the conductivity of steel is very small (λ = 47 W/mK) which is responsible for poorer conduction of heat towards the boiling region. The conductivity of brass (λ = 146 W/mK) is in between these two materials and this order (copper-brass-steel) in relation to MHF propagation velocity is apparent in Fig. 5.10(b). For steel, the solid is not able to supply heat to the surface like copper or brass so a local region on the surface is easily cooled and the MHF point can propagate quickly. In contrast copper can supply heat quickly to the surface and the temperature and surface heat flux remain high so the MHF propagation velocity is lower.

In direct contrast to Fig. 5.10(b), in the case of long resident time conditions for copper, MHF velocity is the highest for copper among all the materials for the same experimental conditions. The mechanism again relates to the temperature distribution when the MHF point started moving. A higher conductivity and thus a longer wetting delay for copper contribute to an overall cooling of the block prior to movement, which ultimately results in the fastest MHF velocity among three materials.

For a constant liquid potential (ΔT_{sub}= 5 K and u = 5 m/s), the block inside temperature distribution when the q_{max} position reach to 10 mm, has been presented for three different materials in Fig. 5.11. For copper, when the q_{max} position, r_q = 10 mm the whole block gets cooling effect (T_i at any where is less than about 230 ^oC) i.e. greater amount of heat is supplied from other portions of the block towards the boiling region. Relatively less crowded isotherms in copper also show that all the temperature gradients on the surface and inside are milder than that of brass and steel. In the case of steel, when r_q=10 mm the same as of copper, due to poorer supply of heat from the other portions, the temperature at z >15 mm and r>20 mm remains at its initial value. Crowded isotherms also indicate a higher gradient of temperature in steel at this situation. All these thermal characteristics of brass are in between copper and steel. In the case of copper and brass, the surface temperature gradient is stable due to heat supply from the other portion of the solid which helps for maintaining the temperature gradient for a long period of time. This consequences a relatively smaller q_{max} velocity for copper and brass than steel (though the temperature gradient is higher in steel) with same liquid velocity and subcooling as shown in Fig. 5.10(b).

5.8 Mechanism of MHF Point Propagation

From the above observations it is apparent that heat transfer is a dominating mechanism for propagation of the maximum heat flux point. When the resident time is short, factors that increase the heat transfer rate such as increasing jet velocity or subcooling also increase the MHF propagation velocity. Also Fig. 5.3 indicates that the surface must cool and that solid temperature is very important in the mechanism for movement rate of the MHF point. When the resident time is long the trends change because the temperature distribution when the MHF point starts moving becomes more important than the initial block temperature.

If it is noted that in Fig. 5.2(b) the heat flux decreases with radial position, the trend for MHF propagation velocity with radial position also can be explained in relation to heat transfer. Near the center of the test piece the MHF propagation velocity is high as a result of the high heat flux. The MHF propagation velocity then decreases as the heat flux decreases. While this is occurring the precursory cooling zone continuously enlarges lowering the surface temperature ahead of the MHF point. The reduction in surface temperature tends to cause an acceleration of the MHF point since less heat needs to be removed to cool the surface. Finally the MHF position accelerates even more rapidly as the PCZ reaches to the circumference of the test piece. In this region the finite solid can no longer supply heat to maintain a high surface temperature.

One problem with this understanding of the propagation mechanism is it almost implicitly assumes that surface temperature defines the balance point for movement of the MHF position. This may not be the case. Certainly the temperature is important and the range of temperatures suitable for continuous wetting must be significantly smaller than the range of initial temperatures in Fig. 5.3(a) for the present experimental results to make sense. However, the existence of a precise surface temperature relating to this balance is not well established.

Note that the present study focuses on the MHF position rather than the visible leading edge of the wetting front. At the maximum heat flux position, like critical heat flux (CHF) from steady state experiments we expect the actual surface superheat is a by-product of the thermal and hydrodynamic balance for the boiling situation rather than simply a constant value. Nonetheless, as was reported previously, at the MHF position for all of the experimental conditions, the temperature was usually around 130-170 °C with a few exceptions reaching as high as 220 °C or as low as 120 °C. Figure 5.3(b) also shows that the surface temperatures at MHF positions remain within a certain range for any initial temperature of the block. From this it is clear that the surface at the MHF position in the

present experiment must cool to somewhere around this range for propagation of the MHF point. With this in mind it is reasonable to suppose that the apparent importance of temperature may simply be the fact that maximum heat flux happens to occur within a temperature range significantly smaller than the range of initial superheats in the experiment.

For all conditions where comparison was made with video images, the MHF position closely followed the visible edge of the wetting front (Figs. 5.1 and 5.2). At first one would suspect that this is simply an effect of rapid cooling of the surface in the transition-boiling region ahead of the MHF point and conditions at the leading visible edge are of primary importance. However, this seems to ignore the effect of conduction on the solid side and the fact that the vigorous boiling upstream tends to splash out much of the liquid away from the surface. An alternative way to look at the data is to suppose that the visible edge of the wetting front cannot advance much beyond the MHF point because most of the coolant supply upstream is splashed out from the surface in the maximum heat flux region. If this is the case, then the position of the MHF point may be of primary importance to wetting front propagation and the precise temperature or conditions at the visible wetting front may even be of less importance. This would help explain why temperature seems to be important for wetting front propagation (Fig. 5.3) when the actual surface temperature at the visible leading edge of the front is far from a constant and shows much scatter.

5.9 Summary and Comments

Due to involvement of many parameters, the maximum heat flux (MHF) propagation characteristics become a complicated phenomenon. More investigation is indispensable to have a clear picture for this important feature of quenching. A mathematical model and correlation have not yet been derived for the present situation.

The internal temperature distribution has been represented in this chapter to help understanding of both the surface and interior phenomena of the solid simultaneously. The wetting front position is always followed by the position of MHF during quenching. MHF propagation velocity strongly depends on the radial temperature gradient in the precursory cooling zone. On the basis of resident time, MHF propagation velocity could be well explained. When this wetting delay is short, MHF propagation velocity increases with jet velocity and subcooling and decreases with block initial temperature. For the short wetting delay, the bulk surface temperature remains high just before the whole surface wetting starts and consequently MHF propagation velocity is smaller for higher block initial temperature. Surprisingly these trends are opposite for the cases with a long wetting delay.

Chapter 6

Width of Boiling Zone in Jet Impingement Quenching

Boiling width increases with the increase of radial position during the movement of wetting front. The definition of boiling width and some of its characteristics have been mentioned in the earlier chapters. A possible effect of boiling width on the estimation and distribution of maximum heat flux and its propagation velocity will be discussed in this chapter.

6.1 Temperature Gradient during Wetting Front Movement

The main objective for estimating the block inside temperature is to investigate the overall cooling of the block just before and during the wetting front movement and to find out its effect on q_{max} velocity. The block inside temperature distribution with the movement of wetting front position has been shown in Fig. 6.1 for a particular experimental condition. The resident time that corresponds to the condition shown here is less than 1sec and the q_{max} position is 6 mm at t = 1.1 s as shown in the figure. The q_{max} velocity at that time is 6.6 mm/s and the value of dT_w/dr at the forward position (precursory cooling zone, PCZ) of q_{max} is 21 ^oC/mm. From the figure it is clear that the temperature inside the block at a vertical position higher than about 12 mm from the surface is almost its initial temperature 400 ^oC. Two arrow heads indicate the inside and the surface temperature gradient and the width of the hatched area indicates the boiling width at that time. One arrow head is at the position of q_{max} and the other is at the forward dry region (PCZ). The longer arrow head represents a higher temperature gradient. From the figure the sequence of how the distribution changes with time can be observed and the surface and the inside parameters are clear during the movement of wetting front. Initially, the higher vertical position does not get any cooling effect due to quenching. When the q_{max} position reached to 40 mm (last sequence), the highest vertical position (at the central line) temperature is almost 300 ^oC. It indicates that finally the whole block gets the cooling effect (though for the short resident time conditions this effect is not so high). The figure reveals that with the movement of

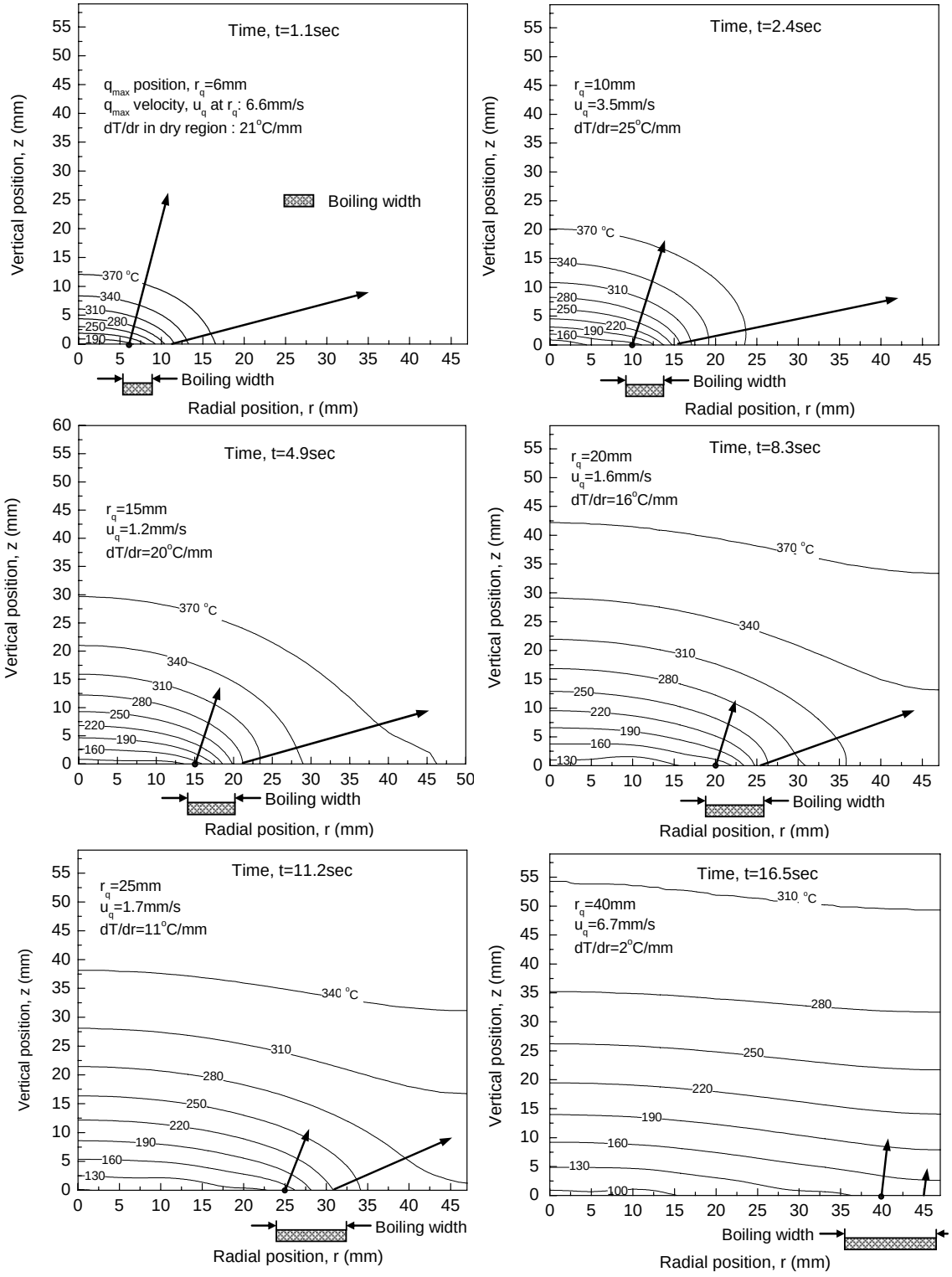

Fig. 6.1: Radial and axial temperature gradient at different position of q_{max} during its movement (Cu, T_b = 400 °C, ΔT_{sub} = 80 K, u = 15 m/s)

q_{max} position, the temperature gradient at both the locations decrease and the isotherms become more and more horizontal. Initially all the isotherms near the q_{max} position are concentric around a small region of high heat transfer. This region may be defined as a heat sink since most of the heat is transferred from this zone. With the increase of q_{max} position, the isotherms are no longer surrounding a narrow region and the sink becomes wider. Therefore, from the analysis of the block inside temperature distribution; it is clear that the most effective heat transfer region increases with the movement of the wetting front. As per the expectation, the video images reveal that the boiling width coincides with the above mentioned heat sink region. Therefore, not only the video images but also the block internal temperature distribution discloses the truth that the boiling width increases with the movement of the wetting front.

6.2 Surface Temperature and Boiling Width

A typical distribution of surface temperature with radial position for a particular experimental condition at different times is shown in Fig. 6.2. The symbol with triangle represents the position of the 'wetting front' (visible leading edge of the boiling region), the solid circle represents the position of 'maximum heat flux' and the rectangular symbol depicts the 'stop boiling' position. The term 'stop boiling' is first introduced in this chapter. The same term was also used by Hammad et al. [63] for the same meaning. As shown in Fig. 5.1 (and also reported by Mozumder at al. [76]), the width of the visible black region is designated as the 'boiling width'. The outer edge of this 'boiling width' is defined as the 'wetting front' and the inner edge is by 'stop boiling'. It is assumed here that the boiling is stopped (or not vigorous) and the forced convection mode of heat transfer becomes dominating in the radial position located at the further inside of the 'stop boiling'. The temperature at the stop boiling is significantly higher than 100 ^{o}C as shown in Fig. 6.2. Therefore, there is a chance of boiling but video clip as represented in Fig. 5.1 shows that the stop boiling region's corresponding color is not dark. The dark region is described as the vigorous boiling region in this study. So, this might be explained in this way that boiling at a lower intensity (not vigorous nucleate) might happen in that position and somehow the visual observation can not detect that.

The main objective of this section is to introduce a possible interrelation between the surface temperature and boiling width. The surface temperature at maximum heat flux

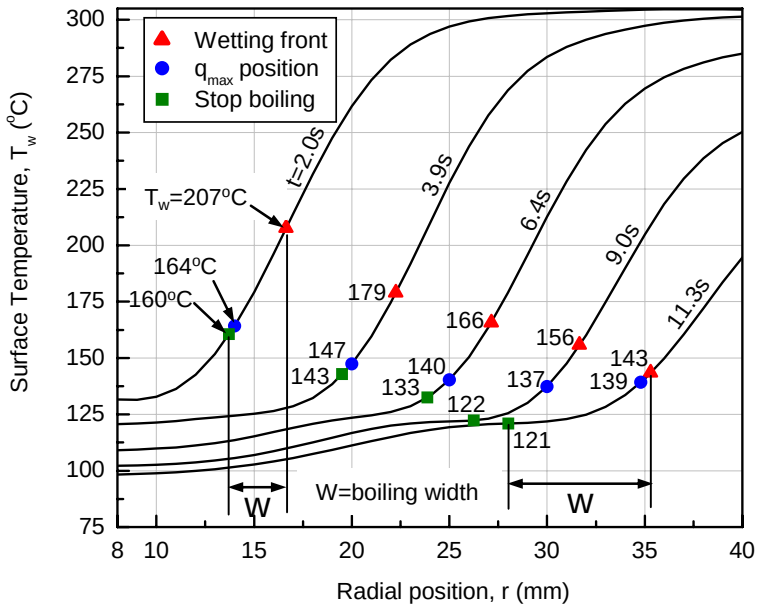

Fig. 6.2: Relation between boiling width and surface temperature
(Bs, T_b = 300 °C, ΔT_{sub} = 50 K, u = 5 m/s)

position is always within a certain range for any experimental condition shown in Table 2.1. This range is 120-200 °C as mentioned in the section 4.1 and this range is considered as the temperature range for the nucleate boiling in this study. In Fig. 6.2, the wetting front and the stop boiling position are detected from the video images. The corresponding surface temperatures at these key positions are estimated from the inverse solution. All of the boiling phenomena for this particular experimental condition are shown in Fig. 6.2. The q_{max} position is always in between the position of wetting front and stop boiling and the surface temperature for q_{max} is also always in between the temperature of the wetting front and the stop boiling as expected.

Figure 6.2 also reveals that the surface radial temperature gradient in the boiling zone decreases with radial position. The nucleate boiling temperature range covers more area if the radial temperature gradient is smaller. Therefore, it is easy to expand the boiling temperature range in the wider region where the temperature gradient is smaller and thus the boiling width, W increases with radial position as shown in Fig. 6.2.

6.3 Boiling Width and Solid Material Property

Variation of block inside temperature distribution for two different materials, copper and brass are exhibited in Fig. 6.3. Two types of comparison can be done from Fig. 6.3; Figs. 6.3(a) and (b) compare the contour plot (isothermal lines) between the time when the q_{max}

position is respectively at 10 and 35 mm for a single material copper. The same comparison can be done if the Figs. 6.3(c) and (d) are considered for brass. Again if Figs. 6.3(a) and (c) are compared, the effect of material on isothermal lines for a specific situation when r_q = 10 mm can be obtained. The same comparison can be done when Figs. 6.3(b) and (d) are considered for r_q = 35 mm.

Figures 6.3(a) and (b) reveal that during the movement of the q_{max} position (from 10 to 35 mm), the overall block temperature dropped down to less than 200 ^oC and the radial temperature gradient, dT_w/dr reached to a small value (as isotherms become less dense). This distribution of isotherms indicates that an overall cooling was done during the wetting front movement. In addition, as discussed in Fig. 6.1, the low density spacing of isotherms indicates that the boiling width is greater. Figs. 6.3(c) and (d) show that only a small portion of the impinged surface cooled during the wetting front movement. The isotherms of Fig. 6.3(d) indicate that the boiling width for steel is not as wide as copper (shown in Fig. 6.3(b)) because of the higher density of isotherms of steel compared to copper. One of

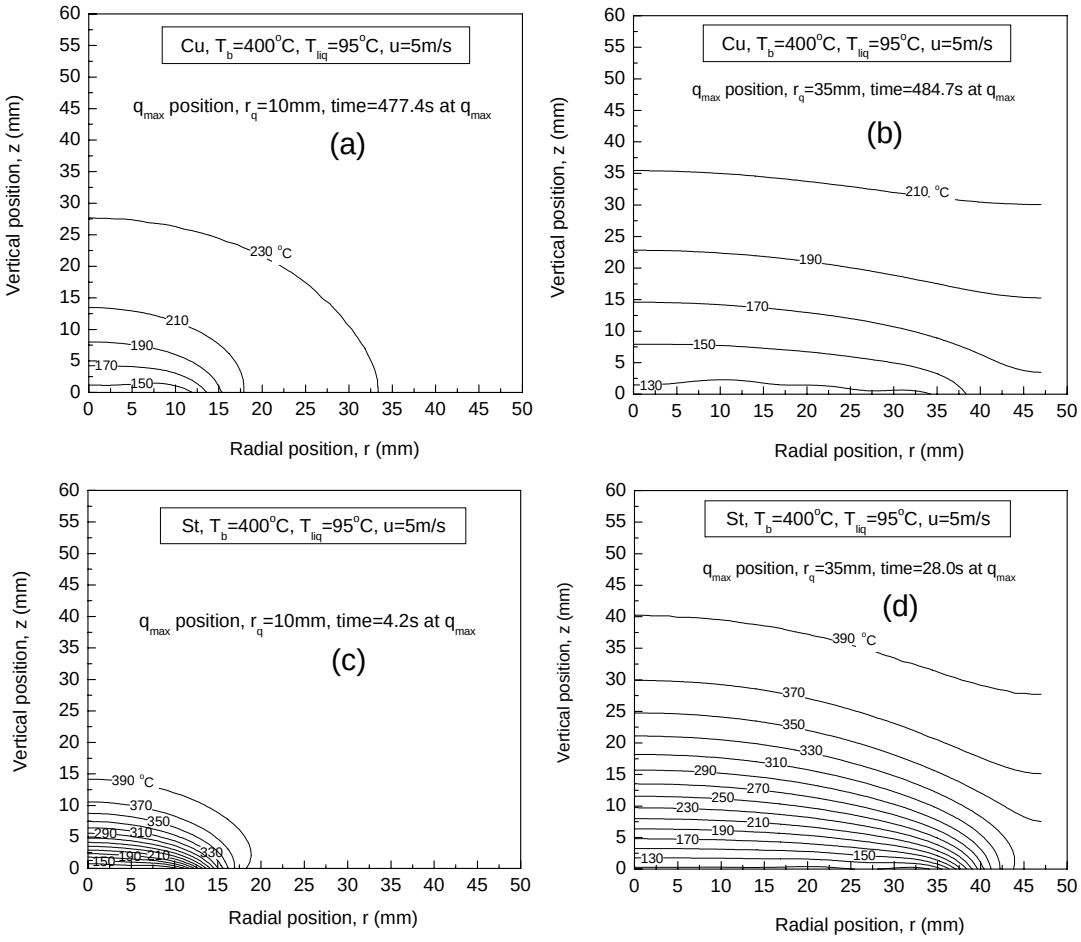

Fig. 6.3: Variation of block inside temperature distribution due to movement of q_{max} position for two different materials (T_b = 400 ^oC, ΔT_{sub} = 5 K, u = 5 m/s)

the important findings from Fig. 6.3 is that for a particular experimental condition and for a certain position of wetting front (or q_{max}), the boiling width should be wider in copper than steel. This verification on the basis of visual observation has been conducted for few available captured video images, one of which is shown in Fig. 6.4. Due to difficulty for capturing quality video images during quenching, the verification within a wide range of experimental conditions has yet to be done. Figures 6.4(a) and (b) reveal that for the same wetting front position, 32 mm, the boiling width for copper is 18.3 mm and that of brass is 13.7 mm. For better estimating the surface heat flux and proposing a quenching model with different materials this trend of boiling width is important.

6.4 Boiling Width, MHF velocity and MHF

6.4.1 Boiling width and MHF propagation velocity: As discussed in the section 5.6 that when the radial temperature gradient dT_w/dr decreases the maximum heat flux point velocity increases. Again, the decrease of value of dT_w/dr is an indication of decreasing the density of isotherms inside the solid (as shown by Fig. 6.1 in section 6.1) and ultimately

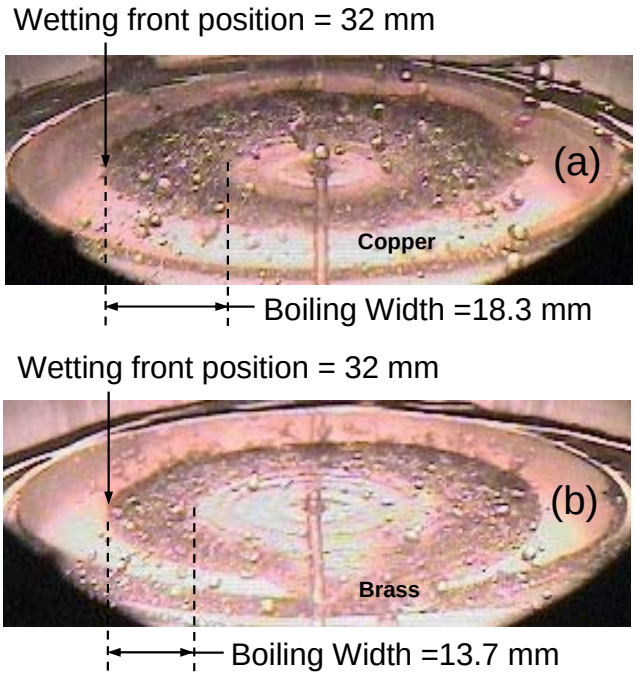

Fig. 6.4: Variation of boiling width with materials for the same wetting front position
(a) Cu, T_b = 300 ^oC, ΔT_{sub} = 20 K, u = 3 m/s, long resident time
(b) Bs, T_b = 300 ^oC, ΔT_{sub} = 20 K, u = 3 m/s, short resident time

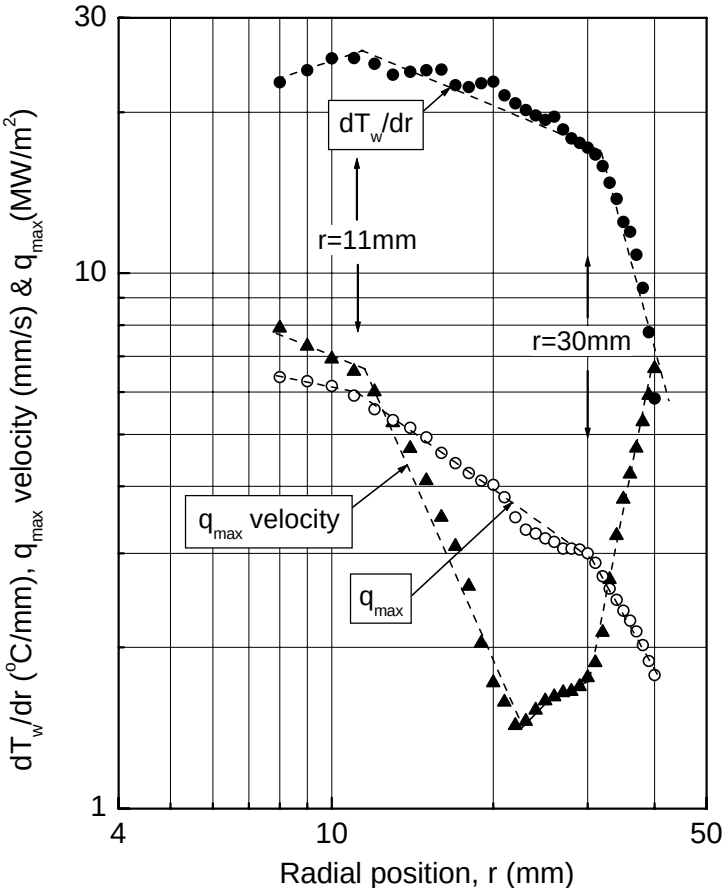

Fig. 6.5: Comparison of dT_w/dr, q_{max} velocity and q_{max} (Bs, T_b = 400 °C, ΔT_{sub} = 80 K, u = 15 m/s)

provides an indication of the increase of boiling width. When the temperature gradient becomes mild, the boiling width increase and heat is transferred from a bigger area which consequences less resistance for the wetting front or q_{max} point to move within this area. Therefore, when the temperature gradient decreases; boiling width increases and MHF velocity increases (in the higher radial position zone) as shown in Fig. 6.5. In the smaller radial position zone, the value of dT_w/dr is so high that though the boiling width increases continuously with radial position, the wetting front could not overcome the resistance due to higher temperature gradient. Actually, a balancing among the liquid thermal potential, hydrodynamic potential and solid thermal potential dominate the phenomena. Therefore it is difficult to explain the characteristics of MHF velocity with a single variable.

6.4.2 Effect of MHF propagation velocity on MHF value estimation: The surface temperature and heat flux data obtained in the present study have originated from a transient experiment. The heat transfer characteristics in transient experiments are a bit different to those of steady state experiments. The limitation due to instrumental facility and the inverse solution might cause a significant deviation of the result from its actual

value in the case of a transient experiment. If the experiment is more transient, the response of the thermocouple might reduce the accuracy of the measurement due to the drastic change of temperature which results an underestimation of surface heat flux by the inverse solution. The thermocouple response is not the only cause for this underestimation of the heat flux data during high a transient experiment. Also the inverse solution itself has time and space resolution limitations. The thermocouple response of the present study is about 0.1sec. So it might play a role for not capable of capturing sudden changes of temperature. But the recent numerical analysis of Woodfield et al. (first author of ref. [24]) shows that thermocouples with zero time lags might underestimate the heat flux data also. Therefore, whatever is the thermocouple response; the more transient the more will be the deviation of measured data from its actual value. The above discussion is necessary to explain the trend of q_{max} , q_{max} velocity and dT_w/dr all together as shown in Fig. 6.5.

The q_{max} velocity decreases with radial position in a higher rate at about r = 11 ± 2 mm and finally it again starts increase at the position of r = 25 ± 5 mm as shown in Fig. 6.5. Both the q_{max} and dT_w/dr change their trend at the same positions. The most important discussion point of view at present is to compare the trend of q_{max} velocity and q_{max} itself. When the value of q_{max} from transient experiment of the present study has been compared with the value of critical heat flux from steady state experiment [70], it is found that both the values decrease with radial position having same slope (at constant rate) in the range r = 11~25 mm [75]. This might be an indication that the accuracy of the estimated q_{max} value is better in this region. If it is true then from Fig. 6.5, it can be agreed that inside and outside of this region the accuracy for the q_{max} value is not as high as in the region r = 11~25 mm. Because if the line for the constant slope (of the region of r = 11-25 mm) as shown in Fig. 6.5 is extended to the other radial positions, it is found that both in the regions r<11 (≈11 ± 2) mm and r>30 (≈25±5) mm, the q_{max} value is a bit underestimated from the expected value on the constant slope line. In these underestimated regions, the MHF velocity is very high compared to the middle region where the q_{max} value has been better estimated. So the MHF velocity might be one of the reasons for the underestimation of the value of q_{max} itself. It can be explained in this way that when MHF velocity is very high, the wetting front moves at a much faster rate over the hot surface and consequently the heat transfer becomes more transient which results in underestimation of the heat flux value. If the MHF velocity over the whole range of radial positions is constant, it can be expected that a same trend of q_{max} over the whole radial position could be obtained unless

other parameters affect the trend. But the reality is different, the MHF velocity changes from position to position and the intensity of transiency changes accordingly. Faster MHF velocity (or wetting front velocity) intensifies the transiency and decreases the heat flux.

It is important to discuss here that the increase of MHF velocity after radial position, r = 25 ± 5 mm can not be interpreted as of the end effect of the test section. The radius of the test section is 47 mm while the analysis conducted in the present study is for r = 5-40 mm. From Fig. 5.10, it is clear that the MHF velocity of copper (T_b = 400 ^oC, ΔT_{sub} = 80 K, u = 15 m/s) starts increasing from r = 20 mm. The block inside temperature distribution for the same experimental condition of copper has been also presented in Fig. 6.1. From the sequence of Fig. 6.1 at time, t = 8.3 s, it is shown that the q_{max} position, r_q is 20 mm and at this time the surface temperature near the circumference is about 330 ^oC which has not yet decreased too much from its initial value 400 ^oC. Thus, by comparing these two figures, it can be revealed that when the MHF velocity starts increasing (at r = 20 mm), the circumferential region of the test block is still hot and which indicates that the increasing trend of the MHF velocity is not determined by the end effect of the test block. In the case of steel, MHF velocity starts increasing from r = 30 mm (Fig. 5.10), it is found that at this position of q_{max}, the surface temperature of the circumferential region is still 400 ^oC which is its initial temperature. This also conforms the independency of end effect on MHF velocity results. The end effect might have a negligible influence on MHF velocity near the circumferential region which might not affect the trend of the result obtained in the present study. A weak end effect independency of MHF velocity is also ensured by another material brass.

6.5 Summary and Comments

A lot of variables are involved in different processes and sub-processes in quenching. Starting from the thermo-physical properties of the solid and liquid, all of the experimental parameters considered are associated with this complicated quenching phenomenon. Some of the important variables other than experimental parameters that have been considered in the present investigation could be mentioned including the resident time, the boiling sound, the wetting front velocity, the maximum heat flux velocity, the flow pattern and so on which were also judged by other researchers as they appeared in the literature. In this chapter a new variable the ‘boiling width’ has been introduced, an extensive studies of which may be for the first time in literature. The moving dark region preceded by the wetting front is described as the boiling width. This boiling width could be considered as a

moving heat source for the modeling/numerical simulation of jet quenching. The effect of the boiling width on jet impingement quenching has been investigated in this chapter. The dominating parameters for the boiling width have been also explored.

Boiling width increases with the increase of radial position. In the central region, the surface radial temperature gradient is high during quenching and the bulk radial temperature gradient decreases with time and radial position. Boiling width is greatly influenced by the radial temperature gradient. The higher the gradient, smaller is the boiling width. When the boiling width is wider, the MHF propagation velocity is higher. On the other hand, MHF propagation velocity has large influence on the q_{max} value and its distribution. Therefore, there is a possibility that boiling width can contribute on the heat flux magnitude and its orientation (or the reverse may be true since this issue is yet to be clarified). Material thermo-physical properties also affect the width of the boiling region. When all the experimental parameters remain the same, for a particular position of wetting front, the boiling width is observed to be wider for copper than brass. More extensive studies for this new parameter ‘boiling width’ are indispensable and may contribute for a clearer understanding of the complicated quenching phenomenon.

Chapter 7

Conclusions and Future Directions

Each chapter gives brief conclusions, comments, and summary of the specific themes investigated relevant to the chapter. The concluding remarks as a whole of this dissertation, the unsolved analysis for this investigation and the future direction of concern are highlighted in this chapter.

7.1 Conclusions

With the combination of different means including an inverse solution, visual observation and audible inspection the present study has been conducted to investigate the distinct features of jet quenching. Much effort has been devoted to find out the key parameters responsible for the resident time (i.e. time from when the jet strikes the surface to when the wetting front starts to move) and temperature at that time, maximum heat flux and its propagation velocity. There are very few publications in the literature that give insight into maximum heat flux and resident time in jet impingement quenching. In this sense the present investigation has made some important contributions in this field. Further comprehensive study is indispensable for understanding these complicated phenomena. Overall intrinsic achievements at present from this investigation are summarized as:

1. The heat flux always attained to its maximum value immediately after the resident time.

2. Initially (before the wetting front movement) the covered central wetted region has a radius of 5 ± 1 mm for copper and 8 ± 3 mm for brass which was almost constant for whole range of experimental conditions in the present study.

3. Resident time could be categorized in three groups on the basis of a velocity-subcooling factor ($u\Delta T_{sub}$) and the shape of the cooling curves.

4. The resident time is a strong function of the properties of the solid material and sub-cooling of the jet. It is also a function of the jet velocity and initial surface

temperature. The proposed correlations for the resident time and temperature agree well with the corresponding values from the experiment and the inverse solution over certain ranges in the present study.

5. The maximum heat flux always occurs during the movement of the wetting front. During this movement the position of the maximum heat flux also moves from the center towards the circumference. During this radial movement, the maximum heat flux is found to occur within the visible boiling region for any experimental condition. Stable nucleate boiling is established at the position of maximum heat flux.

6. Maximum heat flux, MHF is a strong function of jet velocity and thermal properties of block material. It is also a moderate function of jet subcooling. MHF is a weaker function of the block initial temperature, T_b.

7. The maximum heat flux in the region II for copper and brass can be predicted with an accuracy of ± 30 % by Eq. (4.4) together with Eq. (4.1).

8. On the basis of the resident time MHF propagation velocity can be categorized well. For the case of long resident time, the whole block gets a cooling effect before the wetting front starts moving which favors higher MHF propagation velocity. The opposite is true for the short resident time.

9. MHF propagation velocity increases with increasing jet velocity and subcooling and decreases with increasing block initial temperature for a particular radial position in the case of short resident time. This trend is opposite when the experimental conditions are within the long resident time category.

10. MHF propagation velocity sequentially increases from copper, brass and steel for the same experimental conditions for short resident times. The trend is opposite for long resident time conditions (although no long resident time data for steel appeared for T_b = 250-400 ^oC), which reflects the effect of material thermal properties on MHF velocity.

11. Radial temperature gradient, MHF propagation velocity and the value of maximum heat flux all are interrelated and change their trend at particular radial positions. This relation has not yet been clarified.

12. Surface radial temperature gradient decreases and boiling width increases with the increase of radial position and time. Boiling width for copper is wider than that of steel for a particular position of wetting front and for a particular experimental condition.

7.2 Direction for Future Work

In this science era, faster growing technology promotes mankind to augment their standard of living. The prerequisite for this technological development is the research and development in the sector of science and technology. Human beings are eagerly awaiting for the latest invention which leads to the consequence that research and development are an endless job. In this context, the research work delineated in this dissertation may serve as a primary foundation for some of the phenomena which will lead to future study. A lot of investigation is unavoidable for this complicated phenomena. A few directions of future work are depicted here which exclude the fundamental accomplishments of the present study.

7.2.1 Analytical task

Other than experimental work there are some mandatory analytical jobs that have to be performed for clear understanding of quenching mechanism. At the moment the following issues are highlighted that have to be carried out in future studies.

1. An analytical model for the resident time and the surface temperature at the wetting front at resident time is indispensable in jet quenching.

2. The proposed correlations for the resident time and the surface temperature have not yet been non-dimentionalized. The physical interpretation for the group of parameters used in the resident time and temperature correlations has to be clarified.

3. The trend of steel in the correlation of maximum heat flux has not been clarified properly. This could be done with the appropriate modification of the correlation by considering the behavior of steel. The correlation for Region II has been proposed but that of Region I has yet to be explored.

4. The effect of experimental parameters on the MHF velocity has not yet been verified by any analytical model.

5. A thermal and hydrodynamic balancing criteria between the impinged liquid and the solid surface for the movement of the wetting front is the keen interest in the jet impingement quenching which is yet to be done.

7.2.2 Experimental upgrade

Better experimental facility is the preliminary criteria for good data, and then the analysis plays the role for good findings. The used experimental apparatus were so far sophisticated and reliable but the physical phenomena for quenching demands much faster and more precise instruments. Following are some of the critical devices those need to be replaced for better quality of data.

1. The time response for the thermal history measuring device is to be faster as the phenomena is expected to change within a millisecond whereas the time response for the used thermocouple is about 0.1 s.

2. As the phenomena during quenching changes within fraction of a millisecond, faster frame rate per unit time of the high speed video camera is obvious to capture that moment of the phenomena.

3. The temperature of the liquid was difficult to maintain at the desired value especially for long cooling conditions. A feed-back control system could be incorporated which will control the liquid temperature automatically during quenching period by sensing the present liquid temperature and by regulating the heating or cooling system.

References

1. R. G. Owen and D. J. Pulling, Wetting Delay: Film boiling of water jets impinging hot flat metal surfaces, in T. Nejat Veziroglu (Ed.), *Multiphase transport fundamentals*, reactor safety, applications, Clean Energy Research Institute, University of Miami, Vol. 2 (1979) 639-669

2. J. D. Bernardin, and I. Mudawar, The Leidenfrost point: experimental study and assessment of existing models, ASME *Journal of Heat Transfer* 121 (No. 4) (1999) 894-903

3. S. S. Dua and C. L. Tien, An Experimental Investigation of Falling-Film Rewetting, *International Journal of Heat Mass Transfer* 21 (1978) 955–965

4. O. C. Iloeje, D. N. Plummer, W. M. Rohsenow and P. Griffith, Effect of Mass Flux, Flow Quality, Thermal and Surface Properties of Materials on Rewet of Dispersed Flow Film Boiling, Trans. ASME, *Journal of Heat Transfer* 104 (1982) 304–308

5. D. H. Wolf, F. P. Incropera and R. Viskanta, Jet Impingement Boiling, In Advances in *Heat Transfer* (Edited by J. P. Hartnett et al.), Vol. 23, pp. 1–132. Academic Press, New York (1993).

6. Y. Barnea, E. Elias, and I. Shai, Flow and Heat Transfer Regimes During Quenching of Hot Surfaces, *International Journal of Heat Mass Transfer* 37 (1994) 1441–1453

7. Nukiyama. S., The maximum and Minimum Values of Heat Transmitted from Metal to Boiling Water Under Atmosphere Pressure, J. Soc. Mech. Eng., 37, 367-374, 1934 (Translated: *International Journal of Heat Mass Transfer* 9 (1966) 1419-1433

8. S. Kumagai, S. Suzki, Y. Sano and M. Kawazoe, Transition Cooling of a Hot Metal Slab by an Impinging Jet with Boiling Heat Transfer, ASME/JSME *Thermal Engineering Conference* 2 (1995) 347–352

9. Y. Mitsutake and M. Monde, Heat Transfer During Cooling of High Temperature Surface with an Impinging Jet, *Heat and Mass Transfer* 37 (2001) 321–328

10. J. Filipovic, F. P. Incropera, and R. Viskanta, Quenching Phenomena Associated with a Water Wall Jet: I. Transient Hydrodynamic and Thermal Conditions, *Experimental Heat Transfer* 8 (1995) 97–117

11. M. Ciofalo, I. D. Piazza and V. Brucato, Investigation of the Cooling of Hot Walls by Liquid Water Sprays, *International Journal of Heat Mass Transfer* 42 (1999) 1157–1175

12. T. Ueda, S. Tsunenari and M. Koyanagi, An Investigation of Critical Heat Flux and Surface Rewet in Flow Boiling Systems, *International Journal of Heat Mass Transfer* 26 (1983) 1189–1198

13. T. Ueda and M. Inoue, Rewetting of a Hot Surface by a Falling Liquid Film-Effects of Liquid Subcooling, *International Journal of Heat Mass Transfer* 27 (1984) 999–1005

14. J. D. Bernardin, Clinton J. Stebbins and Issam Mudawar, Mapping of impact and heat transfer regimes of water drops impinging on a polished surface, International Journal of Heat Mass Transfer 40 (No. 2) (1997) 247-267

15. D. E. Hall, F. P. Incropera and R. Viskanta, Jet impingement boiling from a circular free-surface jet during quenching: Part2-two-phase jet, ASME *Journal of Heat Transfer* 123 (No. 4) (2001) 911-917

16. J. Hammad, Y. Mitsutake, and M. Monde, Movement of Maximum heat flux and wetting front during quenching of hot cylindrical block, *International Journal of Thermal Sciences* 43 (2004) 743-752

17. M. Monde and Y. Katto, Burnout in a high heat flux boiling system with an impinging jet, *International Journal of Heat and Mass Transfer* 21 (1978) 295-305

18. X. Liu, J. H. Lienhard V, J. S. Lombara, Convective heat transfer by impingement of circular liquid jets, ASME *Journal of Heat Transfer* 113 (1991) 517-582

19. D. E. Hall, F. P. Incropera and R. Viskanta, Jet impingement boiling from a circular free-surface jet during quenching: part1- single-phase jet, ASME *Journal of Heat Transfer* 123 (2001) 901-910

20. H. Lienhard V, X. Liu and L. A. Gabour, Splattering and heat transfer during impingement of a turbulent liquid jet, ASME *Journal of Heat Transfer* 114 (No. 2) (1972) 362-372

21. B. D. G. Piggott, E. P. White and R. B. Duffy, Wetting delay due to film and transition boiling on hot surfaces, *Nuclear Engineering and Design* 36 (1976) 169-181

22. J. Hammad, Characteristics of heat transfer and wetting front during quenching high temperature surface by jet impingement, *PhD thesis*, graduate school of science and engineering, Saga University, Japan, 2004

23. P. L. Woodfield, M. Monde and A. K. Mozumder, The possibility of homogeneous nucleation boiling during transient liquid/solid contact in a jet impingement quench cooling system, *Thermal Science & Engineering* 12 (No. 4) (2004) 39-40

24. P. L. Woodfield, M. Monde and A. K. Mozumder, Observations of high temperature impinging-jet boiling phenomena, *International Journal of Heat and Mass Transfer* 48 (2005) 2032-2041

25. S. K. Bhunia, J. H. Lienhard V, Splattering of turbulent liquid jets impinging on solid targets : Parametric studies, *28th National Heat Transfer Conference*, General paper in heat transfer, ASME HTD, August, 204 (1992) 165-171

26. Y. Iida, K. Okuyama, and K. Sakurai, Peculiar bubble generation on a film heater submerged in ethyl alcohol and imposed a high heating rate over 10^7 Ks^{-1}, *International Journal of Heat and Mass Transfer*, Technical notes, 36 (No. 10) (1993) 2699-2701

27. M. E. Irving and J. W. Westwater, Limitations for obtaining boiling curves by the quenching method with spheres, *Heat Transfer*, 4 (1986) 2061-2066

28. S. Ishigai, S. Nakanishi and T. Ochi, Boiling heat transfer for a plane water jet impinging on a hot surface, Proceedings of the *6th International Heat Transfer Conference* (1978) 445-450

29. T. Ochi, S. Nakanishi, M. Kaji and S. Ishigai, Cooling of a hot plate with an impinging circular water jet, Multiphase-Phase Flow and Heat Transfer III, Part A: Fundamentals (Editors: T. Nejat Veziroglu and Arthur E. Bergles), Elsevier, Amsterdam (1984) 671-681

30. M. A. Ruch and J. P. Holman, Boiling heat transfer to a Freon-113 jet impinging upward onto a flat, heated surface, *International Journal of Heat Mass Transfer* 18 (1975) 51-60

31. H. S. Ragheb, S. C. Cheng and D. C. Groeoneveld, Observations in transition boling of subcooled water under forced convection conditions, *International Journal of Heat Mass Transfer* 24 (No. 7) (1981) 1127-1137

32. N. Hatta, J. Kokado, and K. Hanasaki, Numerical analysis of cooling characteristics for water bar, *Tetsu-to-Hagane*, 67 (1981), 959, in Japanese, English version received December 4, 1981

33. Z. Edelman, E. Elias, and D. Naot, Inverted annular boiling in a stainless-steel tube with steady heat sources, *International Journal of Heat Mass Transfer* 28 (No. 7) (1985) 1281-1292

34. C. F. Ma, and A. E. Bergles, Jet impingement nucleate boiling, *International Journal of Heat Mass Transfer* 29 (No. 8) (1986) 1095-1101

35. T. Nonn, Z. Dagan, and L. M. Jiji, Boiling jet impingement cooling of simulated microelectronic heat sources, ASME, 345 E. 47 St., New York, N. Y. 10017, 88-WA/EEP-3, presented at the *Winter Annual Meeting*, Chicago, Illinois-November 27-December 2, 1988

36. Y. H. Qiu, and Z. H. Liu, Critical heat flux in saturated and subcooled boiling for R-113 jet impingement on the stagnation zone, Applied Thermal Engineering 25 (2005) 2367-2378

37. L. Reichelt, U. Meingast and U. Renz, Calculation Transient Wall Heat Flux from Measurements of Surface Temperature, *International Journal of Heat Mass Transfer* 45 (2002) 579–584

38. F. S. Gunnerson and T. R. Yackle, Quenching and Rewetting of Nuclear Fuel Rods, *Nuclear Technology* 54 (1981) 113-117

39. A. K. Kim and Y. Lee, A Correlation or Rewetting Temperature, *Lett. Heat Mass Transfer* 6 (1979) 117

40. A. M. C. Chan and S. Banerjee, Refilling and Rewetting of a Hot Horizontal Tube, Part I: Experiments, Trans. ASME, *Journal of Heat Transfer* 103 (1981) 281–286

41. J. J. Carbajo, A Study on the Rewetting Temperature, *Nuclear Engineering and Design* 84 (1985) 21–52

42. E. Elias and G. Yadigaroglu, A General One-Dimensional Model for Conduction-Controlled Rewetting of a Surface, *Nuclear Engineering and Design* 42 (1977) 185–194

43. Y. Lee and W. Q. Shen, Effect of Coolant Vapor Quality on Rewetting Phenomena, *International Journal of Heat Mass Transfer* 28 (1985) 139–146

44. A. Yamanouchi, Effect of Core Spray Cooling in Transient State after Loss of Coolant Accident, *Journal of Nuclear Science and Technology* 5 (1968) 547–558

45. B. D. G. Piggot and D. T. C. Porthouse, Water Reactor Emergency Core Cooling: the Effect of Pressure, Subcooling and Surface Condition on the Rewetting of Hot Surface, *UK CEGB RD/B/N2692*, 1973.

46. R. Martini and A. Premoli, A Simple Model for Predicting ECC Transients in Bottom Flooding Conditions, CREST Specialist Meeting on ECC for LWR's, Munich, Oct. (1972) 18–20

47. Y. Lee, W. J. Chen and D. C. Groeneveld, Rewetting of Very Hot Vertical and Horizontal Channels by Flooding, Proc. 6^{th} *International Heat Transfer Conference*, Toronto 5 (1978) 95–101

48. E. Elias and G. Yadigaroglu, The reflooding phase of LOCA in PWRs. Part II : Rewetting and Liquid Entrainment, *Nuclear Safety* 19 (No. 2) March-April (1978) 160-175

49. M. B. David, Y. Zvirin, and Y. Zimmels, Determination of the quenching velocity and rewetting temperature of hot surfaces: Formulation of a nonisothermal microscale hydrodynamic model, *The American Physical society*, Physical Review E, 59 (No. 6) June (1999) 6687-6698

50. T. Nagayoshi, and K. Nishida, Development of a transient boiling transition analysis method based on a film flow model, *Journal of NUCLEAR SCIENCE and TECHNOLOGY* 38 (No. 10) October (2001) 819-825

51. B. D. G. Piggott and R. B. Duffey, The quenching of irradiated fuel pins, *Nuclear Engineering and Design* 32 (1975) 182-190

52. J. J. Carbajo and A. D. Siegel, Review and comparison among the different models for rewetting in LWR's, *Nuclear Engineering and Design* 58 (1980) 33-34

53. E. Oliveri, F. Castiglia, S. Taibi and G. Vella, A new correlation for quench front velocity, *International Journal of Heat Mass Transfer* 25 (No. 10) (1982) 1589-1593

54. X. F. Peng, G. P. Peterson, and B. X. Wang, On the wetting mechanism of liquid flow on hot surface, *International Journal of Heat Mass Transfer* 35 (No. 6) (1992) 1615-1624

55. H. Ohtake, and Y. Koizumi, Study on propagative collapse of a vapor film in film boiling (mechanism of vapor-film collapse at wall temperature above the thermodynamic limit of liquid superheat), *International Journal of Heat and Mass Transfer* 47 (2004) 1965-1977

56. A. K. Satapathy and R. K. Sahoo, Rewetting of an infinite slab with uniform heating under quasi-steady conditions, Trans. ASME, *Journal of Heat Transfer* 124 (2002) 875-880

57. V. K. Dhir, R. B. Duffey and I. Catton, Quenching studies on a zircaloy rod bundle, Trans. ASME, *Journal of Heat Transfer* 103 (1981) 293-299

58. A. K. Saxena, V. V. Raj, and V. G. Rao, Experimental studies on rewetting of hot vertical annular channel, *Nuclear Engineering and Design* 208 (2001) 283-303

59. X. F. Peng, G. P. Peterson, and B. X. Wang, The effect of plate temperature on the onset of wetting, *International Journal of Heat Mass Transfer* 35 (1992) 1605-1613

60. K. H. sun, G. E. Dix and C. L. Tien, Effect of precursory cooling on falling-film rewetting, Trans. ASME, *Journal of Heat Transfer* 97 (1975) 360-365

61. W. J. Chen, Y. Lee, and D. C. Groeneveld, Measurement of boiling curves during rewetting of a hot circular duct, *International Journal of Heat and Mass Transfer* 22 (1978) 973-976

62. J. Filipovic, F. P. Incropera, and R. Viskanta, Rewetting temperatures and velocity in a quenching experiment, *Experimental Heat Transfer* 8 (1995) 257-270

63. Hammad, J. A., Characteristics of heat transfer and wetting front during quenching high temperature surface by jet impingment, *Ph. D. thesis*, Graduate school of science and engineering, Saga University, Japan, March 2004

64. J. Hammad, M. Monde and Y. Mitsutake, Characteristics of heat transfer and wetting front during quenching by jet impingement, *Thermal Science & Engineering* 12 (No. 1) (2004) 19-26

65. M. Monde, H. Arima, W. Liu, Y. Mitutake and J. A. Hammad, An analytical solution for two-dimensional inverse heat conduction problems using laplace transform, *International Journal of Heat and Mass Transfer* 46 (2003) 2135-2148

66. J. Hammad, M. Monde, Y. Mitsutake and H. Arima, Determination of surface temperature and heat flux using inverse solution for two dimensional heat conduction, *Thermal Science & Engineering* 10 (No. 2) (2002) 17-26

67. P. L. Woodfield, M. Monde and Y. Mitsutake, Implementation of an analytical two-dimensional inverse heat conduction technique to practical problems, *International Journal of Heat and Mass Transfer* 49 (2006)187-197

68. H. S. Carslaw and J. C. Jaeger, *Conduction of Heat in Solids*, second edition, Oxford University Press, 1959, pp. 87-88

69. A. K. Mozumder, M. Monde and P. L. Woodfield, Delay of wetting propagation during jet impingement quenching for a high temperature surface, *International Journal of Heat and Mass Transfer* 48 (2005) 5395-5407

70. M. Monde, K. Kitajima, T. Inoue and Y. Mitsutake, Critical heat flux in a forced convection subcooled boiling with an impinging jet, *Heat Transfer*, 7 (1994), 515-520

71. M. Monde, Critical heat flux in saturated forced convective boiling on a heated disk with an impinging jet, *Warme- und Stoffubertragung* 19 (1985) 205-209

72. Y. Haramura and Y. Katto, A new hydrodynamic model of critical heat flux, applicable widely to both pool and forced convection boiling on submerged bodies in saturated liquids, *International Journal of Heat and Mass Transfer* 26 (1983) 389-398

73. E. J. Watson, The radial spread of a liquid jet over a horizontal plane, *J. Fluid Mech.* 20 (1964) 481-499

74. M. Monde, Critical heat flux in saturated forced convection boiling on a heated disk with one or multiple impinging jets, *Trends in Heat, Mass & Momentum Transfer* 1(1991) 33-44

75. A. K. Mozumder, M. Monde, P. L. Woodfield and M. A. Islam, Maximum Heat Flux in Relation to Quenching of a High Temperature Surface with Liquid Jet Impingement, *International Journal of Heat and Mass Transfer* 49 (2006) 2877-2888

76. A. K. Mozumder, P. L. Woodfield, M. A. Islam, and M. Monde, Maximum Heat Flux Propagation Velocity during Quenching by Water Jet Impingement, submitted to *International Journal of Heat and Mass Transfer* (2006)

77. Lienhard, J. H., Correlation for the limiting liquid superheat, *Chem. Eng. Sci.* 31 (1976) 847-849

78. K. H. Chang, and L. C. Witte, Liquid-solid contact during flow film boiling of subcooled Freon-11, *Journal of Heat Transfer* 112 (1990) 465-471

79. A. F. Cokmez-Tuzla, K. Tuzla, and J. C. Chen, Characteristics of liquid-wall contact in post-CHF flow boiling, *International Journal of Heat and Mass Transfer* 43 (2000) 1925-1934

80. S. J. Kline, and F. A. McClintock, Describing uncertainties in single-sample experiments, *Mechanical Engineering*, January (1953) 3-8

81. Y. Mitsutake, Characteristics of Transient Heat Transfer during Impinging Jet Cooling, in Japanese, *Doctoral thesis*, Graduate school of science and engineering, Saga University, Japan, March 2002

Appendix A

Phenomena Immediately after the Commencement of Jet Impingement

At the very early stage immediately after the jet impingement on the hot solid surface, the observed phenomena are different from that after few milli-seconds. The phenomena within the first few milli-seconds have not yet been clarified. A possible explanation of the early stage cooling will be discussed in this chapter.

A.1 Observation Just after the Commencement of Jet Impingement

Two sequences of video images immediately after the commencement of the jet striking jet on the hot solid surface initially heated to 500 ^{o}C are exhibited in Fig. A.1. Immediately after the jet impingement on the brass surface, the flow was found explosive and noisy where splashed liquid moved away in all possible directions. While for steel a circular shiny liquid sheet was observed at the center of the block as shown up to 30 ms. During this period, the flow was very calm and quiet and no boiling sound was detected. It is understood that the jet hardly made contact with the surface at this stage. Rather some pre-existing hot air at the surface and a small amount of vapor formed at the top surface of the impinging jet play an important role in making the jet slide over the surface in a shape like a sheet as shown. Heat transfer from the hot surface lowers the surface tension of the liquid and limits the size of the shiny sheet by forming numerous tiny liquid drops at its fringe as shown in the figure for steel.

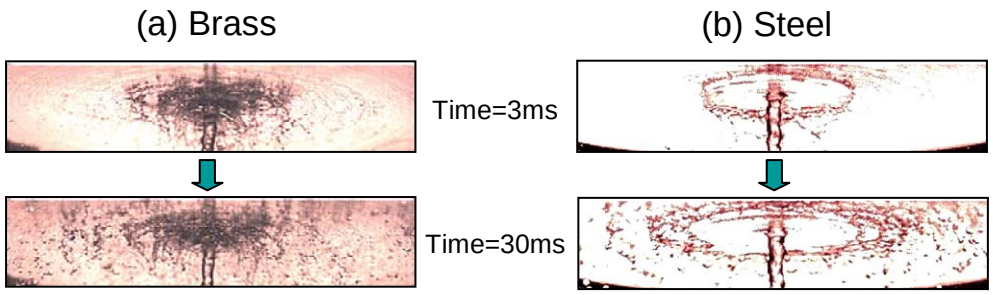

Fig. A.1: Visual observation at the commence of jet for T_b = 500 ^{o}C and u = 5 m/s (a) ΔT_{sub} = 50 K and (b) ΔT_{sub} = 20 K

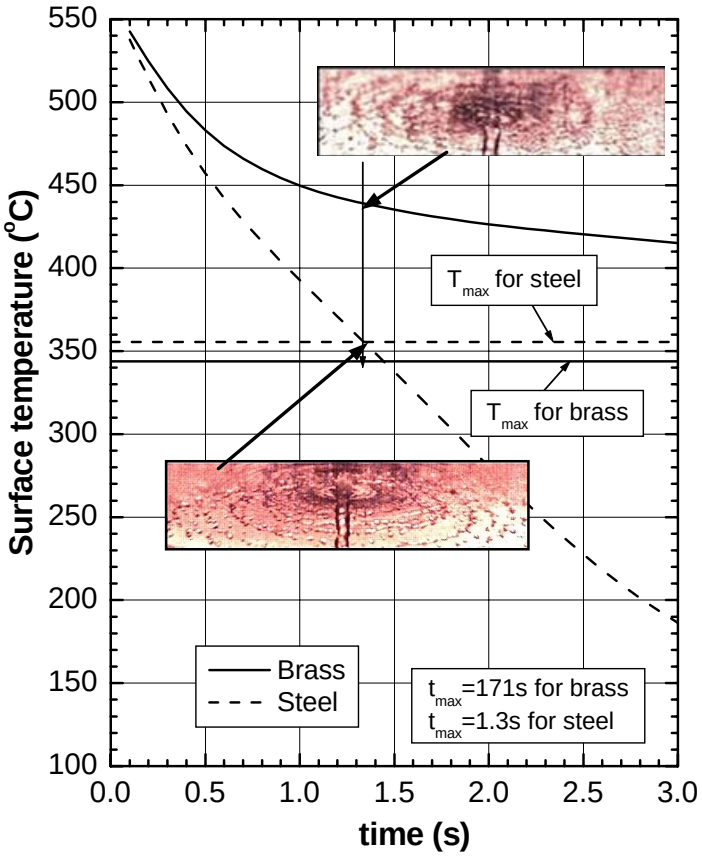

Fig. A.2: Video images together with maximum allowable surface temperature for liquid-solid contact (T_b = 550 °C, ΔT_{sub} = 20 K, u = 5 m/s)

A.2 Maximum Allowable Surface Temperature for Solid-Liquid Contact

Figure A.2 exhibits changes of solid surface temperatures with time at the center of steel and brass blocks both heated initially to 550 °C and quenched by water with a jet of ΔT_{sub} = 20 K and u = 5 m/s. Each of the horizontal lines represents the limiting surface temperature T_{max} that allows solid-liquid contact during quenching. Considering the fact that the jet impingement on a solid surface forms a two-semi-infinite-body contact problem and taking the thermodynamic limiting temperature T_{tls}, which can be well predicted by Lienhard [77], as shown by Eq. (A.1) to be the interface temperature, Eq. (A.2) can be used to estimate the T_{max} according to Carslaw and Jaeger [68].

$$T_{tls} = T_c\left[0.905 + 0.095\left(\frac{T_{sat}}{T_c}\right)^8\right] \tag{A.1}$$

$$\frac{T_{\max} - T_{tls}}{T_{tls} - T_{liq}} = \sqrt{\frac{(\rho c\lambda)_l}{(\rho c\lambda)_s}} \tag{A.2}$$

It is learned from Fig. A.2 that just after the jet impingement the surface temperatures were well above the T_{max} indicating no sustainable solid-liquid contact and became equal to T_{max} at about t_{max} = 1.3 s for steel beyond which the surface cooled below this limiting temperature maintaining solid-liquid contact during the quench. While the surface temperature is well above the T_{max} line as shown in the Fig. A.2. The time t_{max} when the brass surface temperature becomes equal to T_{max} is about 171 s for the quench conditions of Fig. A.2. Two video images are also shown in this figure at a time of 1.3 s when the steel surface temperature equals T_{max}. The video image for steel demonstrates sustainable solid-liquid contact at this time, while for brass it is far beyond such contact and shows a state of explosive flow with splashed liquid moved away radially outward. Solid thermo-physical properties are presumably responsible for the difference in cooling curves and video images.

Chang and Witte [78] provided some important information regarding this solid-liquid contact during the flow film boiling of subcooled Freon-11. Many studies have been done by assuming a continuous vapor film exists between the liquid and the heater surface throughout the film boiling region and several experimental studies [79] have shown that brief random contacts between the liquid and the surface occur in some portions of this region. Chang and Witte [78] found that liquid-solid contacts occurred in a small scale mode in most of their experiments, where the surface temperature was greater than the homogeneous nucleation temperature of R-11. In contrast, large-scale contacts took place just prior to unexpected intermediate transition in some cases. In the large-scale mode, liquid-solid contacts became longer and more intense, causing a cold spot to form. This led to very large temperature drops that shifted the boiling behavior to a significantly lower wall superheat.

A.3 Repetition of Cooling Phenomena: A Conceptual Interpretation

It is realized that neither video observation nor temperature history could help to find a clue for understanding the phenomena that happen at the early stages during jet impingement quenching of a high temperature surface. As the surface temperature during the early stages is well above the thermodynamic limiting temperature that allows solid-liquid contact, the jet may impact the surface by the hydrodynamic forces and bounce immediately because of possible bubble formation during the brief contact making the surface dry again. These events of wet and dry may continue at different frequencies until the surface temperature becomes equal to T_{max} that allows sustainable solid-liquid contact.

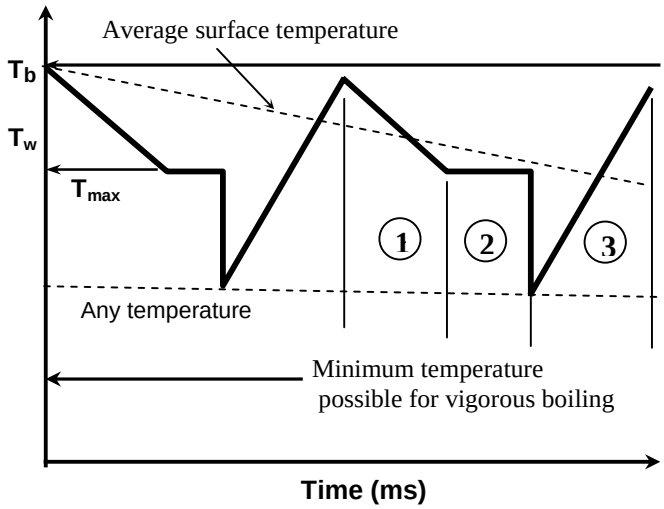

Fig. A.3: Repetition of cooling curve just after the commencement of jet impingement (a conceptual interpretation)

Figure A.3 demonstrates a concept of how the surface temperature may change with these wet and dry phenomena during very early stages of jet impingement quenching. The dark solid line in Fig. A.3 is the possible change in surface temperature T_w during very early stages of quenching. Other solid horizontal lines drawn in the figure are T_b, T_{max} and any temperature for possible vigorous boiling. The upper dashed line is the average temperature that may be predicted by the inverse solution. The regions, circled 1, 2 and 3, are the events making a cycle of wet and dry phenomena during quenching. At first (during the event 1), the surface temperature decreases because of heat transfer by radiation and conduction through gas/vapor in the gap between jet and impinging surface. During the second event (circled 2), the solid-liquid contact is established for a moment and vapor forms by vapor explosion and/or homogeneous nucleation by cooling the surface down to any temperature as shown. Finally, the jet is bounced back by the vapor and the surface temperature is raised by heat conduction from the hotter zone of the block. As the time passes on, the average surface temperature decreases and the above events take relatively longer time to repeat. And thus the period of the cycle becomes larger. An accurate prediction of the change of surface temperature and its frequency may help predict surface heat flux correctly. This could in turn tell us about the type of boiling phenomena at the early stages.

The result of Cokmez-Tuzla et al. [79] could be mentioned here as one of the evidents for the repetition of cooling curve. They conducted an analysis for the quantitative charateristics of liquid-wall contacts in the vicinity of quench fronts for flow boiling, with emphasis on the time fraction of contacts. In order to detect and record potential liquid contacts in the vicinity of an advancing quench front, a special rapid-response probe was

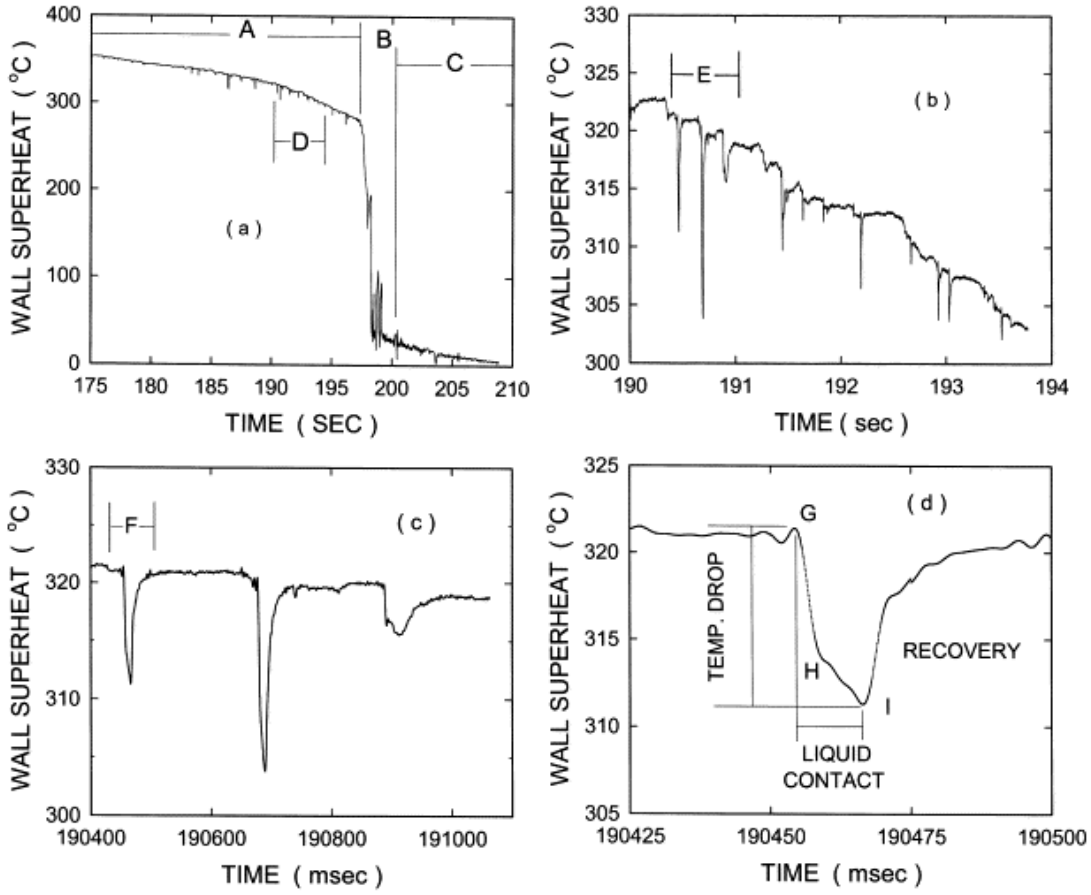

Fig. A.4: A sample contact probe signal indicating variation of instantaneous wall surface temperature during a reflood test [79]

utilized which time response was determined to be better than 0.1 ms to sense 99% of any sudden temperature change. The frequency of the probe was 16,000 data point per second.

To explain the phenomena, an experimental result of Cokmez-Tuzla et al. [79] is exhibited in Fig. A.4. Following their explanation, the surface temperature initially stayed at high superheat of about 300-400 ^{o}C (region A) and decreases gradually with intermittent sudden drops and recoveries as represented in the Fig. A.4(a). This region clearly corresponds to the film boiling regime. As the quench front approached, the surface temperature dropped at a faster rate (region B). This region, with its large temperature drops and recoveries, indicates a transition boiling mechanism. The region C indicates convective nucleate boiling where the surface temperature is very close to the saturation temperature of the liquid. An expanded view of the region D is shown in the Fig. A.4(b). In this expanded scale, a sudden temperature drop (up to 15 ^{o}C) clearly indicates a high cooling mechanism even at the high wall super-heat of 320 ^{o}C. The first three quenching contacts of Fig. A.4(b) are further expanded in Fig. A.4(c) and magnify only one contact

(region F) which is shown in Fig. A.4(d). Figure A.4(d) reveals that the wall temperature is constant before point G and then drops at a rate of 4550 ^{o}C/s (between points G and H) which is reduced to 760 ^{o}C/s between points H and I. Finally, after the point I, the surface temperature recovers to its initial value. From this observed results, Cokmez-Tuzla et al. [79] concluded that the fast cooling of the surface temperature between points G and I is due to the cooling by a liquid droplet which is in contact with the wall. Therefore, the conceptual interpretation as delineated in the Fig. A.3 could be treated as a potentially possible elucidation. Further investigation regarding this mechanism is indispensable.

A.4 Summary and Comments

The definition of Leidenfrost temperature in jet impingement quenching is one of the keen interests. After getting a clear picture of the Leidenfrost phenomena, a new milestone in thermal science will be achieved. Many researchers and scientists have been focusing their efforts to inaugurate the territory of Leidenfrost. The analysis incorporated in this chapter is a part of this ongoing venture. It is reasonable that the possibility of homogeneous nucleation and the presence of the interrelating Leidenfrost phenomena might subsist at the high temperature of the solid especially at the very early stages of the jet impingement. The phenomena observed and a conceptual explanation have been depicted in this chapter. No direct evidence or measurement of the phenomena that happened just immediately after the jet impingement has been identified from the present investigation. Different indirect measures are adopted to simulate the phenomena.

The flow pattern just after the commencement of the jet impingement is influenced by the thermo-physical properties of the solids. An allowable maximum temperature of the solid that permits the solid-liquid contact has been estimated on the basis of the thermodynamic limit of the liquid superheat and on the basis of the concept of the solid-liquid interface temperature. It agrees well to a certain extent with the observable phenomena. A conceptual interpretation regarding the repetition of cooling at the very early stages of the jet impingement is outlined. An evidence of this interpretation has been also referred. Possibility of homogeneous nucleation at the very early stages of the jet impingement has been contemplated as the solid surface temperature is so high to easily interpret that. The ultimate aim, the Leidenfrost phenomena, is so complicated that the present achievements can only represent a small but important step towards this goal.

.

Appendix B

Inverse Solution

Inverse solutions are concerned with determining causes for a desired or an observed effect. Inverse solutions most often do not fulfill postulates of well-posedness. From an inverse solution it is possible to obtain more than one cause/solution from the same effect. Therefore, inverse heat conduction problems might not have a solution in the strict sense; solutions might not be unique and/or might not depend continuously on the data. In fact, what ever is the reliability, it is impossible to directly measure the temperature and heat flux of the impinged surface from the present experiment. A well established and more reliable inverse solution of heat conduction [65-67] is adopted during this research work. The inverse solution procedure is implemented by fitting the thermocouple readings to equations in the form of Eq. (B.1) for each depth using a least-squares method to determine the coefficients $P_{j,k}^{(n)}$.

$$f(\tau,\gamma,\zeta_n) = \sum_{j=0}^{N_j} J_0(m_j\gamma)\cdot\sum_{k=0}^{N}\frac{P_{j,k}^{(n)}\cdot\tau^{k/2}}{\Gamma(k/2+1)} \quad at\ n=1,2 \tag{B.1}$$

Where, $f(\tau,\gamma,\zeta_n)$ is temperature variation function on plane $\zeta=\zeta_n$ beneath the surface

The unsteady heat conduction equation and Eq. (B.1) are transformed to the Laplace domain and then solved. Using an approximate inverse Laplace transform procedure the solutions for the surface temperature and heat flux are obtained explicitly in the form of Eq. (B.2) and Eq. (B.3) respectively.

$$\theta_w(\tau,\gamma) = \sum_{j=0}^{N_j}\sum_{\ell=-1}^{N} G_{j,\ell}^{(1,2)}\cdot\frac{\tau^{\ell/2}}{\Gamma(\ell/2+1)}\cdot J_0(m_j\gamma) - \sum_{j=0}^{N_j}\sum_{\ell=-1}^{N} G_{j,\ell}^{(2,1)}\cdot\frac{\tau^{\ell/2}}{\Gamma(\ell/2+1)}\cdot J_0(m_j\gamma) \tag{B.2}$$

$$\Phi_w(\tau,\gamma) = \sum_{j=0}^{N_j}\sum_{\ell=-1}^{N} H_{j,\ell}^{(1,2)}\cdot\frac{\tau^{\ell/2}}{\Gamma(\ell/2+1)}\cdot J_0(m_j\gamma) - \sum_{j=0}^{N_j}\sum_{\ell=-1}^{N} H_{j,\ell}^{(2,1)}\cdot\frac{\tau^{\ell/2}}{\Gamma(\ell/2+1)}\cdot J_0(m_j\gamma) \tag{B.3}$$

Where, *Jo* is Bessel function, τ is non-dimensional time, ζ is non-dimensional distance in axial direction, γ is non-dimensional distance in radial direction of the block and m_j is eigen value. The coefficients $G_{j,l}^{(m,n)}$ and $H_{j,l}^{(m,n)}$, the mathematical derivation and practical implementation of the inverse solution have been discussed in detail in [65-67].

Appendix C

Thermo-Physical properties of Materials

Thermo-physical properties of working fluid and solid are tabulated in this section.

Table C.1: Thermo-physical properties of water *

T_{liq} (^oC)	Density (kg/m^3)	Specific heat (J/kg.K)	Conductivity (W/mK)	Diffusivity (m^2/s)	Viscosity (m^2/s)	Prandtl number
20	997.755	4183.65	0.59909	$1.44x10^{-7}$	$1.03x10^{-6}$	7.2077
50	987.830	4178.50	0.64000	$1.55x10^{-7}$	$5.44x10^{-7}$	3.5086
80	971.635	4199.35	0.64684	$1.64x10^{-7}$	$3.62x10^{-7}$	2.2054
95	961.123	4214.00	0.67848	$1.67x10^{-7}$	$3.05x10^{-7}$	1.8253

Table C.2: Thermo-physical properties of test section materials **

Material	Temp. (^oC)	Density, ρ (kg/m^3)	Sp. heat, c (kJ/kg.K)	Conductivity, λ (W/mK)	Diffusivity, a (m^2/s)	$\sqrt{\rho c\lambda}$ ($kJ/m^2K\sqrt{s}$)
Copper	100	8862	0.393	379	$1.088x10^{-4}$	36.33
	200	8831	0.406	374	$1.041x10^{-4}$	36.62
	300	8794	0.416	369	$1.008x10^{-4}$	36.74
	400	8752	0.425	363	$9.759x10^{-5}$	36.75
Brass (70% Cu, 30% Zn)	100	8530	0.389	128	$3.857x10^{-5}$	20.61
	200	8530	0.414	144	$4.077x10^{-5}$	22.55
	300	8530	0.444	147	$3.881x10^{-5}$	23.60
	400	8530	0.477	147	$3.612x10^{-5}$	24.46
Steel (0.45% C)	100	7833	0.485	52	$1.368x10^{-5}$	14.06
	200	7806	0.509	48	$1.208x10^{-5}$	13.81
	300	7775	0.545	45	$1.061x10^{-5}$	13.81
	400	7741	0.589	42	$9.211x10^{-6}$	13.84

*Based on standard text book

**Based on JSME Heat Transfer Hand Book, 1993, The Japan Society of Mechanical Engineers ed.

Appendix D

Uncertainty Analysis

No measurement made is ever exact. The exactness of measurement is always limited by the degree of refinement of the apparatus used, by skill of the observer, and by the basic physics in the experiment. In doing experiments we are trying to establish the best values of certain quantities, or trying to validate a theory. We must also give a range of possible true values based on our limited number of measurements. Why should repeated measurements of a single quantity give different values? Mistakes on the part of the experimenter are possible, but we do not include these in our discussion. A careful researcher should not make mistakes! (or at least he or she should recognize them and correct the mistakes.) Even use of the synonymous terms uncertainty, error, or deviation to represent the variation in the measurement data sometimes can be ambiguous. Two types of error are possible. Systematic error is the one which is the result of a mis-calibrated device, or a measuring technique which always makes the measured value larger (or smaller) than the "true" value. Even when systematic errors are eliminated there will remain a second type of variation in measurement values of a single quantity. These remaining deviations will be classed as random errors, and can be dealt with in a statistical manner.

For a single observation, the error, which is the difference between the true and observed values, is a certain fixed number. But the uncertainty, or what one thinks the error might be, may vary considerably depending upon the particular circumstances of observation. "Variable" means a basic quantity observed directly in the laboratory as opposed to the "result" which is obtained by making corrections to or calculations with the recorded values of the variables. The recorded values of the variables are called "data". In a few cases, of course, the results are the same as the data. "Propagation of uncertainty" will mean the way in which uncertainties in the variables affect the uncertainty in the results.

Therefore, the term "Uncertainty" may be defined as the parameter, associated with the result of a measurement that characterizes the description of the values that could reasonable be attributed to the measurement. Uncertainty analysis is a powerful tool for improving the values of experimental work, and can be applied during all phases of an experimental program. Uncertainty analysis is an essential ingredient in planning, controlling, and reporting experiments. Uncertainty analysis is also necessary for the results to be used to their fullest value.

D.1 Uncertainty Terminology of Primary Measurands

Basic definitions of frequently used terminology of primary measurands in uncertainty analysis are presented in this section.

D.1.1 Precision limit, P: The ±P interval about a result (single or average) is the experimenter's 95% confidence estimate of the band within which the mean of many such results would fall, if the experiment were repeated many times under the same conditions and using the same equipment. The precision limit is thus an estimate of the scatter (or lack of repeatability) caused by random error and unsteadiness. The precision limit of a measurand could be calculated as two times the standard deviation of unsteadiness of a set of observations measured with the apparatus in normal running condition. A sufficiently large number of sample (>30) should be taken over a sufficiently long sampling period in order for unsteadiness values to be representative of the process.

D.1.2 Bias limit, B: The bias limit is an estimate of the magnitude of the fixed, constant error. When the true bias error in a result is define as β, the quantity B is the experimenter's 95% confidence estimate such that $|\beta| \leq B$. The bias element cannot be sampled (via replication) within available procedure and its existence is what mandates the need of cross-checks and closures via theory. The bias limit includes the estimated bias errors of calibration standards and in the calibration procedure, and less-than-perfect curve fitting of the calibration data.

D.1.3 Uncertainty, *w*: The ±*w* interval about the result is the band within which the experimenter is 95% confident the true value of the result lies. The 95% confidence uncertainty (also uncertainty interval), *w* is calculate from Eq. (D.1)-

$$w = [P^2+B^2]^{1/2} \qquad \text{(D.1)}$$

D.2 Uncertainty Propagation into Experimental Results

As it is discussed earlier that the error in the experimental results initiates from the deviation of the primary measured quantity and finally it propagates into the derived quantity/results which is based on the primary measurands. The variable which is measured independently during experiment is described as primary measurands. To know how reliable the experimental result is, it is necessary to compute the uncertainty in the results form the estimates of uncertainty in the measurands. This computation process is described as "Propagation of Uncertainty". Kline and Mc.clintock [80] nicely described a mathematical technique for estimation of uncertainty propagation into experimental results.

D.2.1 Uncertainty in variables: Kline and Mc.clintock [80] described the uncertainty in each variable as-

$$\text{Variable value} = m \pm w \tag{D.2}$$

Where, m is the mean (arithmetic mean of the observed value) and w is the uncertainty interval. The uncertainty interval, w is not a variable but a fixed value selected so that the experimenter would be willing to wager that the error is less than w.

D.2.2 Uncertainty in estimated result: If R is linear function of n independent variables, $v_1, v_2, \ldots v_n$ each of which is normally distributed, then the relation between the interval for the variables w_i, and the interval for the result W_R is as follows:

$$W_R = \left[\left(\frac{\partial R}{\partial v_1} w_1 \right)^2 + \left(\frac{\partial R}{\partial v_2} w_2 \right)^2 + - - - - - + \left(\frac{\partial R}{\partial v_n} w_n \right)^2 \right]^{1/2} \tag{D.3}$$

Equation (D.3) might be used directly as an approximation for calculating the uncertainty interval in the result. Equation (D.2) can be also considered separately in computing the precision and bias components of uncertainties when the functional form of R is known.

D.3 Uncertainty in the Present Experiment

Examples of uncertainty calculation for the present experiment are incorporated in this section. Few values during the estimation of uncertainty are adopted from Mitsutake [81]. Uncertainties of the primary measured quantities are incorporated. The uncertainty of the inverse solution has not yet been included.

D.3.1 Uncertainty of jet velocity: The location of strain meter is shown in Fig. D.1. Let V_2 = jet velocity = u

From the equation of continuity:

$$A_2V_2 = A_1V_1$$

$$\Rightarrow V_2 = \frac{A_1V_1}{A_2} \Rightarrow u = \left(\frac{d_1}{d_2}\right)^2 V_1$$

Here, d_2 = Jet diameter = d and d_1 = Pipe diameter = d_o (= 23.7 mm)

$$\therefore \quad u = \left(\frac{d_o}{d}\right)^2 V_1 \Rightarrow V_1 = u\left(\frac{d}{d_o}\right)^2$$

Applying Bernoulli's equation between point 1 and 2 the following equation is obtained:

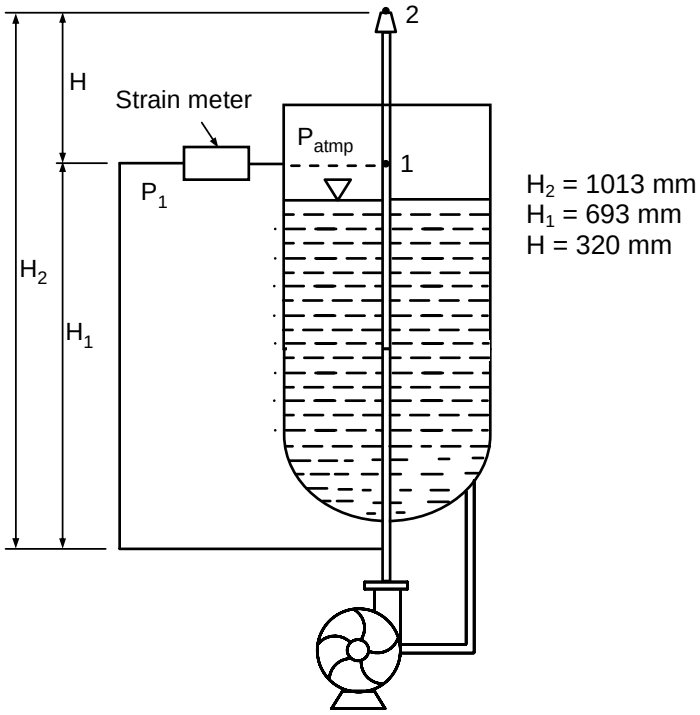

Fig. D.1: Strain meter location in the experimental set-up

$$\frac{P_2}{\rho_l g}+\frac{V_2^{\,2}}{2g}+H_2=\frac{P_1}{\rho_l g}+\frac{V_1^{\,2}}{2g}+H_1$$

$$\Rightarrow \frac{V_2^{\,2}}{2g}-\frac{V_1^{\,2}}{2g}=\frac{P_1-P_2}{\rho_l g}+H_1-H_2$$

$$\Rightarrow \frac{u^2}{2g}-\frac{\left\{u\left(\frac{d}{d_o}\right)^2\right\}^2}{2g}=\frac{P_1-P_2}{\rho_l g}+H_1-H_2$$

$$\Rightarrow \frac{u^2}{2g}-\frac{u^2\left(\frac{d}{d_o}\right)^4}{2g}=\frac{P_1-P_2+H_1\rho_l g-H_2\rho_l g}{\rho_l g}$$

$$\Rightarrow \frac{u^2}{2g}\left\{1-\left(\frac{d}{d_o}\right)^4\right\}=\frac{P_1-P_{atmp}+H_1\rho_l g-H_2\rho_l g}{\rho_l g}$$ [$P_2 = P_{atmp}$ = Atmospheric pressure and P_1-P_{atmp} = strain meter pressure reading]

$$\Rightarrow \frac{u^2}{2g}\left\{1-\left(\frac{d}{d_o}\right)^4\right\}=\frac{P_1-P_{atmp}+\rho_l g\left(H_1-H_2\right)}{\rho_l g}$$

$$\Rightarrow u^2\left\{1-\left(\frac{d}{d_o}\right)^4\right\}=\frac{2\left\{P_1-P_{atmp}-H\rho_l g\right\}}{\rho_l}$$

$$\therefore u=\frac{\sqrt{\frac{2(\Delta P)}{\rho_l}}}{\sqrt{\left\{1-\left(\frac{d}{d_o}\right)^4\right\}}}$$ [Let, $\Delta P = P_1 - P_{atmp}$-$gH\rho_l$]

(A) Uncertainty of jet velocity from the flow rate measurement:

Jet velocity,
$$u=\frac{Q/t}{\frac{\pi}{4}d^2}=\frac{4Q}{\pi d^2 t} \qquad \text{(D.4)}$$

Where, Q = Total volume of water collected in time, t and d = jet diameter

According to Eq. (D.3), the uncertainty in the velocity estimation by using Eq. (D.4) is-

$$W_u=\left[\left(\frac{\partial u}{\partial Q}w_Q\right)^2+\left(\frac{\partial u}{\partial d}w_d\right)^2+\left(\frac{\partial u}{\partial t}w_t\right)^2\right]^{1/2} \qquad \text{(D.5)}$$

An example has been considered from a set of run for the present experiment where, Jet diameter, d = 2 mm, strain meter voltage reading, V = 0.593 V, Time of water collection, t = 154.5 seconds, Total volume of water collected, Q = 3384 ml, Water temperature, T_{liq} =

20 ^{o}C, ΔP = 2.92x10^{4} Pa and jet velocity [from Eq. (D.4)], u = 6.97 m/s. During the measurement of volume of water the bias limit, w_{QB} was 2.5 ml [half of the least count (5 ml) of the measuring flask which is easily readable and it's a standard practice) and the precision limit, w_{QP} was about 10 ml (random variation of the measured volume from different readings for a fixed time and which is approximately two times of the standard deviation of random data).

So,

$$w_Q = \sqrt{w^2_{QB} + w^2_{QP}} = \sqrt{(\text{Least count}/2)^2 + w_{QP}{}^2} = \sqrt{(5.0/2)^2 + 10.0^2}\ \text{ml} = 1.0308\text{X}10^{-5}\ \text{m}^3$$

$$w_d = \sqrt{w^2_{dB} + w^2_{dP}} = \sqrt{(\text{Least count}/2)^2 + w_{dP}{}^2} = \sqrt{(0.05/2)^2 + 0.0^2}\ \text{mm} = 2.5\text{X}10^{-5}\ \text{m}$$

$$w_t = \sqrt{w^2_{tB} + w^2_{tP}} = \sqrt{(\text{Least count}/2)^2 + w_{tP}{}^2} = \sqrt{(0.01/2)^2 + 0.15^2}\ \text{s} = 0.1501\,\text{s}$$

Now, the change of velocity with respect to volume-

$$\frac{\partial u}{\partial Q} = \frac{4}{\pi d^2 t} = \frac{4}{\pi\left(2\text{x}10^{-3}\right)^2 \text{x}154.5} = 2060.2582$$

Change of jet velocity with respect to jet diameter-

$$\frac{\partial u}{\partial d} = \frac{-8Q}{\pi d^3 t} = \frac{-8\left(3384\text{x}10^{-6}\right)}{\pi(154.5)\text{x}\left(2\text{x}10^{-3}\right)^3} = -6971.9136$$

Change of jet velocity with respect to time-

$$\frac{\partial u}{\partial t} = \frac{-4Q}{\pi d^2 t^2} = \frac{-4\left(3384\text{x}10^{-6}\right)}{\pi\left(2\text{x}10^{-3}\right)^2 \text{x}(154.5)^2} = -0.045126$$

Now, putting all these values in Eq. (D.5)-

$$W_u = \left[\left\{2060.2582\text{x}\left(1.0308\text{x}10^{-5}\right)\right\}^2 + \left\{-6971.9136\text{x}\left(2.5\text{x}10^{-5}\right)\right\}^2 + \left\{-0.045126\text{x}(0.1501)\right\}^2\right]^{1/2}$$
$$= 0.1757\ m/s$$

Therefore, the relative uncertainty for the measurement of jet velocity by the flow measurement (fm) technique, $\left|\frac{W_u}{u}\right|_{fm} = \frac{0.1757}{6.97} = 2.5208\%$

(B) Uncertainty of jet velocity from the calibration curve fitting error:

If the strain meter constant is α [Pa/$\mu\varepsilon$], the strain is ε_p [$\mu\varepsilon$] and the voltage is V_p [volt] then the corresponding pressure,

$$\Delta P = \left(\frac{\varepsilon_p}{V_p}\alpha\right) \text{x } \textit{strain meter voltage reading} - \rho_l g H$$
$$= 54502.7\text{x } \textit{strain meter voltage reading} - 3139.2 \quad [Pa]$$
$$= 54502.7\text{x}0.593 - 3139.2 \ \ Pa$$
$$= 2.92\text{x}10^4 \ Pa$$

The empirical correlation for the estimation of the jet velocity from the measured pressure as shown in Fig. D.2 is given below:

$$\textit{Re ynolds number}, R_{ed} = \frac{ud}{\nu_l} = 0.9641\left[\frac{d}{\nu_l}\sqrt{\frac{\Delta P}{\rho_l}}\right]^{1.0328} \tag{D.6}$$

Standard deviation of Reynolds number, $\sigma R_{ed} = 289.5986$

So, the deviation of jet velocity from the calibration data-

$$\delta u = \frac{\sigma R_{ed}\nu_l}{d} = \frac{289.5986\text{x}\left(1.0327\text{x}10^{-6}\right)}{2\text{x}10^{-3}} = 0.1495 \ m/s$$

The relative uncertainty due to the calibration error, $\left|\frac{\delta u}{u}\right|_{clbr} = \frac{0.1495}{6.97} = 2.1449\ \%$

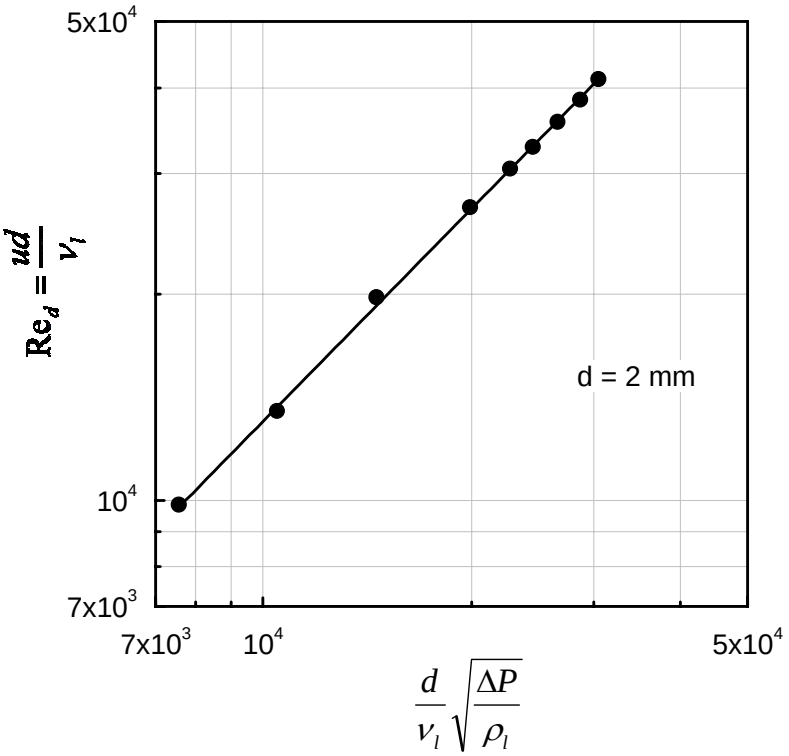

Fig. D.2: Calibration curve for the jet velocity estimation

(C) Uncertainty of pressure measurement due to the strain meter: Uncertainty of pressure value of strain meter from the readout (RO) mechanism,

$$\delta(\Delta P)_{DP} = \pm 0.2\ \%\ \text{of RO}$$
$$= \pm (0.2/100)\text{x}(3.2320 \times 10^4)\ \text{Pa}$$
$$= \pm 64.64\ \text{Pa}$$

Uncertainty of readings of voltage, $\delta(V)_{DV} = \pm 0.045\%$ of readings

Full scale strain, $\varepsilon_o = 1000\ \mu\varepsilon$, full scale voltage, $V_o = 0.5V$ and the strain meter constant, $\alpha = 65.3809\ \text{Pa}/\mu\varepsilon$.

$$\therefore \delta(V)_{DV} = \pm\frac{0.045}{100}\text{X}0.5\ V$$
$$= \pm 2.25\text{X}10^{-4}\ V$$

Uncertainty of strain meter reading, $\delta\varepsilon_{DP} = \pm 0.5\ \%$ of full scale

$$= \pm (0.5/100)\text{x}1000\ \mu\varepsilon$$
$$= \pm 5\ \mu\varepsilon$$

Therefore, the total uncertainty of pressure measurement from the strain meter,

$$\delta(\Delta P) = \sqrt{\left|\delta(\Delta P)_{DP}\right|^2 + \left\{\alpha\frac{\varepsilon_o}{V_o}\left|\delta(V)_{DV}\right|\right\}^2 + \left\{\alpha\left|\delta\varepsilon_{DP}\right|\right\}^2}$$
$$= 334.5259\ Pa$$

The relative uncertainty of velocity due to strain meter $= \left|\frac{\partial u}{\partial(\Delta P)}\right|.\left|\frac{\delta(\Delta P)}{u}\right|$

Here, $\frac{\partial u}{\partial(\Delta P)}$ indicates the partial derivative of u with respect to ΔP, where u is a function of ΔP. From the empirical correlation [Eq. (D.6)] of velocity it is estimated that-

$$\left[\frac{\partial \text{u}}{\partial(\Delta \text{P})}\right]_{\text{at u}=6.97\ \text{m/s}} = 1.1447\text{x}10^{-4}\ \frac{\text{m/s}}{\text{Pa}}$$

So, $\left|\frac{\partial u}{\partial(\Delta P)}\right|.\left|\frac{\delta(\Delta P)}{u}\right| = (1.1447\text{x}10^{-4})\text{x}\left(\frac{334.5259}{6.97}\right) = 0.5494\ \%$

(D) Overall uncertainty propagation into jet velocity: The overall relative uncertainty, $\left|\frac{\delta u}{u}\right|$ propagation into jet velocity from different sources can be express as follows:

$$\left|\frac{\partial u}{u}\right| = \left|Uncertainties\ during\ \ flow\ rate\ measurement\right| + \left|Uncertainties\ \ from\ calibration\right|$$
$$+ \left|Uncertainties\ \ from\ the\ strain\ meter\right|$$
$$= \left|\frac{W_u}{u}\right|_{fm} + \left|\frac{\delta u}{u}\right|_{clbr} + \left|\frac{\partial u}{\partial(\Delta P)}\right|_{at\ a\ constant\ u} \cdot \left|\frac{\delta(\Delta P)}{u}\right| \qquad (D.7)$$

Putting all the necessary values in Eq. (D.7)-

$$\left|\frac{\delta u}{u}\right| = \pm[2.5208 + 2.1449 + 0.5494]\,\%$$

$= \pm 5.22\ \%$ at $T_{liq} = 20\ ^oC$

D.3.2 Uncertainty of block initial temperature, T_b:

Overall relative uncertainty, $\left|\frac{\delta T_b}{T_b}\right|$ for the block initial temperature, T_b measurement is as follows-

$\left|\frac{\delta T_b}{T_b}\right|$ = Uncertainty due to thermocouple error (Manufacturer's claim), $\left|\frac{\delta T_{TC}}{T_b}\right|$

+ Uncertainty from the data acquisition system, $\left|\frac{\partial T_{conv}}{\partial E}\right|_{at\ a\ constant\ T_b} \cdot \left|\frac{\delta E}{T_b}\right|$

+ Uncertainty due to calibration inaccuracy, $\left|\frac{\delta T_{clbr}}{T_b}\right|$

+ Uncertainty from the zero temperature (ice box) setting, $\left|\frac{\delta T_{zero}}{T_b}\right|$

Now, for a set of data where, $T_b = 250\ ^oC$

$\delta T_{TC} = 0.15\ ^oC$ (Manufacturer's claim)

$$\therefore \left|\frac{\delta T_{TC}}{T_b}\right| = \frac{0.15\ ^oC}{250\ ^oC} = \pm\ 0.06\ \%$$

Again, error in the data acquisition system, δE = Error from the amplifier, δE_{amp} + Error from the Analog-Digital (A/D) converter, $\delta E_{A/D}$

δE_{amp} = Standard deviation, $\sigma_{amp,\,err} = \pm\ 0.006$ mV

And, $\delta E_{A/D} = \frac{Error\ in\ voltage\ reading}{Gain} = \frac{\pm\ 2.44\ mV}{610} = \pm\ 0.004\ mV$

So, $\delta E = \delta E_{amp} + \delta E_{A/D}$

$= \pm 0.01$ mV

Again, $T_{conv}(E) = 3.2043x10^{-2} + 2.5448x10^{1}E - 0.57181E^{2} + 0.10624E^{3} - 7.5316x10^{-3}E^{4} + 1.79497x10^{-4}E^{5}$

The above equation is recommended for the temperature range 0 ~ 400 ^{o}C. The standard deviation for the fitting curve of the above equation, $\sigma_{Terr} = \pm 0.12\ ^{o}C$

$$\therefore \left|\frac{\delta T_{clbr}}{T_b}\right| = \pm\frac{0.12\ ^{o}C}{250\ ^{o}C} = \pm 0.048\ \%$$

The zero setting error, $\delta T_{zero} = \pm 0.1\ ^{o}C$ (approximately)

$$\therefore \left|\frac{\delta T_{zero}}{T_b}\right| = \pm\frac{0.1\ ^{o}C}{250\ ^{o}C} = \pm 0.04\ \%$$

By using all of the above necessary values, the total uncertainty for the block initial temperature, T_b measurement is as follows:

$\delta T_b = \pm 0.46\ ^{o}C$ at $T_b = 250\ ^{o}C$

D.3.3 Uncertainty of liquid temperature, T_{liq}:

Thermocouple uncertainty, $\delta T_{TC} = 0.15\ ^{o}C$ (Manufacturer's claim)

The temperature voltage conversion equation:

$T_{conv}(E) = 0.1367 + 2.4882x10^{1}E - 1.2056x10^{-1}E^{2}$

This equation is recommended between the temperature 0~100 ^{o}C.

The standard deviation, $\sigma_{Terr} = \pm 0.09\ ^{o}C$

Error from the data acquisition system, $\frac{\delta E}{E} = \pm 0.045\ \%$ ($\delta E = \pm 0.045$ % of reading)

Error from the zero setting (ice box) of thermocouple = $\pm 0.1\ ^{o}C$ (approximately)

The overall relative uncertainty,

$$\left|\frac{\delta T_{liq}}{T_{liq}}\right| = \left|\frac{\delta T_{TC}}{T_{liq}}\right| + \left|\frac{\delta T_{conv}}{T_{liq}}\right| + \left|\frac{\partial T_{conv}}{\partial E}\right|_{T=T_{liq}} \cdot \left|\frac{\delta E}{T_{liq}}\right| + \left|\frac{\delta T_{zero}}{T_{liq}}\right|$$

For $T_{liq} = 50\ ^{o}C$, the total uncertainty, $\delta T_{liq} = \pm 0.2\ ^{o}C$.